DISCRETE VARIABLE REPRESENTATION

OF THE ANGULAR VARIABLES

IN QUANTUM THREE-BODY SCATTERING

BY

DAVID CABALLERO

A Dissertation submitted to the Faculty of
Claremont Graduate University and
California State University, Long Beach
in partial fulfillment of the requirements for the
degree of Doctor Of Philosophy in the Graduate
Faculty of Engineering and Industrial Applied
Mathematics

Claremont Graduate University
California State University, Long Beach
2011

APPROVAL OF THE REVIEW COMMITTEE

This thesis has been duly read, reviewed, and critiqued by the Committee listed below, which hereby approves the manuscript of David Caballero as fulfilling the scope and quality requirements for meriting the degree of Doctor Of Philosophy in the Graduate Faculty of Engineering and Industrial Applied Mathematics

Alfonso Rueda, Ph.D., Chair
California State University, Long Beach

C.Y. Hu, Ph.D.
California State University, Long Beach

Ellis Cumberbatch, Ph.D.
Claremont Graduate University

Ali Nadim, Ph.D.
Claremont Graduate University

Abstract

Discrete Variable Representation

Of The Angular Variables

In Quantum Three-Body Scattering

by

David Caballero

Claremont Graduate University: 2011

There are many numerical methods to study the quantum mechanical three-body scattering system using the Schrodinger equation. Traditionally, a partial-wave decomposition of the total wave function is carried out first, allowing the scattering system to be solved one partial wave at a time. This is convenient when the interaction is central, causing the total angular momentum to be conserved during the collision process. This is not possible in the presence of a non-central interaction such as a laser field, where the total angular momentum is not conserved during the collision process. The Discrete Variable Representation is a new method for solving the quantum-mechanical three-body scattering problem to obtain the total cross section. The implementation of this new method for the two-body problem has been successfully applied to real

systems. The extension to the three-body problem is the next logical step. For this thesis bipolar spherical harmonics are used in the implementation of the three-body Discrete Variable Representation. This Discrete Variable Representation is capable of working with any combination of interactions, including non-central interactions. The total cross section computation for a three-particle elastic-scattering numerical example is used to illustrate the potential of this Discrete Variable Representation method. The three-particle system consists of a positron scattering against a ground state hydrogen atom (an electron bound to a proton).

ACKNOWLEDGMENTS

The author would like to thank the members of the committee for their help and advice in the preparation of this thesis.

The author is particularly grateful to Dr. Hu for her invaluable advice, immense help and direction in making this thesis possible.

The author is also grateful for the generous allocation of computer time and for the use of computer resources made possible by the NSF, Texas Advanced Computing Center (TACC) and the Teragrid allocation committee.

TABLE OF CONTENTS

APPENDIX

APPENDIX

LIST OF TABLES

TABLE

LIST OF FIGURES

FIGURE

FIGURE

FIGURE

FIGURE

FIGURE

FIGURE

CHAPTER 1

INTRODUCTION

Quantum mechanics came about during the early twentieth century through the works of a number of physicists like Bohr, Schrodinger, Dirac, Heisenberg and many others. It provides a mathematical frame work to calculate the dynamic properties of atomic and nuclear interaction systems.

Almost everything known about particles at the quantum scale has been found by scattering experiments. Thus a mathematical frame work describing the scattering process can be used to stimulate a quantum scattering experiment by explaining the underlying details of the results of the scattering process.

However, computational difficulty has severely limited the calculation of the three-body problem. Only recently, with the advent of massive parallel computers, has progress been made towards solving the three-body problem. Even using today's computer systems, new computational methods are needed to apply the quantum mechanical equations to obtain solutions to the precision necessary for current scattering experiments.

Current researches are developing new numerical methods for the application of quantum mechanics to the most general low energy quantum three-body scattering system. The method in this thesis provides a step towards that goal.

The method described in this thesis produces the total and differential scattering cross sections that can be compared directly with experimental data. In this research the experimental data consists of a positron scattering against a ground state hydrogen atom (which consists of a proton and an electron). This scattering process is denoted as $(e^+ + H)$.

As this method becomes more refined it could simulate anti-hydrogen production experiments in external fields since it would indicate how to obtain the largest cross sections corresponding to anti-hydrogen production.

The long range Coulomb interaction is a major difficulty in obtaining solutions to the Schrodinger equation governing the $(e^+ + H)$ scattering process. There are many methods to study this problem using the Schrodinger equation[1,2,3,4,5,6,7,8,9]. However, the method that provides the most complete picture for low-energy scattering is the Modified Faddeev Method (MFE),

especially when there are rearrangement channels, and all three particles are different. The modified Faddeev method involves the solving of a set of coupled equations that is well suited to analyze multi-channel scattering processes with a long range potential[10,11].

The efficiency of the numerical solution to the MFE and other implementations of the Schrodinger equation are a function of the choice of basis functions used in the expansion of the wave function. The expansion and projection of the basis functions reduces the differential problem to a large set of coupled linear equations. The solution to these problems requires the manipulation of large matrices and a poor choice of basis functions can make the problem unwieldy in both matrix density and computer time required for a solution.

One effective method to solve the equations is to expand the wave function in terms of global basis functions[12,13]. Once the angular momentum states have been projected out, diagonalizing the kinetic energy operator, a Gaussian quadrature procedure is used for the numerical integration of the potential operator. For three-body scattering an efficient method for evaluating the MFE equations is to use a bipolar spherical harmonics

expansion to represent all the angular momentum states[14,15]. Once the angular momentum states have been projected out, a Quintic-Hermite polynomial spline and collocation procedure is used for the x and y coordinate numerical calculations[16,17,18,19,20,21,22,23].

The three-body problem in this form may be solved using partial-wave decomposition. For scattering problems this is convenient when the interaction is central so that the total angular momentum is conserved. With this method the solution is obtained one partial wave at a time.

This approach becomes impractical for scattering in the presence of a non-central interaction such as the presence of a laser field or when the collision energy increases so that many rearrangement channels are possible.

The Discrete Variable Representation (DVR) is a basis-set representation in which the matrix elements of a multiplicative potential energy operator V(x) are diagonal[24]. DVRs can be in many types of functions, such as polynomial, trigonometric or angular spherical harmonics[25]. In 1965 Harris chose a polynomial basis to diagonalize the position operator x, or a monotonically increasing or decreasing function of x. He then stated

that this basis also diagonalizes V(x)[26]. In 1968, Dickinson showed that if the basis were polynomials multiplied by a weight W(x) then the matrix element computation (using DVR) would be equivalent to using an N-point Gaussian quadrature[27,28]. In 1992, Light used the DVR method to solve the nuclear Schrodinger equation[29].

The use of Discrete Variable Representation in the two-body problem has been successfully applied to other physical systems[30,31,32,33,34]. The extension to the three-body problem has also been investigated by defining a three-variable DVR as the direct product of three distinct one-variable radial DVRs, one for each dimension x, y, and z[35]. The advantage of the DVR is that the matrix elements of the potential energy are diagonal when projected out at the DVR grid points. The coupled kinetic energy matrix elements are left to be evaluated analytically or numerically. By diagnolizing the potential, and numerically integrating the kinetic energy, computational efficiency is obtained without the use of partial waves.

The method proposed for this thesis uses the Discrete Variable Representation as the angular basis functions used in the expansion of the wave function to solve the Schrodinger equation. Once proven, this method may be

implemented into the Modified Faddeev Method. Following the spirit of Hu and Kvitsinsky, who use the bipolar spherical harmonics consistently as a convenient set of basis functions to solve the Modified Faddeev Equations, the DVR basis functions used to solve the Schrodinger equation are also based on the bipolar spherical harmonics rather than a direct product in the implementation of the three-body four-variable DVR. The DVR calculation is partial wave independent and will lend itself well to calculations of non-central interactions. Quintic splines and three-body e+H radial basis functions are implemented in the x and y coordinate numerical calculations after the DVR angular basis functions have been projected out.

This thesis computes the scattering cross section for a three-particle elastic-scattering problem numerically. The numerical example is used to illustrate the potential of the Discrete Variable Representation method to solve the general three-particle scattering problem.

CHAPTER 2

COMPUTATIONAL METHODOLOGY

The description of the discretization of the Schrodinger equation is given in this chapter. The first section discusses a convenient coordinate system used to simplify the mathematics. The second section describes the DVR basis functions that are used to simplify the Schrodinger equation when these functions are projected out of the wave function. The third section describes the radial basis functions that are used to interpolate the resulting radial wave function. The fourth section gives the discretized Schrodinger equation using the results of the previous 3 sections. The fifth section describes the asymptotic boundary conditions and the amplitude function. The sixth section describes the boundary conditions near the interaction region. The final section describes the scattering cross section obtained from the amplitude function.

A detailed description of each of these sections is given in the appendix.

2.1 Three-body Elastic-scattering Coordinates

Appendix A contains more details of the mathematics behind this overview of the Mass-scaled Jacobi coordinates[36,37,38]. The mass-scaled electron-atomic units have $\eta = e = m_e = K = 1$ so that the unit of length is the electron Bohr radius a = 1 corresponding to the length in MKS units of $a^{MKS} = \eta^2/Km_e e^2$ = 0.529169x10^{-10} M. Similarly, the unit of energy is E = 1, and the electron Bohr energy E_B = -½ corresponding to E_B^{MKS} = -2.179698535x10^{-18} J = -13.623 eV.

Three-body kinematics is conveniently described using Jacobi vectors. There are three domains of configuration space that give rise to three sets of Jacobi coordinates. A set of Jacobi coordinates is chosen that best describes the asymptotic state of the problem to be solved. For positron-hydrogen scattering the three sets of Jacobi coordinates which represent the three possible asymptotic scattering states are shown in Figure 1.

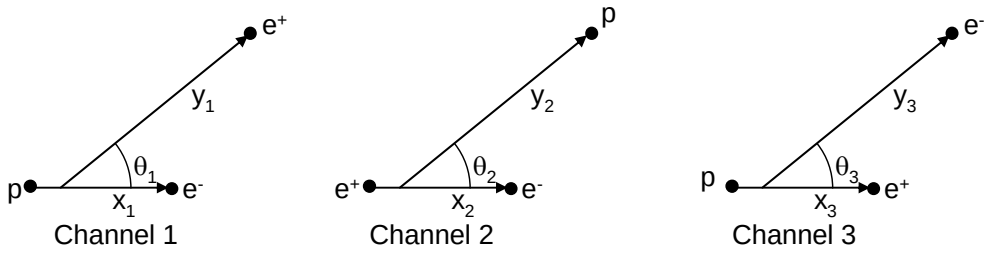

Figure 1. Jacobi Coordinates

The convenient set of indices used in the physics community is used to describe the mass-scaled Jacobi equations. The relationship between the mass-scaled Jacobi coordinates are summarized by defining the indices (α, β, γ) as cyclic (1, 2, 3) where (1, 2, 3) represents the Jacobi channel and (1, 2, 3) also represents the particles (e^+, e^-, p) respectively. Also defined are the pairs $\alpha = (\beta, \gamma)$, $\beta = (\gamma, \alpha)$ and $\gamma = (\alpha, \beta)$.

Let m_α and r_α be the mass and position vector for the particle indexed by α. Then the mass-scaled Jacobi vectors are defined by

$$\bar{x}_\alpha = t_\alpha(\bar{r}_\beta - \bar{r}_\gamma) \qquad \text{Eq. 1}$$

$$\bar{y}_\alpha = \mu_\alpha\left(\bar{r}_\alpha - \frac{m_\beta \bar{r}_\beta - m_\gamma \bar{r}_\gamma}{m_\beta + m_\gamma}\right) \qquad \text{Eq. 2}$$

where

$$t_\alpha = \sqrt{\frac{2m_\beta m_\gamma}{m_\beta + m_\gamma}} \qquad \text{Eq. 3}$$

and

$$u_\alpha = \sqrt{\frac{2m_\alpha (m_\beta + m_\gamma)}{M}} \qquad \text{Eq. 4}$$

and M is the total atomic mass $m_1 + m_2 + m_3$.

Note that $t_\alpha^2/2$ is the reduced mass of the pair α, and $u_\alpha^2/2$ is the reduced mass of the particle α and the pair α.

The Jacobi vectors of different channels are related by orthogonal transformations

$$\bar{x}_\beta = c_{\beta\alpha}\bar{x}_\alpha + s_{\beta\alpha}\bar{y}_\alpha \qquad \text{Eq. 5}$$

$$\bar{y}_\beta = -s_{\beta\alpha}\bar{x}_\alpha + c_{\beta\alpha}\bar{y}_\alpha \qquad \text{Eq. 6}$$

where the mass dependent coefficients are

$$c_{\beta\alpha} = -\sqrt{\frac{m_\alpha m_\beta}{(m_\alpha + m_\gamma)(m_\beta + m_\gamma)}} \qquad \text{Eq. 7}$$

$$s_{\beta\alpha} = (-1)^{\beta-\alpha}\,\mathrm{sgn}(\alpha-\beta)\sqrt{1-c_{\beta\alpha}^2} \qquad \text{Eq. 8}$$

For scattering problems, a more convenient set of local coordinates are the lengths of the mass-scaled Jacobi vectors and the angle between them,

$$x_\alpha = |\bar{x}_\alpha| \qquad \text{Eq. 9}$$

$$y_\alpha = |\bar{y}_\alpha| \qquad \text{Eq. 10}$$

$$z_\alpha = \cos(\theta_\alpha) = \frac{\bar{x}_\alpha \bullet \bar{y}_\alpha}{x_\alpha y_\alpha} \qquad \text{Eq. 11}$$

and the coordinate transformation for the lengths are

$$x_\beta^2 = c_{\beta\alpha}^2 x_\alpha^2 + s_{\beta\alpha}^2 y_\alpha^2 + 2 s_{\beta\alpha} c_{\beta\alpha} x_\alpha y_\alpha z_\alpha \qquad \text{Eq. 12}$$

$$y_\beta^2 = s_{\beta\alpha}^2 x_\alpha^2 + c_{\beta\alpha}^2 y_\alpha^2 - 2 s_{\beta\alpha} c_{\beta\alpha} x_\alpha y_\alpha z_\alpha \qquad \text{Eq. 13}$$

$$z_\beta = \frac{(c_{\beta\alpha}^2 - s_{\beta\alpha}^2) x_\alpha y_\alpha z_\alpha - s_{\beta\alpha} c_{\beta\alpha} (x_\alpha^2 - y_\alpha^2)}{x_\beta y_\beta} \qquad \text{Eq. 14}$$

In mass-scaled coordinates the Coulomb potential, V_α, for the α particle pair is given by

$$V_\alpha = t_\alpha e_\beta e_\gamma / x_\alpha \qquad \text{Eq. 15}$$

Defining $q_\alpha = t_\alpha e_\beta e_\gamma$ as the mass-scaled charge for the pair, the Coulomb potential for the pair $\alpha = (\beta,\gamma)$ becomes

$$V_\alpha(x_\alpha) = q_\alpha / x_\alpha \qquad \text{Eq. 16}$$

In terms of the rotational angular momentum of the bound pair given by the operator, $\hat{l}_{x_\alpha}$, and of the orbital angular momentum of the free particle about the bound pair, $\hat{l}_{y_\alpha}$, the quantum-mechanical form of the mass-scaled Schrodinger equation, with pair wise Coulomb potentials, is

$$\left(-\frac{1}{x_\alpha}\frac{\partial}{\partial x_\alpha^2} x_\alpha - \frac{1}{y_\alpha}\frac{\partial}{\partial y_\alpha^2} y_\alpha + \frac{\hat{l}_{x_\alpha}^2}{x_\alpha^2} + \frac{\hat{l}_{y_\alpha}^2}{y_\alpha^2} + \frac{q_\alpha}{x_\alpha} + \frac{q_\beta}{x_\beta} + \frac{q_\gamma}{x_\gamma} \right) \Psi = E\Psi \qquad \text{Eq. 17}$$

This thesis computes the cross section results for positron-hydrogen elastic-scattering. For convenience of calculations, the Jacobi coordinates indexed by 1 is implemented into the Schrodinger equation since it is best related to the asymptotic physics.

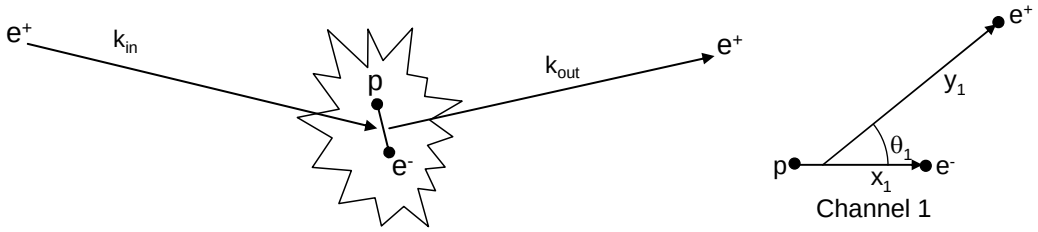

Figure 2. Selected Jacobi Coordinates.

Hereafter $\alpha = 1$ and the subscript is dropped from the equations. $\beta = 2$ and $\gamma = 3$ remain in the equations as needed.

The previous equation is rewritten as

$$\left(-\frac{1}{x}\frac{\partial}{\partial x^2}x-\frac{1}{y}\frac{\partial}{\partial y^2}y+\frac{\hat{l}_x^2}{x^2}+\frac{\hat{l}_y^2}{y^2}+\frac{q}{x}+\frac{q_2}{x_2}+\frac{q_3}{x_3}\right)\Psi = E\Psi \qquad \text{Eq. 18}$$

For convenience let the wave function be represented by

$$\Psi(\bar{x},\bar{y}) = \Psi(x,y,\Omega_x,\Omega_y) = \frac{\tilde{\Psi}(x,y,\Omega_x,\Omega_y)}{xy} \qquad \text{Eq. 19}$$

where

Ω_x = angle representation of the pair of angles (θ_x, ϕ_x) that indicate the polar and azimuthal angles of the x coordinate axis

Ω_y = angle representation of the pair of angles (θ_y, ϕ_y) that indicate the polar and azimuthal angles of the y coordinate axis

Substituting Eq. 19 into Eq. 18, the wave function differential equation becomes

$$-\frac{\partial^2\tilde{\Psi}}{\partial x^2}-\frac{\partial^2\tilde{\Psi}}{\partial y^2}+\frac{\hat{l}_x^2\tilde{\Psi}}{x^2}+\frac{\hat{l}_y^2\tilde{\Psi}}{y^2}-E\tilde{\Psi}+\left(\frac{q}{x}+\frac{q_2}{x_2}+\frac{q_3}{x_3}\right)\tilde{\Psi}=0 \qquad \text{Eq. 20}$$

2.2 Discrete Variable Representation

Appendix B contains more details of the mathematics behind this overview of the DVR basis representation. Solving the time independent two-body Schrodinger equation using an angular two-variable DVR approach has been successfully implemented. The DVR is a unitary transformation of a Finite Basis Representation (FBR) defined for some quadrature scheme associated with the FBR. The two-variable angular basis functions are a linear combination of spherical harmonics. The radial functions are not expanded but are approximated using splines or some other approximating technique.

Since the three-body angular four-variable DVR is analogous to the two-body angular two-variable DVR, a description of the two-body DVR is described first and then extended to the three-body DVR.

The derivation of a set of two-variable angular DVR basis functions begins by defining N Gauss points on a two-dimensional unit sphere $\Omega_j = (\theta_{i\theta},\phi_{i\phi})$ where θ is the spherical coordinate polar angle and ϕ is the spherical coordinate azimuthal angle. The index j represents the angular grid point indicated by the pair of indices (i_θ,i_ϕ).

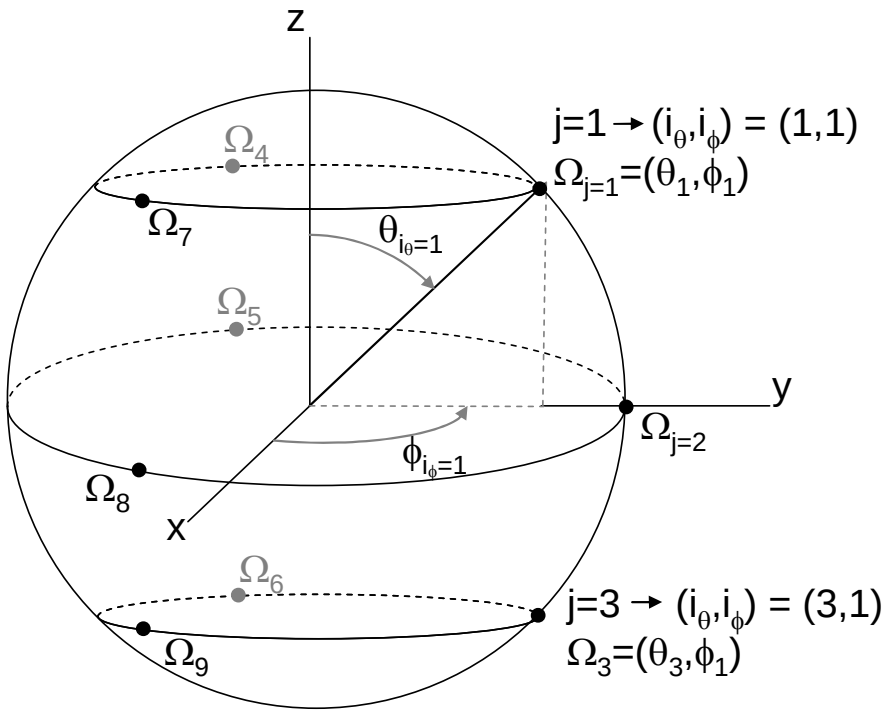

Figure 3. N=9 Point DVR Angular Grid.

Also defined with this grid are a set of associated Gauss-quadrature weights w_j, and a set of DVR basis functions $\phi_j(\Omega)$. By construction, these functions satisfy the property

$$\phi_i(\Omega_j) = \delta_{ij}/\sqrt{w_j} \qquad \text{Eq. 21}$$

where δ_{ij} is the Kronecker delta function.

On this grid the two-dimensional Gauss quadrature approximation for a function $g(\Omega)$ is[39,40]

$$\int g(\Omega)d\Omega \approx \sum_{k=1}^{N} g(\Omega_k)w_k \qquad \text{Eq. 22}$$

The DVR functions are orthogonal

$$\int \phi_i^*(\Omega)\phi_j(\Omega)d\Omega = \sum_{k=1}^{N} \phi_i^*(\Omega_k)\phi_j(\Omega_k)w_k = \delta_{ij} \qquad \text{Eq. 23}$$

The advantage of the DVR basis functions is that the potential matrix of a multiplicative potential is diagonal in angular space

$$\int \phi_i^*(\Omega)V(\Omega,r)\phi_j(\Omega)d\Omega \approx \sum_{k=1}^{N} \phi_i^*(\Omega_k)V(\Omega,r)\phi_j(\Omega_k)w_k = V(\Omega_i,r)\delta_{ij} \qquad \text{Eq. 24}$$

The angular DVR basis functions are constructed from the FBR basis functions as described in appendix B. For the case of spherical harmonic FBR basis functions, which are orthonormal

$$\int J_\nu^*(\Omega)J_{\nu'}(\Omega)d\Omega = \delta_{\nu\nu'} \qquad \text{Eq. 25}$$

the DVR basis functions are given by

$$\phi_j(\Omega) = \sqrt{w_j} \sum_{\nu=1}^{N} (S_{j\nu})^* S_\nu(\Omega) \qquad \text{Eq. 26}$$

with

$$S_\nu(\Omega) = \sum_{\nu'=1}^{N} C_{\nu\nu'} J_{\nu'}(\Omega) \qquad \text{Eq. 27}$$

being the digital Gram-Schmidt orthogonalization of the FBR spherical harmonic basis functions, $J_\nu(\Omega)$. The Gram-Schmidt orthogonalization is required so that the basis functions are orthogonal in the Gauss integration

$$\int S_i^*(\Omega) S_j(\Omega) d\Omega = \sum_{k=1}^{N} S_i^*(\Omega_k) S_j(\Omega_k) w_k = \delta_{ij} \qquad \text{Eq. 28}$$

Let the index ν represents the pair of angular momentum quantum numbers (l,m) with $0<=l<=l_{max}$ and $-l<=m<=l$ and the index j represents the angular grid point indicated by the pair (i_θ, i_ϕ). w_j are the appropriately selected Gaussian weights. There is not a set of unique quantum numbers, grid points and weights for the DVR basis[42]. The selection of the convenient set of quantum numbers, angular grid points and weights used for this thesis is described in appendix B.

For this thesis the total number of angular momentum quantum numbers, ν, is equal to the total number of angular

quadrature points, j. The total number is also an odd number. This is not a strict requirement on the use of DVR functions[43]. However, for the selection of angular basis functions, the selection of angular quantum grid points, and the selection of grid angles, the Gram-Schmidt expansion fails when the total number of DVR basis functions is an even number since the basis functions are not linearly independent on the grid.

The FBR transformation to DVR is a unitary transformation thus completeness is also obtained

$$\sum_{k=1}^{N} S_k^*(\Omega_i)\sqrt{w_i}S_k(\Omega_j)\sqrt{w_j} = \delta_{ij} \qquad \text{Eq. 29}$$

This guarantees the DVR basis functions obey the property given by Eq. 21.

In this angular two-variable DVR approach the two-body wave function is expanded, using spherical coordinates, appropriately selected weights and Gram-Schmidt coefficients, as

$$\tilde{\Psi}(r,\Omega) \approx \sum_{j=1}^{N} \psi_j(r)\phi_j(\Omega) = \sum_{j=1}^{N}\sum_{\nu=1}^{N} \sqrt{w_j}(S_{j\nu})^* S_\nu(\Omega)\psi_j(r) \qquad \text{Eq. 30}$$

When evaluated at the k^{th} angular grid point, the wave function reduces to the corresponding radial expansion

coefficient, $\psi_k(r)$, divided by the square root of the corresponding weight.

$$\tilde{\Psi}(r,\Omega_k)=\sum_{j=1}^{N}\psi_j(r)\phi_j(\Omega_k)=\sum_{j=1}^{N}\psi_j(r)\frac{\delta_{jk}}{\sqrt{w_k}}=\frac{\psi_k(r)}{\sqrt{w_k}} \qquad \text{Eq. 31}$$

When solving the time independent three-body Schrodinger equation (Eq. 20), the four-variable angular finite basis is chosen to be the bipolar spherical harmonics.

$$\begin{aligned}\mathrm{Y}_{l_x,l_y}^{L,M}(\hat{x},\hat{y}) &= \sum_{m_x+m_y=M}(\mathrm{Y}_{l_x}^{m_x}(\theta_x\phi_x)\mathrm{Y}_{l_y}^{m_y}(\theta_y\phi_y)C_{l_x,m_x,l_y,m_y}^{L,M}) \\ &= [\mathrm{Y}_{l_x}^{m_x}(\hat{x})\otimes\mathrm{Y}_{l_y}^{m_y}(\hat{y})]^{L,M}\end{aligned} \qquad \text{Eq. 32}$$

where

L = Total angular momentum quantum number, $L = (l_x+l_y), (l_x+l_y-1), \ldots, |l_x-l_y|$

M = Total angular momentum projection

l_x = Rotational angular momentum of the bound pair

l_y = The orbital angular momentum of the free particle about the bound pair

m_x = Bound pair angular momentum projection along the relative coordinate x-axis

m_y = Orbital angular momentum projection along the relative coordinate y-axis

$C_{l_x,m_x,l_y,m_y}^{L,M}$ = Clebsch-Gordon vector coupling coefficient, $\langle l_x,l_y,m_x,m_y|l_x,l_y,L,M\rangle$

$\hat{x}$ = angle representation of the pair of angles Ω_x = (θ_x, ϕ_x)

$\hat{y}$ = angle representation of the pair of angles Ω_y = (θ_y, ϕ_y)

To give the bipolar basis a convenient one-dimensional look the following notation is implemented

ν = index representing the quartet of quantum numbers (L, M, l_x, l_y)

Ω = angle representation of the quartet of angles ($\hat{x}$, $\hat{y}$) = (θ_x, ϕ_x, θ_y, ϕ_y)

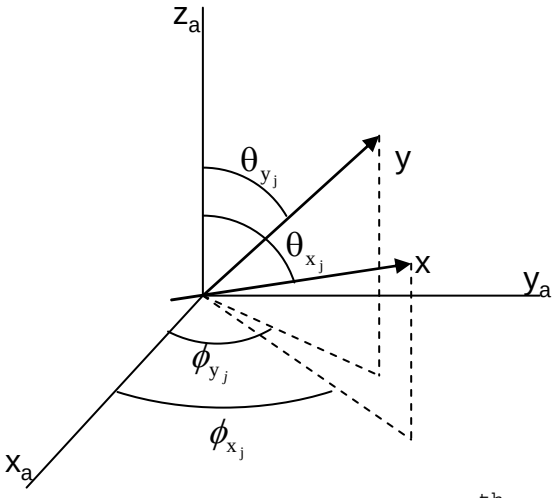

Figure 4. Jacobi Coordinates At j^{th} Grid Point.

Using this notation, the bipolar basis function is rewritten as

$$Y_\nu(\Omega) = \sum_{m_x+m_y=M} (Y_{l_x}^{m_x}(\hat{x}) Y_{l_y}^{m_y}(\hat{y}) C_{l_x,m_x,l_y,m_y}^{L,M}) \qquad \text{Eq. 33}$$

Let

i = index representing the quartet of indices (i_{θ_x}, i_{ϕ_x}, i_{θ_y}, i_{ϕ_y})

Ω_i = angular Gaussian quadrature point indexed by i, ($\theta_{i_{\theta_x}}$, $\phi_{i_{\phi_x}}$, $\theta_{i_{\theta_y}}$, $\phi_{i_{\phi_y}}$)

N_x = Number of Ω_x Gaussian quadrature points relative to the x-axis, $N_{\theta_x} * N_{\phi_x}$

N_y = Number of Ω_y Gaussian quadrature points relative to the y-axis, $N_{\theta_y} * N_{\phi_y}$

N = Total number of four-dimensional Gaussian quadrature points, $N_x * N_y$

The bipolar basis function evaluated at the i^{th} Gaussian quadrature grid point is denoted as $Y_\nu(\Omega_i)$ and is given by

$$Y_\nu(\Omega_i) = \sum_{m_x+m_y=M} (Y_{l_x}^{m_x}(\theta_{i_{\theta_x}}, \phi_{i_{\phi_x}}) Y_{l_y}^{m_y}(\theta_{i_{\theta_y}}, \phi_{i_{\phi_y}}) C_{l_x,m_x,l_y,m_y}^{L,M}) \qquad \text{Eq. 34}$$

The bipolar spherical harmonics are orthogonal

$$\int Y_\nu^*(\Omega) Y_{\nu'}(\Omega) d\Omega = \delta_{\nu\nu'} \qquad \text{Eq. 35}$$

Analogous to the two-body case, the three-body angular DVR basis functions are constructed from the FBR

basis functions, as described in appendix B. The four-variable angular DVR basis functions are given by

$$\phi_j(\Omega) = \sqrt{W_j}\sum_{\nu=1}^{N}(S_{j\nu})^* S_\nu(\Omega) \qquad \text{Eq. 36}$$

with

$$S_\nu(\Omega) = \sum_{\nu'=1}^{N} C_{\nu\nu'} Y_{\nu'}(\Omega) \qquad \text{Eq. 37}$$

being the digital Gram-Schmidt orthogonalization of the bipolar spherical harmonics basis functions, $Y_v(\Omega)$, to ensure the Gauss approximation is orthogonal

$$\int S_\nu^*(\Omega) S_{\nu'}(\Omega) d\Omega = \sum_{k=1}^{N} S_\nu^*(\Omega_k) S_{\nu'}(\Omega_k) W_k = \delta_{\nu\nu'} \qquad \text{Eq. 38}$$

Again the total number of angular grid points is an odd number so that the Gram-Schmidt orthogonalization process is successful.

Analogous to the two-dimensional angular case we have the DVR property

$$\phi_i(\Omega_j) = \delta_{ij} / \sqrt{W_j} \qquad \text{Eq. 39}$$

and the DVR functions are orthogonal

$$\int \phi_i^*(\Omega)\phi_j(\Omega) d\Omega = \sum_{k=1}^{N} \phi_i^*(\Omega_k)\phi_j(\Omega_k) W_k = \delta_{ij} \qquad \text{Eq. 40}$$

and complete

$$\sum_{i=1}^{N} \phi_i^*(\Omega_k)\sqrt{W_k}\,\phi_i(\Omega_{k'})\sqrt{W_{k'}} = \delta_{kk'} \qquad \text{Eq. 41}$$

The weights are appropriately chosen Gaussian quadrature weights:

$$w_{i_\theta} = \left(\frac{\sqrt{2}}{\sin(\theta_{i_\theta}) P'_{N_\theta}(\cos(\theta_{i_\theta}))} \right)^2 \qquad \text{Eq. 42}$$

$$w_{i_\phi} = 2\pi / N_\phi \qquad \text{Eq. 43}$$

$$W_i = w_{i_x} * w_{i_y} = w_{i_{\theta_x}} * w_{i_{\phi_x}} * w_{i_{\theta_y}} * w_{i_{\phi_y}} \qquad \text{Eq. 44}$$

Note that the Gram-Schmidt modified bipolar spherical harmonic functions have the properties:

$$< \nu \mid \nu' >= \sum_{i=1}^{N} (S_{i\nu})^* S_{i\nu'} W_i = \delta_{\nu\nu'} \qquad \text{Eq. 45}$$

$$< i \mid i' >= \sum_{\nu=1}^{N} (S_{i\nu})^* S_{i'\nu} \sqrt{W_i W_{i'}} = \delta_{ii'} \qquad \text{Eq. 46}$$

where S_{iv} represents $S_i(\Omega_v)$.

As an example of the importance of using the Gram-Schmidt orthogonalization, Table 1 lists the results of the orthogonality and completeness properties of the off diagonal matrix elements of the Gauss quadrature representations. The top row in the table lists the DVR grid size for the table column beneath the heading. The numerical values of $Y_v(\Omega)$ and $S_v(\Omega)$ are evaluated at the DVR angular grid points using double precision computer representation.

The second and third rows show that the orthogonality and completeness properties fail when using the $Y_\nu(\Omega)$ representation. The fourth and fifth rows show that the orthogonality and completeness properties are obtained when using the Gram-Schmidt $S_\nu(\Omega)$ representation.

Table 1. Orthogonality And Completeness.

DVRsize->	9x9	9x25	25x9	25x25	9x49	25x49	49x9	49x25	49x49
$\sum_{i=1}^{N}(Y_{i\nu})^* Y_{i\nu'} W_i$	164	597	597	2237	1289	5202	1289	5202	12000
$\sum_{\nu=1}^{N}(Y_{i\nu})^* Y_{i'\nu}\sqrt{W_i W_{i'}}$	427	1595	1595	5890	3780	13885	3780	13885	32644
$\sum_{i=1}^{N}(S_{i\nu})^* S_{i\nu'} W_i$	$1x10^{-12}$	$4x10^{-11}$	$4x10^{-11}$	$2x10^{-9}$	$1x10^{-9}$	$5x10^{-8}$	$1x10^{-9}$	$5x10^{-8}$	$2x10^{-6}$
$\sum_{\nu=1}^{N}(S_{i\nu})^* S_{i'\nu}\sqrt{W_i W_{i'}}$	$5x10^{-12}$	$2x10^{-10}$	$3x10^{-10}$	$3x10^{-8}$	$9x10^{-9}$	$6x10^{-7}$	$1x10^{-8}$	$6x10^{-7}$	$5x10^{-5}$

As the DVR grid size increases, the accuracy of the orthogonality and completeness properties of the Gram-Schmidt representation decreases when using double precision numerical representation. As the size of the DVR grid size increases, higher precision representation is required to maintain high accuracy results.

Note that the completeness and orthogonality of the $S_\nu(\Omega)$ functions ensures that the matrix elements of the multiplicative potential are diagonal.

For the finite basis, the total angular momentum quantum number, L, is between 0 and L_{max} where L_{max} is the product of l_{max} of each Jacobi axis: $L_{max} = l_{xmax} * l_{ymax}$.

Table 2 lists the values of L_{max} for each three-body angular DVR basis function size.

Table 2. Maximum Total Angular Momentum Index.

DVRsize->	9x9	9x25	25x9	25x25	9x49	25x49	49x9	49x25	49x49
L_{max}	4	6	6	8	8	10	8	10	12

A six variable wave function $\Psi(x,\theta_x,\phi_x,y,\theta_y,\phi_y)$ is approximated using the angular four-variable DVR functions as follows

$$\tilde{\Psi}(x,y,\Omega) \approx \sum_{j=1}^{N} \psi_j(x,y)\phi_j(\Omega) = \sum_{j=1}^{N}\sum_{\nu=1}^{N} \sqrt{W_j}\,(S_{j\nu})^* S_\nu(\Omega)\psi_j(x,y) \qquad \text{Eq. 47}$$

where $\psi_j(x,y)$ are the two-variable radial expansion coefficients.

When evaluated at the k^{th} angular grid point the wave function reduces to the corresponding radial expansion coefficient, $\psi_k(x,y)$, divided by the square root of the corresponding weight.

$$\tilde{\Psi}(x,y,\Omega_k) = \sum_{j=1}^{N} \psi_j(x,y)\phi_j(\Omega_k) = \sum_{j=1}^{N} \psi_j(x,y)\frac{\delta_{jk}}{\sqrt{W_k}} = \frac{\psi_k(x,y)}{\sqrt{W_k}} \qquad \text{Eq. 48}$$

2.3 Radial Splines And Spline Basis

Appendix C describes the detailed mathematics for the Hermite Quintic Splines that are used to numerically evaluate the radial coefficient of the wave function that

results after the angular DVR basis functions have been projected out.

Since the three-body spline basis is a direct product of the two-body spline basis, a description of the two-body spline basis is described first and then extended to the three-body spline basis.

In the two-dimensional angular DVR case we are left to evaluate the radial coefficients, $\psi_k(r)$. Interpolation is the process of estimating the intermediate values of a continuous function from discrete samples. The radial coordinate is discretized over a radial grid. These discrete points are called knots. The set of points that make up the grid is represented by

$$\{ x_i^k \} = \{ x_0^k = r_{min},\ x_1^k,\ x_2^k,\ \ldots,\ x_{N_k}^k = r_{max} \} \qquad \text{Eq. 49}$$

where N_k is the number of segments between the knots: N_k = number of knots + 1.

In between each set of knots is a set of points called collocation points. A fundamental property of interpolation functions is that they must coincide with the sampled data at the collocation points. Each set of collocation points consists of N_f points. For example if f is the sampled function and g is the corresponding

interpolation function then $f(r_k) = g(r_k)$ where r_k is a collocation point.

Hermite Quintic splines are a set of three interpolation functions defined on two adjacent intervals describe by three continuous knots $[x_{i-1}^k, x_i^k] \cup [x_i^k, x_{i+1}^k]$. These functions are zero outside their intervals.

The quintic spline basis consists of $N_k * N_f$ piecewise polynomials of fifth degree. Using Hermite Quintic splines the interpolating function is written as

$$g(r) = \sum_{rs=0}^{N_k N_f - 1} A_{rs} \phi_{rs}(r) \qquad \text{Eq. 50}$$

where $\phi_{rs}(r)$ is the $(rs)^{th}$ indexed Quintic spline function A_{rs} is the corresponding scaling coefficient, N_k is the number of knots and N_f is the number of collocation points between knots. Plots of the quintic spline functions are given in Appendix C.

Over any one interval, $[x_{i-1}^k, x_i^k]$, there are six non-automatic zero basis functions and six scaling coefficients to be evaluated.

Gauss-Legendre collocation points are found between each adjacent pair of knots. For Quintic splines $N_f = 3$ collocation points are required for the Gauss quadrature integration approximation to be a reasonable approximation

to the function. This assumes that the function being approximated is smooth enough over the interval that a fifth order polynomial can approximate it.

For the three-dimensional two-body wave function, after the DVR basis are projected out, the radial wave function is approximated using the quintic spline basis functions

$$\psi_j(r) = \sum_{rs=0}^{N_k N_f - 1} A_{j,rs}\phi_{rs}(r) \qquad \text{Eq. 51}$$

In this DVR quintic spline approach the two-body wave function is expanded as

$$\tilde{\Psi}(r,\Omega) \approx \sum_{j=1}^{N}\sum_{\nu=1}^{N}\sqrt{w_j}(S_{j\nu})^* S_\nu(\Omega) \sum_{rs=0}^{N_k N_f - 1} A_{j,rs}\phi_{rs}(r) \qquad \text{Eq. 52}$$

When evaluated at the k^{th} angular grid point, the following equality is obtained

$$\tilde{\Psi}(r,\Omega_k) = \frac{1}{\sqrt{w_k}} \sum_{rs=0}^{N_k N_f - 1} A_{k,rs}\phi_{rs}(r) \qquad \text{Eq. 53}$$

For the three-body case, the two-dimensional knots are the direct product of the one-dimensional knots. The two-dimensional collocation points are also the direct product of the one-dimensional collocation points. The two-dimensional quintic spline basis functions are a direct product of two one-dimensional quintic spline basis

functions. The two-dimensional radial wave function is written as

$$\psi_k(x,y) = \sum_{rs_y=0}^{N_{k_y}N_f-1} \sum_{rs_x=0}^{N_{k_x}N_f-1} A_{k,rs_y,rs_x} \phi_{rs_y}(y) \phi_{rs_x}(x) \qquad \text{Eq. 54}$$

where N_{ky} are the number of knots on the Jacobi y-axis, N_{kx} are the number of knots on the Jacobi x-axis and it is assumed that both axis use the same spline basis so that N_f is the same for both axis. Similarly, rs_y is the spline index for the y-axis and rs_x is the spline index for the x-axis.

In this DVR quintic spline approach the three-body wave function is expanded as

$$\tilde{\Psi}(x,y,\Omega) \approx \sum_{j=1}^{N} \sum_{\nu=1}^{N} \sqrt{W_j} (S_{j\nu})^* S_\nu(\Omega) \sum_{rs_y=0}^{N_{k_y}N_f-1} \sum_{rs_x=0}^{N_{k_x}N_f-1} A_{j,rs_y,rs_x} \phi_{rs_y}(y) \phi_{rs_x}(x) \qquad \text{Eq. 55}$$

When evaluated at the k^{th} angular grid point

$$\tilde{\Psi}(r,\Omega_k) = \frac{1}{\sqrt{W_k}} \sum_{rs_y=0}^{N_{k_y}N_f-1} \sum_{rs_x=0}^{N_{k_x}N_f-1} A_{k,rs_y,rs_x} \phi_{rs_y}(y) \phi_{rs_x}(x) \qquad \text{Eq. 56}$$

As described in Appendix C, if the quintic spline approach cannot meet the Gauss quadrature integration approximation requirements over an interval between two knots, then another set of basis functions must be chosen to approximate the function over that interval.

It was found empirically that the positron-proton scattering basis functions provide a better wave function approximation near the interaction region on the y-axis than Hermite splines alone. These basis functions are given in Appendix C and denoted by $F_{rs_y}(y)$.

When these basis functions are implemented along with the quintic splines then the two-dimensional radial wave function approximation is given by

$$\psi_k(x,y) = \begin{cases} \sum_{rs_y=0}^{N_{k_y}N_f-1} \sum_{rs_x=0}^{l_{y,\max}} A_{rs_y,rs_x} F_{rs_y}(y)\phi_{rs_x}(x) & y \le y_t \\ \sum_{rs_y=0}^{N_{k_y}N_f-1} \sum_{rs_x=0}^{N_{k_x}N_f-1} A_{rs_y,rs_x} \phi_{rs_y}(y)\phi_{rs_x}(x) & otherwise \end{cases} \qquad \text{Eq. 57}$$

where y_t is the first collocation point after the second knot.

Note that the polynomial order of $F_{rs_y}(y)$ is related to the number of DVR basis functions via the angular momentum number $l_{y,max}$. Depending on this number, the number of collocation points between the first and second knots may be different than that for quintic splines in order for the Gauss quadrature integration to be valid for these basis functions on this interval.

For notation, in the next sections whenever the radial expansion is denoted, it is given as

$$\psi_k(x,y) = \sum_{rs_y=0}^{N_{k_y}N_f-1} \sum_{rs_x=0}^{N_{k_x}N_f-1} A_{k,rs_y,rs_x} \phi_{rs_y}(y) \phi_{rs_x}(x) \qquad \text{Eq. 58}$$

with the understanding that the over the first y interval, the first y basis functions are $F_{rs_y}(y)$. Only when the $F_{rs_y}(y)$ basis functions are specifically described will they be denoted properly (i.e. when the boundary conditions are described).

Appendix C also describes how to discretize a linear differential equation involving the wave function by evaluating at the selected collocation points. The result is a linear set of algebraic equations that are solved yielding the spline scaling coefficients.

2.4 Numerical Schrodinger Equation

Appendix D describes the mathematics for the discretization of the Schrodinger equation using the mass-scaled Jacobi vectors given in channel 1, implementing the DVR basis functions and implementing the radial splines. Appendix D describes both the two-body case and the three-body case so that the reader can see the analogy between the cases. Only the three-body results are discussed in this section.

Substituting the DVR expanded wave function

$$\tilde{\Psi}(x,y,\Omega) \approx \sum_{j=1}^{N}\sum_{\nu=1}^{N}\sqrt{W_j}(S_{j\nu})^{*}S_{\nu}(\Omega)\psi_j(x,y) \qquad \text{Eq. 59}$$

into the relative motion Schrodinger equation

$$-\frac{\partial^2\tilde{\Psi}}{\partial x^2}-\frac{\partial^2\tilde{\Psi}}{\partial y^2}+\frac{\hat{l}_x^2\tilde{\Psi}}{x^2}+\frac{\hat{l}_y^2\tilde{\Psi}}{y^2}-E\tilde{\Psi}+\frac{q}{x}\tilde{\Psi}+\frac{q_2}{x_2}\tilde{\Psi}+\frac{q_3}{x_3}\tilde{\Psi}=0 \qquad \text{Eq. 60}$$

and evaluating a DVR angular grid point, denoted with index k, angle Ω_k, we get the following differential equation for the radial wave function

$$0=\sum_{j=1}^{N}\left[\left(-\frac{\partial^2}{\partial x^2}-\frac{\partial^2}{\partial y^2}+\left(\frac{q}{x}+\frac{q_2}{x_2\big|_{\Omega_k}}+\frac{q_3}{x_3\big|_{\Omega_k}}-E\right)\right)\delta_{k,j}+\frac{Sl_xS_{k,j}}{x^2}+\frac{Sl_yS_{k,j}}{y^2}\right]\psi_j(x,y) \qquad \text{Eq. 61}$$

where

$$Sl_xS_{k,j}=\sqrt{W_kW_j}\sum_{\nu=1}^{N}\sum_{\nu'=1}C_{\nu\nu'}(l'_x(l'_x+1))Y_{k\nu'}(S_{j\nu})^{*} \qquad \text{Eq. 62}$$

$$Sl_yS_{k,j}=\sqrt{W_kW_j}\sum_{\nu=1}^{N}\sum_{\nu'=1}C_{\nu\nu'}(l'_y(l'_y+1))Y_{k\nu'}(S_{j\nu})^{*} \qquad \text{Eq. 63}$$

$x_\beta\big|_{\Omega_k}$ is the transformation of the x β-Jacobi coordinate to the x α-Jacobi coordinates using the coordinate transformation for the lengths as described previously with z_α being the cosine of the angle between the β-Jacobi

coordinates defined by angles Ω_k. In this description α = 1 and β = 2 and 3.

Notice that the potential has been diagonalized. Only the $Sl_xS_{k,j}$ and $Sl_yS_{k,j}$ terms are off diagonal and most of these terms are zero due to the properties of the DVR (the Gram-Schmidt orthogonalized bipolar spherical harmonics).

Since there are N DVR indices, k = 1 to N, a set of N coupled differential equations is obtained for the set of N radial coefficients, $\psi_j(x,y)$.

Substituting the radial spline expansion into this set of differential equations yields the following set of coupled linear differential equations for the unknown coefficients, A_{j,rs_y,rs_x}

$$0 = \sum_{j=1}^{N} \sum_{rs_y=0}^{N_f N_{ky}-1} \sum_{rs_x=0}^{N_f N_{kx}-1} A_{j,rs_y,rs_x} \left\{ \left[\left(\frac{q}{x} + \frac{q_2}{x_2\big|_{\Omega_k}} + \frac{q_3}{x_3\big|_{\Omega_k}} - E \right) \delta_{k,j} + \left(\frac{Sl_x S_{k,j}}{x^2} + \frac{Sl_y S_{k,j}}{y^2} \right) \right] \phi_{rs_x}(x) \phi_{rs_y}(y) - \left(\phi_{rs_y}(y) \frac{\partial^2 \phi_{rs_x}(x)}{\partial x^2} + \phi_{rs_x}(x) \frac{\partial^2 \phi_{rs_y}(y)}{\partial y^2} \right) \delta_{k,j} \right\} \qquad \text{Eq. 64}$$

There are $N*(N_{kx}*N_f)*(N_{ky}*N_f)$ unknown coefficients if only quintic splines are implemented. Otherwise the number of coefficients is given by $N*[(N_{kx}*N_f)*((N_{ky}-$

1)*N_f)+N'_f)], where N'_f is the number of positron-proton scattering basis functions implemented between the first and second y-axis knots.

Using the spline solution technique described in Appendix C to obtain an algebraic equation for the coefficients, each equation is evaluated at all the collocation points. There are N DVR angles, (N_{kx}-1)*N_f collocation points along the x-axis and (N_{ky}-1)*N_f collocation points along the y-axis, giving a total of N*(N_{kx}-1)*N_f*(N_{ky}-1)*N_f equations. Boundary conditions supply the remaining equations to provide a unique solution for the coefficients.

As described in Appendix B, since the mass of the proton is much greater than that of the positron or electron, the x and y Jacobi axes have their origins nearly aligned. If the axes collocation points are chosen so that the some collocation points are the same for each axis, then there are cases that correspond with the electron coinciding with the positron causing numerical instability due to the potential energy between the two-particles.

The DVR y-axis azimuthal grid points are shifted so that the y-axis is not parallel to the x-axis. This mitigates the interference between the two-particles.

2.5 Asymptotic Boundary Conditions

Appendix D also defines the boundary conditions that describe the physics of the elastic-scattering process. When the scattered particle is far away from the scattering center so that the center's influence on the particle is negligible, the scattered particle is a free particle. This region is called the asymptotic region.

In the asymptotic, region the scattered particle wave function is the sum of an incoming plane wave and an outgoing spherical scattered wave with an angular dependent amplitude factor[43]. The hydrogen wave function is unchanged. Thus the three particle asymptotic wave function is

$$\Psi(\bar{x},\bar{y}) = A\phi(\bar{x})\left(e^{i\bar{k}\bullet\bar{y}} + \frac{e^{iky}}{y}f(\theta)\right) \qquad \text{Eq. 65}$$

where A is the normalization constant, $\bar{k}$ is the incoming particle momentum vector, $\bar{y}$ is the outgoing vector direction, $f(\theta)$ is the scattering amplitude factor and is the shift in the outgoing wave function amplitude and θ is

the angle between the incoming direction vector and the Jacobi y-axis vector. $\phi(\bar{x})$ is the bound particle hydrogen wave function which for convenience is denoted as $\phi(\bar{x}) = \phi^h(\bar{x})/x$.

For convenience let $\Psi(\bar{x},\bar{y}) = \tilde{\Psi}(\bar{x},\bar{y})/xy$, and the asymptotic wave function is written as

$$\tilde{\Psi}(\bar{x},\bar{y}) = A\left(y\phi^h(\bar{x})e^{i\bar{k}\bullet\bar{y}} + \phi^h(\bar{x})e^{iky}f(\theta)\right) \qquad \text{Eq. 66}$$

where

$$\phi^h(\bar{x}) = \phi^h(x)\,Y_{lm}(\theta_x,\phi_x) \qquad \text{Eq. 67}$$

and $\phi^h(x)$ is the product of x and the hydrogen radial wave function, $R_{nl}(x)$.

The scattering amplitude is found by matching the outgoing wave above and the expanded interior wave function at the asymptotic distance at a DVR angle. The following technique is implemented to obtain the boundary conditions as well as the scattering amplitude.

By evaluating $\tilde{\Psi}(\bar{x},\bar{y})$ at the j^{th} DVR grid angle and at two adjacent asymptotic y collocation points, y and y', $f(\theta)$ is eliminated yielding the equality

$$\psi_j(x,y) - e^{ik(y-y')}\psi_j(x,y') = A\phi^h(\bar{x})\sqrt{W_j}\,(ye^{ikycos(\theta_{kj})} - y'e^{iky'cos(\theta_{kj})-ik(y'-y)}) \qquad \text{Eq. 68}$$

where θ_{kj} represents the angle between the incoming direction vector and the Jacobi y-axis vector corresponding to the j grid angle. The incoming wave vector $\bar{k} = k\hat{k}$ has orientations given by the angles on the y-axis angular grid (θ_y, ϕ_y).

The goal of this thesis is to find an approximating wave function that allows the derivation of the amplitude function to determine the scattering cross section. Since an approximated wave function is being implemented using a finite number of partial angular momenta an approximated boundary condition for that wave function must also be implemented to obtain a reasonable match at the asymptotic boundary.

The expanded form of $e^{i\bar{k}\bullet\bar{y}} = e^{ikycos(\theta_{ky})}$ using angular basis functions is given by

$$e^{ikycos(\theta_{ky})} = \sum_{l_y} e^{il_y/2}(2l_y+1)\, j_{l_y}(kr) P_{l_y}(\cos(\theta_{ky})) \qquad \text{Eq. 69}$$

where θ_{ky} is the angle between the incoming vector k and the outgoing vector y.

The expanded asymptotic wave function is given by

$$\tilde{\Psi}(\bar{x},\bar{y}) = A\phi^h(\bar{x}) y \sum_{l_y} e^{il_y/2}(2l_y+1)\, j_{l_y}(kr) P_{l_y}(\cos(\theta_{ky})) + A\phi^h(\bar{x}) e^{iky} f(\theta_{ky}) \qquad \text{Eq. 70}$$

The amplitude function, $f(\theta_{ky})$, is also expanded

$$\mathrm{f}(\theta_{ky}) = \frac{1}{2\mathrm{ik}} \sum_{l_y} (2\mathrm{l_y} + 1)(s_{l_y} - 1) P_{l_y}(\cos(\theta_{ky})) \qquad \text{Eq. 71}$$

where s_{ly} represents the l^{th} diagonal element of the scattering or S operator. The actual value of s_{ly} is not computed nor required for asymptotic matching.

In each of these expansions the sum over l_y goes from zero to infinity. If this sum is truncated then these expansion equations become approximations. In the approximated asymptotic wave function the sum over l_y goes from 0 to the maximum l_y given in the DVR quartet of quantum numbers (L, M, l_x, l_y) used for the wave function approximation. That is, the sum goes from 0 to $l_{y,max}$.

Using this notation the asymptotic wave function is represented by

$$\tilde{\Psi}_{\mathrm{asym}}(\bar{\mathrm{x}}, \bar{\mathrm{y}}) \approx A\phi^h(\bar{\mathrm{x}}) y \sum_{l_y} \mathrm{e}^{\mathrm{i}l_y \pi/2} (2\mathrm{l_y} + 1)\, j_{\mathrm{l_y}}(ky) P_{l_y}(\cos(\theta_{ky})) + A\phi^h(\bar{\mathrm{x}}) \mathrm{e}^{\mathrm{iky}} \frac{1}{2\mathrm{ik}} \sum_{l_y} (2\mathrm{l_y} + 1)(s_{l_y} - 1) P_{l_y}(\cos(\theta_{ky})) \qquad \text{Eq. 72}$$

which is rewritten as

$$\tilde{\Psi}_{\mathrm{asym}}(\bar{\mathrm{x}}, \bar{\mathrm{y}}) \approx A\phi^h(\bar{\mathrm{x}}) S_{yk}(y) + A\phi^h(\bar{\mathrm{x}}) \mathrm{e}^{\mathrm{iky}} G_{yk} \qquad \text{Eq. 73}$$

where

$$S_{yk}(y) = \sum_{l_y} i^{l_y} y j_{\mathrm{l_y}}(ky)(2\mathrm{l_y} + 1) P_{l_y}(\cos(\theta_{ky})) \qquad \text{Eq. 74}$$

$$f(\theta_{ky}) \approx G_{yk} = \frac{1}{2\mathrm{ik}} \sum_{l_y} (2\mathrm{l_y} + 1) P_{l_y}(\cos(\theta_{ky}))(s_{l_y} - 1) \qquad \text{Eq. 75}$$

Evaluation at the DVR angle j for the outgoing y-axis finds

$$\psi_{\mathrm{j}}(\mathrm{x}, \mathrm{y}) \approx A\phi^{h}(\bar{\mathrm{x}}_{\mathrm{j}})(S_{jk}(y) + \mathrm{e}^{\mathrm{iky}} G_{jk}) \qquad \text{Eq. 76}$$

where the hydrogen wave function is evaluated only at the two appropriate x-axis angles out of the four angles the index j represents.

$$S_{jk}(y) = \sum_{l_y} i^{l_y} y j_{\mathrm{l_y}}(ky)(2\mathrm{l_y} + 1) P_{l_y}(\cos(\theta_{kj})) \qquad \text{Eq. 77}$$

$$f(\theta_{kj}) \approx G_{jk} = \frac{1}{2\mathrm{ik}} \sum_{l_y} (2\mathrm{l_y} + 1) P_{l_y}(\cos(\theta_{kj}))(s_{l_y} - 1) \qquad \text{Eq. 78}$$

Using the approximated asymptotic wave function, evaluating at two different scattering distances y and y' in the asymptotic region, and eliminating G_{jk} yields the following asymptotic boundary condition

$$\psi_{\mathrm{j}}(x, y) - \mathrm{e}^{\mathrm{ik(y-y')}} \psi_{\mathrm{j}}(x, y') = A\sqrt{\mathrm{W_j}}\phi^{h}(\bar{\mathrm{x}}_{\mathrm{j}})(S_{jk}(y) - \mathrm{e}^{\mathrm{ik(y-y')}} S_{jk}(y')) \qquad \text{Eq. 79}$$

Using the derivative at two different scattering distances yields boundary conditions for the derivatives

$$\psi'_{\mathrm{j}}(x, y) - \mathrm{e}^{\mathrm{ik(y-y')}} \psi'_{\mathrm{j}}(x, y') = A\sqrt{\mathrm{W_j}}\phi^{h}(\bar{\mathrm{x}}_{\mathrm{j}})(S'_{jk}(y) - \mathrm{e}^{\mathrm{ik(y-y')}} S'_{jk}(y')) \qquad \text{Eq. 80}$$

Continuing, the second derivative yields another boundary condition

$$\psi''_{\mathrm{j}}(x,y) - \mathrm{e}^{\mathrm{ik(y-y')}}\psi''_{\mathrm{j}}(x,y') = A\sqrt{\mathrm{W_j}}\phi^h(\overline{\mathrm{x}}_{\mathrm{j}})S''_{jk}(y) - \mathrm{e}^{\mathrm{ik(y-y')}}S''_{jk}(y') \qquad \text{Eq. 81}$$

with

$$S'_{j,k}(y) \approx \sum_{l_y} i^{l_y}(2\mathrm{l_y}+1)P_{l_y}(\cos(\theta_{kj}))(j_{\mathrm{l_y}}(ky) + kyj'_{\mathrm{l_y}}(ky)) \qquad \text{Eq. 82}$$

and

$$S''_{j,k}(y) \approx \sum_{l_y} i^{l_y}(2\mathrm{l_y}+1)P_{l_y}(\cos(\theta_{kj}))(2kj'_{\mathrm{l_y}}(ky) + k^2 yj''_{\mathrm{l_y}}(ky)) \qquad \text{Eq. 83}$$

$S_{j,k}$ and its derivatives are a function only of the y-axis components, (θ_y, ϕ_y), of the 4 angles the index j represents.

Note that the amplitude function, evaluated at the j^{th} DVR grid angle, is written as

$$\mathrm{f}(\theta_{ky})\Big|_{kj} = \frac{\mathrm{e}^{-\mathrm{iky}}\psi_{\mathrm{j}}(x,y)}{AY_0^0(\hat{x}_j)\phi^h(\mathrm{x})\sqrt{\mathrm{W_j}}} - \mathrm{e}^{-\mathrm{iky}}S_{jk}(y) \qquad \text{Eq. 84}$$

where S_{jk} is a function only of the y-axis angular components that j represents, and the hydrogen angular component is only a function of the x-axis angular components that j represents.

The amplitude function represents the full scattering amplitude matrix $f(k_{j1}, y_{j2})$ where j_1 and j_2 each run over all the possible grid points indexed from 1 to N. That is, the matrix represents all incoming directions as well as all outgoing directions.

2.6 Near Interaction Region Boundary Conditions

In addition to the asymptotic region boundary conditions, boundary conditions are required in the interaction region. At x = 0 or y = 0 the boundary condition

$$\psi_j(0,y)=0$$
$$\psi_j(x,0)=0 \qquad \text{Eq. 85}$$

is implemented. This maintains that for the limit that x goes to zero and/or y goes to zero the full wave function, $\Psi(\bar{x},\bar{y})=\tilde{\Psi}(x,y,\Omega_x,\Omega_y)/(xy)$, remains finite.

Since this thesis focuses on elastic-scattering it is expected that the wave function for the scattered particle near the interaction region at locations that do not interfere with the hydrogen particle's electron should have a similar functional form of the previously derived wave function for a particle scattering off a proton. That is, the quintic spline y basis functions are replaced by the positron-proton scattering basis functions.

This quintic spline replacement is done since the proton-proton scattering basis functions are of higher order than quintic splines as $l_{y,max}$ increases.

The low order positron-proton scattering basis functions are given by

$$F_{l_y}(y) = \sqrt{2\pi} e^{-iky} C_{l_y} (ky)^{l_y+1} [1+...] \qquad \text{Eq. 86}$$

with

$$C_l^2 = \left[\frac{2^l}{(2l+1)!} \right]^2 (l^2+1/k^2)((l-1)^2+1/k^2)...(1+1/k^2) \frac{2\pi/k}{e^{2\pi/k}-1}$$

$$C_1^2 = \left[\frac{2}{(3)!} \right]^2 (1+1/k^2) \frac{2\pi/k}{e^{2\pi/k}-1} \qquad \text{Eq. 87}$$

$$C_0^2 = \frac{2\pi/k}{e^{2\pi/k}-1}$$

However, these constants are not used since only the form of the basis functions is required in the spline expansion

$$F_{l_y}(y) = e^{-iky} (ky)^{l_y+1} \qquad \text{Eq. 88}$$

Using these basis functions for small y allows a better fit of the splines to the scattering wave function. That is, the Gauss quadrature integration approximation is valid in this region. Of course, if more collocation points are required, due to the order of the basis functions, they must also be added between the first two knots.

The cumulative probability of the ground state hydrogen wave function near zero is given in Figure 5.

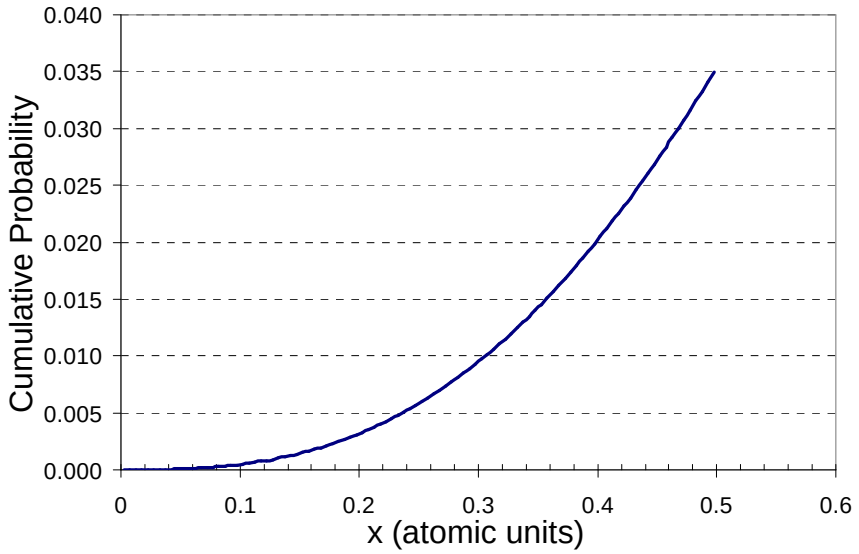

Figure 5. Cumulative Probability Of The Ground State Hydrogen Electron At Radial Position x.

As long as the probability of the hydrogen electron interaction with the incoming particle is small, then replacing the quintic y basis functions by the positron-proton scattering basis functions should yield a good representation of the total wave function.

Since the wave function is approximated by

$$\psi_k(x,y) = \begin{cases} \sum_{rs_y=0}^{N_{k_y}N_f-1} \sum_{rs_x=0}^{l_{y,\max}} A_{rs_y,rs_x} F_{rs_y}(y)\phi_{rs_x}(x) & y \le y_t \\ \sum_{rs_y=0}^{N_{k_y}N_f-1} \sum_{rs_x=0}^{N_{k_x}N_f-1} A_{rs_y,rs_x} \phi_{rs_y}(y)\phi_{rs_x}(x) & \textit{otherwise} \end{cases} \qquad \text{Eq. 89}$$

where y_t is the first collocation point after the second knot and is selected in the region where the cumulative probability of the hydrogen electron at its radial

position is small, the boundary conditions for the wave function and its first and second derivative must be

$$\sum_{\mathrm{rs_x}=0}^{\mathrm{N_f N_{kx}}-1}\sum_{\mathrm{rs_y}=l_{y,\max}+1}^{N_f N_{ky}-1+(l_{y,\max}+1)-N_f}\mathrm{A_{k,rs_y,rs_x}}\phi_{\mathrm{rs_y}}(\mathrm{y_t})\phi_{\mathrm{rs_x}}(\mathrm{x})-\sum_{\mathrm{rs_x}=0}^{N_f N_{kx}-1}\sum_{rs_y=0}^{l_{y,\max}}A_{k,rs_y,rs_x}F_{rs_y}(y_{\mathrm{t}})\phi_{rs_x}(x)=0 \quad \text{Eq. 90}$$

$$\sum_{\mathrm{rs_x}=0}^{\mathrm{N_f N_{kx}}-1}\sum_{\mathrm{rs_y}=l_{y,\max}+1}^{N_f N_{ky}-1+(l_{y,\max}+1)-N_f}\mathrm{A_{k,rs_y,rs_x}}\phi'_{\mathrm{rs_y}}(\mathrm{y_t})\phi_{\mathrm{rs_x}}(\mathrm{x})-\sum_{\mathrm{rs_x}=0}^{N_f N_{kx}-1}\sum_{rs_y=0}^{l_{y,\max}}A_{k,rs_y,rs_x}F'_{rs_y}(y_{\mathrm{t}})\phi_{rs_x}(x)=0 \quad \text{Eq. 91}$$

$$\sum_{\mathrm{rs_x}=0}^{\mathrm{N_f N_{kx}}-1}\sum_{\mathrm{rs_y}=l_{y,\max}+1}^{N_f N_{ky}-1+(l_{y,\max}+1)-N_f}\mathrm{A_{k,rs_y,rs_x}}\phi''_{\mathrm{rs_y}}(\mathrm{y_t})\phi_{\mathrm{rs_x}}(\mathrm{x})-\sum_{\mathrm{rs_x}=0}^{N_f N_{kx}-1}\sum_{rs_y=0}^{l_{y,\max}}A_{k,rs_y,rs_x}F''_{rs_y}(y_{\mathrm{t}})\phi_{rs_x}(x)=0 \quad \text{Eq. 92}$$

In other words, the wave function using the positron-proton scattering basis functions must yield the same value at y_t as the wave function using the quintic spline basis functions.

Note that

$$F'_{l_y}(y)=F_{l_y}(ky)[(l+1)/y-ik] \quad \text{Eq. 93}$$

$$F''_{l_y}(y)=F_{l_y}(ky)[l(l+1)-k^2y^2-i2k(l+1)y]/y^2 \quad \text{Eq. 94}$$

2.7 Scattering Cross Section

The scattering cross section is obtained from the amplitude function by assuming that the asymptotic particle is a free particle and has a free particle wave function modified by the amplitude function.

For a given input direction, the amplitude function for the outgoing j^{th} DVR grid angle is related to the wave function by

$$\phi^h(\mathrm{x})\mathrm{f}(\theta_{ky})\Big|_{k,j} = \frac{\mathrm{e}^{-\mathrm{iky}}\psi_{\mathrm{j}}(x,y)}{AY_0^0(\hat{x}_j)\sqrt{\mathrm{W_j}}} - \phi^h(\mathrm{x})\mathrm{e}^{-\mathrm{iky}}S_{jk}(y) \qquad \text{Eq. 95}$$

Since only the y-axis is required to compute the scattering cross section, the radial hydrogen wave function is projected out of this equation.

$$\mathrm{f}^{\mathrm{p}}(\theta_{kj}) = <\phi^h(\mathrm{x})\,|\,\phi^h(\mathrm{x})\mathrm{f}(\theta_{ky})\Big|_{kj}>_x = \qquad \text{Eq. 96}$$

$$<\phi^h(\mathrm{x})\,|\,\frac{\mathrm{e}^{-\mathrm{iky}}\psi_{\mathrm{j}}(x,y)}{AY_0^0(\hat{x}_j)\sqrt{\mathrm{W_j}}}>_x - <\phi^h(\mathrm{x})\,|\,\phi^h(\mathrm{x})\mathrm{e}^{-\mathrm{iky}}S_{jk}(y)>_x$$

where

$$<f\,|\,g>_x = \sum_{i_x}^{N_{kx}N_f-1} f^*(x_{i_x})g(x_{i_x})x_{i_x}^2 w_x \qquad \text{Eq. 97}$$

is the Gauss quadrature integration over the x coordinates.

The resulting amplitude function, $\mathrm{f}^{\mathrm{p}}(\theta_{kj})$, no longer has any dependency on x.

Figure 6 illustrates the general coordinate diagram for the incoming particle k vector and the outgoing j^{th} DVR grid angle axis configuration.

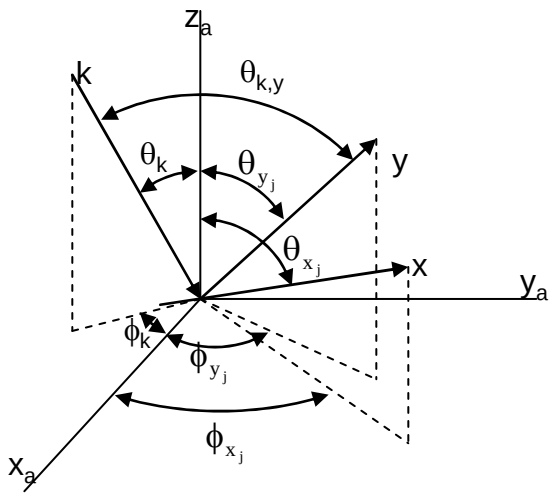

Figure 6. Coordinate Diagram For The Incoming Vector And The j^{th} DVR Grid Angle.

The angle between the incoming vector and the outgoing Jacobi y-axis is found by

$$\cos(\theta_{ky}) = \cos(\theta_{yj})\cos(\theta_k)+\sin(\theta_{yj})\sin(\theta_k)\cos(\phi_{yj}-\phi_k) \quad \text{Eq. 98}$$

The cross section is given by

$$\sigma_k = \int \frac{d\sigma}{d\Omega} d\Omega = \int | f^p(\theta_{kj}) |^2 \sin(\theta_{kj}) d\theta_{kj} d\phi_{kj} \quad \text{Eq. 99}$$

Since the potential is spherically symmetric the selection of the incoming direction is arbitrary. Also, the integration over the arbitrary azimuthal angle, ϕ_{kj}, is trivial since the amplitude function is independent of this angle.

To make the cross section calculations more convenient, the coordinate system is rotated so that the k vector is along the z-axis, $\theta_k = 0$. The angle between the

k and y axes in the original coordinates, θ_{ky}, is exactly the same as the polar angle of the j^{th} y-axis in the rotated coordinate system θ_{yj} so that and $\cos(\theta_{ky}) = \cos(\theta_{yj})$. The y-axis azimuthal angle, ϕ_{yj} remains arbitrary with respect to the amplitude function. The amplitude function remains unchanged: $f^p(\theta_{ky}) = f^p(\theta_{yj})$.

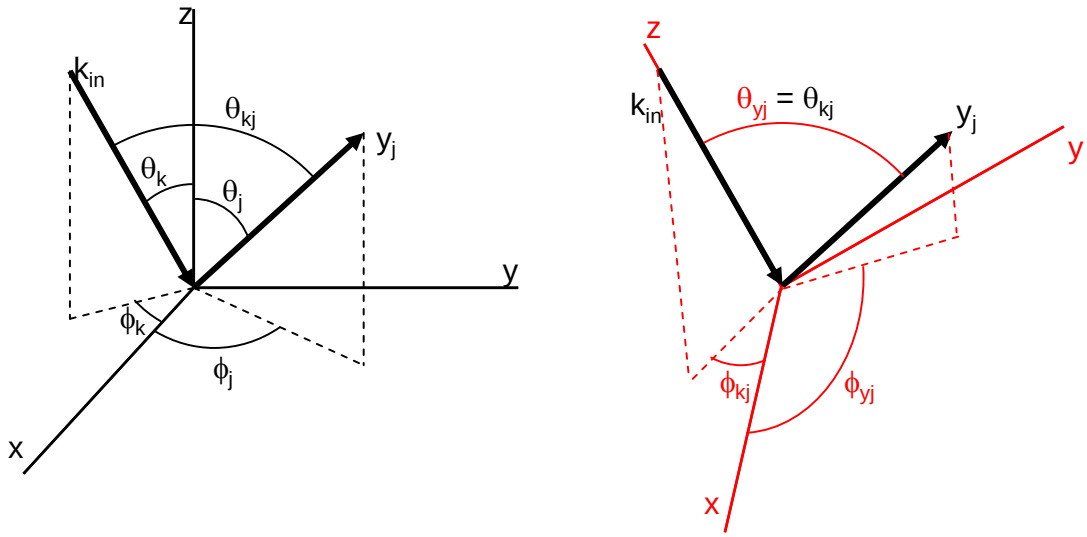

Figure 7. Rotated Coordinate System.

Thus the total cross section is now given by

$$\begin{aligned}\sigma_k &= \int |f^p(\theta_{y_j})|^2 \sin(\theta_{y_j}) d\theta_{y_j} d\phi_{y_j} \\ &= \int |f^p(\theta_{y_j})|^2 d\Omega_{y_j} \\ &= \frac{1}{4\pi}\int |f^p(\theta_{y_j})|^2 d\Omega_{y_j} d\Omega_{x_j} \\ &= \frac{1}{4\pi}\int |f^p(\theta_{y_j})|^2 d\Omega_j \\ &= \frac{1}{4\pi}\sum_j |f^p(\theta_{y_j})|^2 W_j\end{aligned} \qquad \text{Eq. 100}$$

using the DVR quadrature integration.

CHAPTER 3

RESULTS

The scattering cross section is computed for a positron scattering with a ground state hydrogen atom which consists of a proton and a bound electron.

The results of numerous independent scattering calculations obtained by researchers are quantified in reference 44. In particular reference 44 gives the elastic scattering cross sections for the positron-Hydrogen problem that has been obtained by the research community. Verification of the results of the DVR technique described in this paper is obtained by comparing the resulting converged cross sections to the elastic scattering results given in reference 44. The DVR grid that generates the smallest set of coupled equations is the 9x9 grid yielding 81 DVR basis functions. The incoming particle's k vector angular orientation is chosen as one of the DVR y-axis grid angles. The potential function symmetry implies that results for equal cross sections are independent of the incoming angle chosen.

3.1 Selection Of Knots And Angular Grid

For the numerical ground state radial hydrogen wave function, it has been found empirically that good convergence using quintic splines are obtained using only eight strategically placed x-axis knots with values between 0 and 20. Specifically placing the knots at 0, 0.5, 1.0, 2.5, 5.0, 8.5, 11, and the cut off point at 20 allows the quintic spline implementation to closely approximate the radial hydrogen wave function and its derivatives. Figure 8 shows a plot of the wave function and the spline fit values. R(x), R'(x), R"(x) are the ground state wave function and its first and second derivatives respectively. Rs(x), R's(x) and R"s(x) are the spline fits.

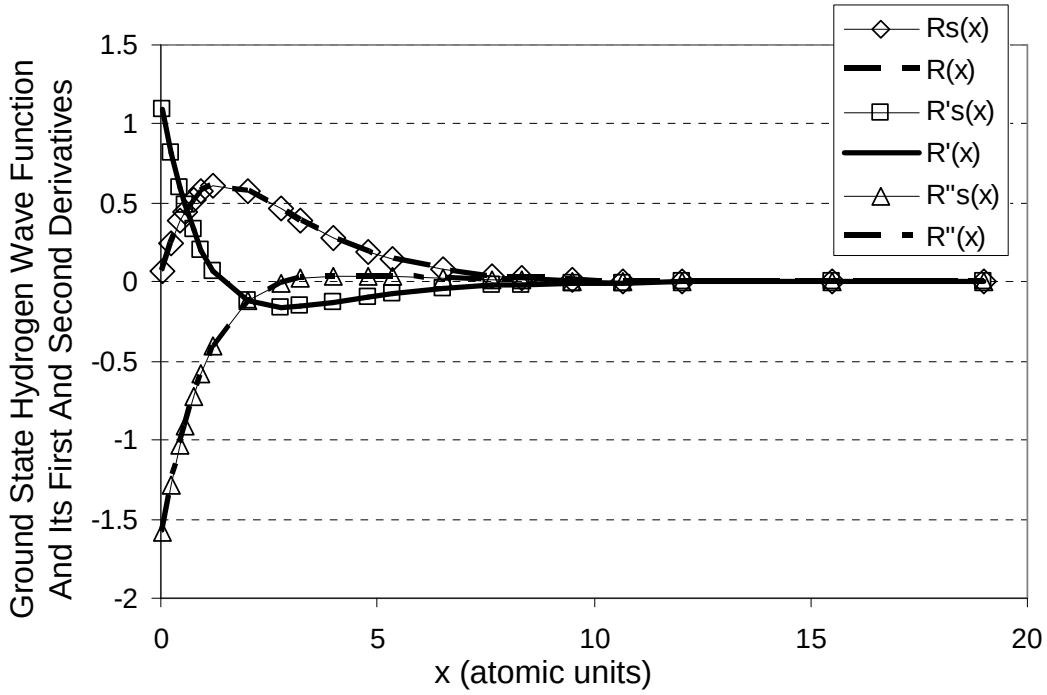

Figure 8. Ground State Hydrogen Wave Function And Its First And Second Derivatives.

The maximum error between the spline fits and the wave function is on the order of 10^{-4}.

The y-axis spatial knot locations had to be chosen with sufficient density to properly fit the asymptotic wave function as well as the wave function in the interaction region. The asymptotic wave function for elastic-scattering has a De Broglie wavelength $\lambda = 2\pi/k$. The number of knots and y-axis cut off point had to be chosen so that the asymptotic region would be obtained. The number of knots also had to be traded against the resulting matrix size and computer resources. As a

result, a sufficient cut off point was found to be at y = 80 with 35 equally spaced segments between 0 and 80.

The smallest DVR set that can be implemented to obtain a reasonable cross section result is a N = 81 set of DVR basis functions, consisting of N_x = 9 and N_y = 9. Using 8 x-knots and 36 y-knots for the spatial coordinates, this yields a matrix size of ~187,500 x 187,500 complex elements or ~375,000 x 375,000 real elements.

The next smallest DVR set of basis functions consists of N = 225 elements, consisting of N_x = 9 and N_y = 25. If this set is implemented the resultant matrix size is ~500,000 x 500,000 complex elements or 1,000,000 x 1,000,000 real elements. The next size DVR basis function set is N = 625 which results in a matrix size of 7,700,000 square.

On the University Of Texas Sun Constellation Linux Cluster Ranger parallel computer system, the N = 81 DVR generated matrix equation requires ~5,600 core hours to obtain a solution using the SCALAPAK software. Solving the N = 225 DVR generated matrix equation requires ~145,635 core hours. Due to limits on the computer resources, only the N = 81 DVR set of equations can

currently be solved to convergence. The results are shown in this section.

Other computer resources and software are currently being investigated including parallel and sparse matrix computing techniques such as TAUCS, BSCLIB-EXT, SuperLU, PARDISO, UMFPACK, Sparse Matrix SCALAPAK, and MUMPS[46]. Once these techniques have advanced to the point where they can solve problems of the size generated by this DVR technique, additional analysis can be performed yielding higher fidelity cross section results.

3.2 Results Using Y-Axis Azimuthal Shift 26.8^0

Using quintic splines only, convergence of the solution is found using the x-axis and y-axis knots described above.

Figure 9 shows the DVR results, using a y-axis shift of 26.8^0, plotted alongside that of reference 44 for k = 0.2, 0.3, 0.4, 0.5, 0.6 and 0.7.

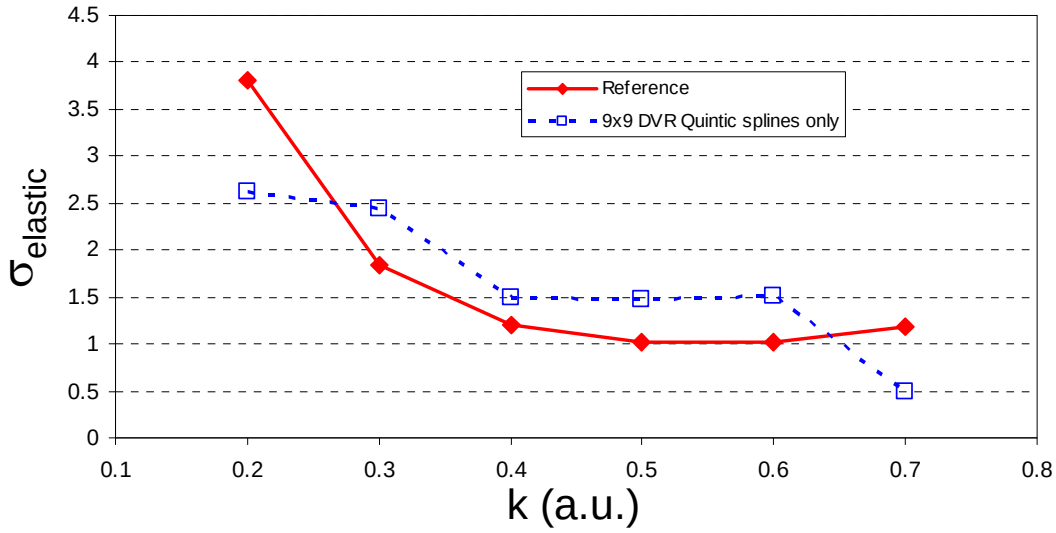

Figure 9. Elastic Cross Section Vs Incoming Momentum Using Quintic Splines Only.

In general, the results at k = 0.2 are not expected to be well converged since the De Broglie wavelength at this energy is fairly long. As the wavelength increases, the asymptotic region also increases. In this case the asymptotic region is beyond the y-axis cut off point. Implementing a longer cut off point requires additional y-axis spatial coordinates. Additional spatial coordinates increases the size of the matrix which increases the required computer resources.

On the other hand, at k = 0.7 the system is close to the bound $(e^+ + e^-)$ positronium formation which has a profound polarization effect on the scattering process. The current DVR formulization does not have the structure

for the (e^+ + e^-) virtual positronium formation, especially in the x-direction which currently uses the hydrogen wave function spline approximation and grid points. Solving for this case also requires more spatial coordinates on both the x and y axes, increasing the size of the matrix and the required computer resources.

Considering the small DVR basis size used in this calculation, the agreement is very good at the 0.3 to 0.6 energies. Figure 9 demonstrates the proof of principle of the DVR technique. As the size of the set of DVR basis increases, the y-axis angular momentum also increases and the use of the positron-proton basis becomes important.

Using quintic splines and positron-proton basis functions, convergence of the solution is recomputed using the same spatial and angular grid for the previous case, except that the first non zero y-axis knot was placed at 0.25, 0.5, and 0.8. The first collocation point after the first knot is denoted as y_{1st}. The positron-proton scattering basis functions are implemented in the region between 0 and y_{1st}. The quintic splines are implemented in the y_{1st} to the asymptotic region. The near zero matching boundary condition occurs at y_{1st}. Figure 10 shows the 9x9

DVR results plotted with that of reference 44. Again, a y-axis azimuthal shift of 26.8^0 is implemented.

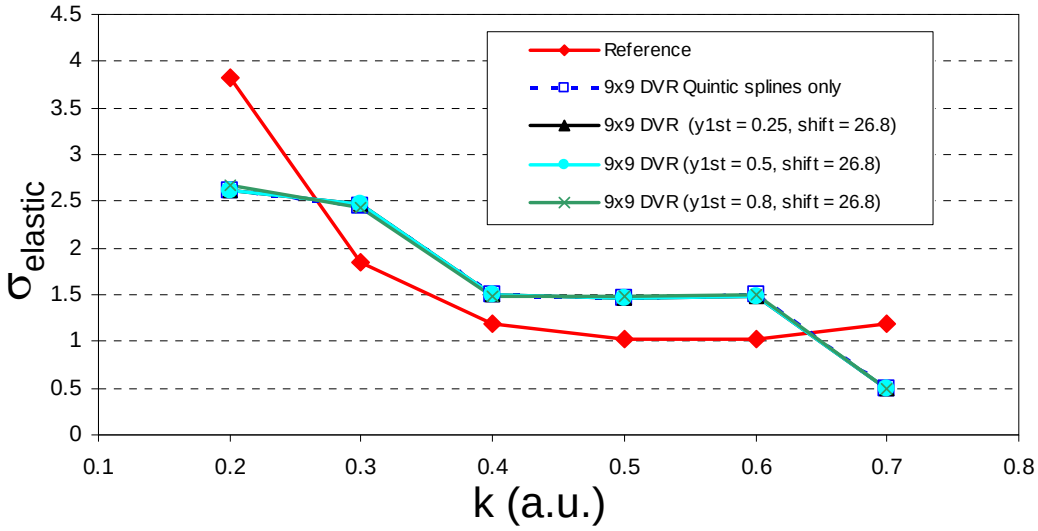

Figure 10. Elastic Cross Section Vs Incoming Momentum Using 26.8^0 y-axis Azimuthal Shift.

In the figure all the DVR data are close in value so that each curve's data point is at the same location.

The results show that for the 9x9 DVR, Quintic splines perform just as well as using mixed spatial basis functions. Table 3 lists the numerical results.

Table 3. Elastic Cross Section Vs Incoming Momentum.

k-->	0.2	0.3	0.4	0.5	0.6	0.7
Reference	3.815	1.848	1.194	1.025	1.029	1.181
Quintic Basis	2.623	2.500	1.496	1.469	1.508	0.496
Mixed Basis (y1st = 0.25)	2.607	2.464	1.507	1.464	1.488	0.493
Mixed Basis (y1st = 0.5)	2.611	2.465	1.507	1.467	1.480	0.493
Mixed Basis (y1st = 0.8)	2.668	2.435	1.485	1.479	1.508	0.498

The agreement between the techniques is very good. More DVR basis functions are required for better accuracy in the results. Table 3 demonstrates the proof of principle of the DVR technique. Table 3 also demonstrates that for the small size DVR basis, quintic splines alone produce the same results as the mixed basis. However, as the number of DVR angular basis functions increase, and thus as the maximum angular momentum quantum number increases, the positron-proton scattering basis functions contribution to the wave function increases. Using quintic splines alone degrades the wave function approximation as previously explained.

3.3 Results And Analysis Of Other Y-Axis Azimuthal Shifts

Although the accuracy of the results should increase as the density of the DVR basis function increases, it is instructional to demonstrate results using the 9x9 DVR basis using different y-axis azimuthal angular shifts. Results are shown using different shifts, namely 0^0, 10^0, 20^0, 26.8^0, and 30^0.

As the DVR density increases, these axes angular locations are automatically included in the angular grid, or angles near these angles. For example, without

shifting, the 9x9 angular grid y-axis azimuthal angular grid points are 60^0, 180^0, and 240^0. For an nx25 angular grid the y-axis azimuthal grid points are 36^0, 108^0, 180^0, 252^0 and 324^0. For an nx49 angular grid the angles are 25.7^0 to 334.28^0 in steps of 51.43^0. As the density increases, more contributions due to the increase in input and output directions yield more accuracy in the final cross section.

However, the effects of the different axis directions can be studied using the 9x9 basis and different shift angles. For example, if no shift of the angle is used to obtain cross sections, the results become numerically unstable due to the potential between the positron and the electron. The first knot used for the hydrogen wave function spline fit was at 0.5. If this same knot location is used for the y-axis spline fitting, then the two axes have identical collocation points between 0 and this knot. If there is no shifting, then there are only seven different angles between the x and y axis out of the 81 possibilities: 0^0 9 cases, 50.77^0 12 cases, 66.42^0 12 cases, 101.54^0 6 cases, 108.44^0 24 cases, 120^0 6 cases and 143.13^0 12 cases.

In the 0^0 cases, for the collocation points that are very near each other, the potential between the positron and electron is evaluated at nearly the same location, causing a spike in the values q_2/x_2 of Eq. 18. In addition, the next closest angle is 50.77^0, so that there is significantly less interaction between the two-particles. The transition between the two configurations is not as smooth as it would be if the density of angles was increased. Low angle density allows a very powerful contribution to be dominant over the very weak contributions.

Figures 11a - 11d show plots of the radial wave function for the first incoming direction (y-axis) for k = 0.3 to 0.6 respectively for the case where the shift is 0^0.

Notice that, along the line where the y-axis values are the same as the x-axis values the wave function quality degrades. This degradation also increases dramatically as the energy (k) increases.

Contrast that to Figures 12a - 12d which show plots of the radial wave function for the first incoming direction for k = 0.3 to 0.6 respectively for the case

where the shift is 26.8^0. This is the shift that was chosen to show the results that were shown previously in Figures 9 and 10 and Table 3.

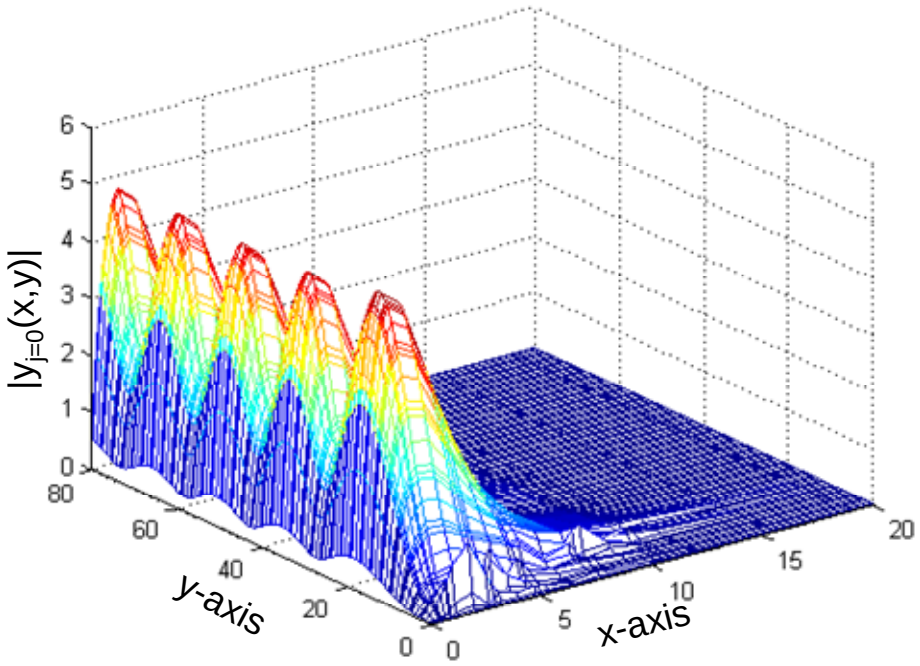

Figure 11a. Radial Wave Function (j=0) For First Y Knot = 0.5, k = 0.3 And 0^0 Y-Axis Azimuthal Shift.

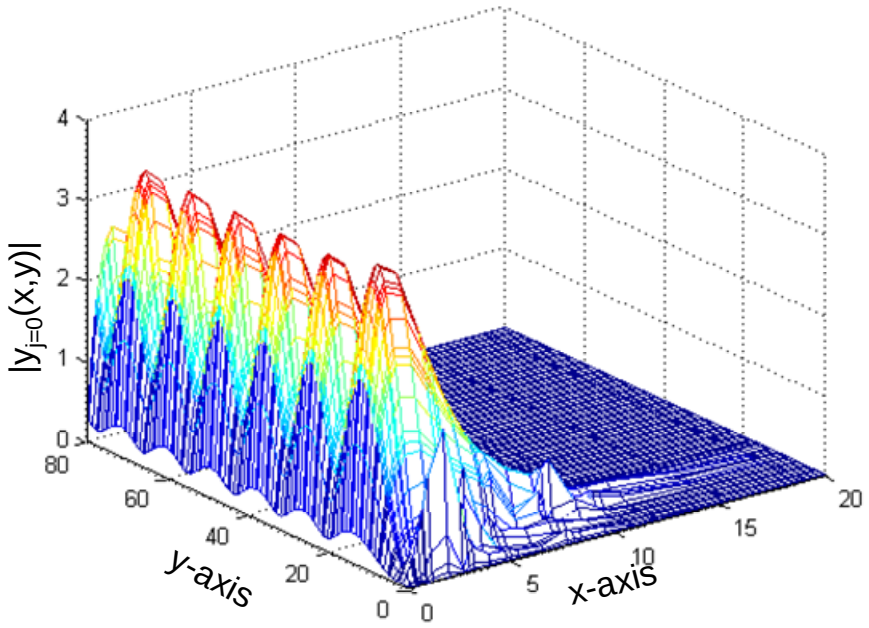

Figure 11b. Radial Wave Function (j=0) For First Y Knot = 0.5, k = 0.4 And 0^0 Y-Axis Azimuthal Shift.

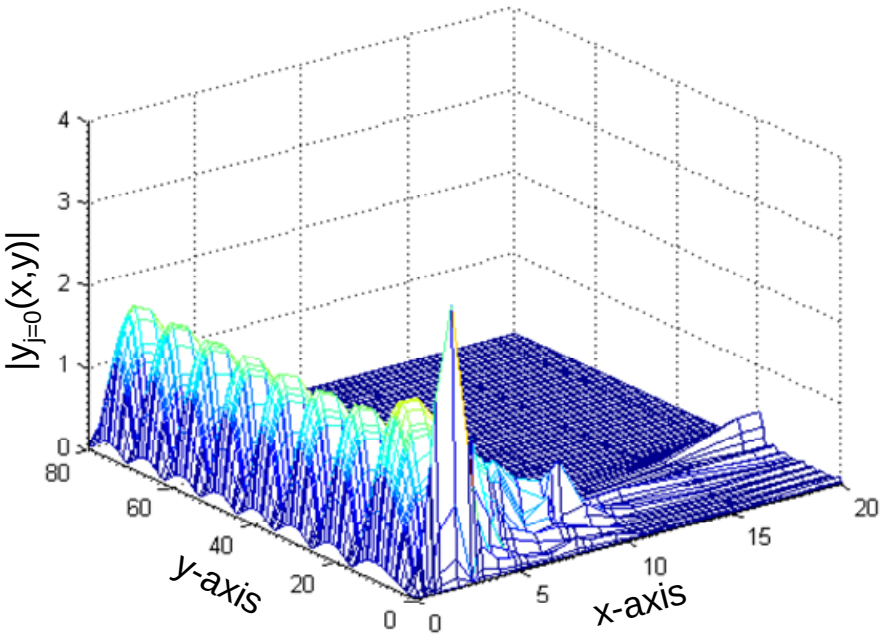

Figure 11c. Radial Wave Function (j=0) For First Y Knot = 0.5, k = 0.5 And 0^0 Y-Axis Azimuthal Shift.

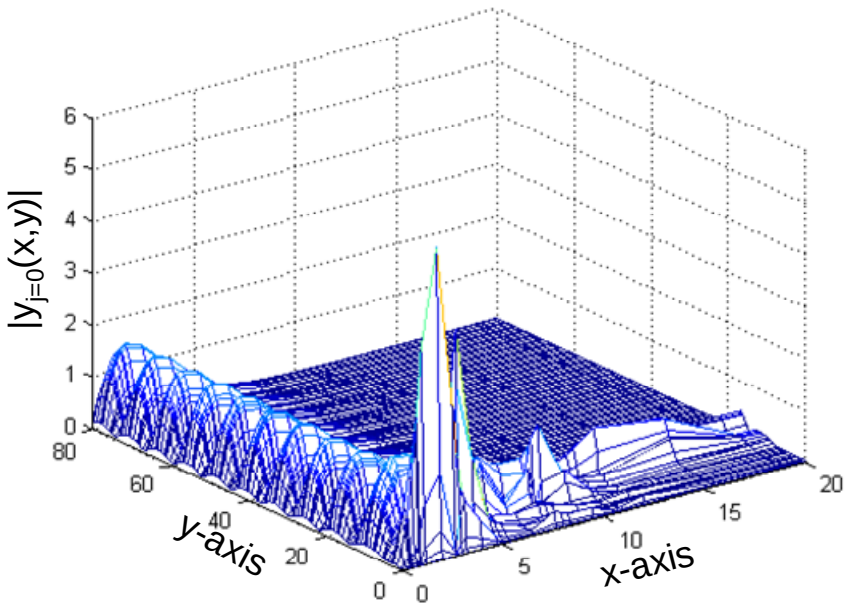

Figure 11d. Radial Wave Function (j=0) For First Y Knot = 0.5, k = 0.6 And 0^0 Y-Axis Azimuthal Shift.

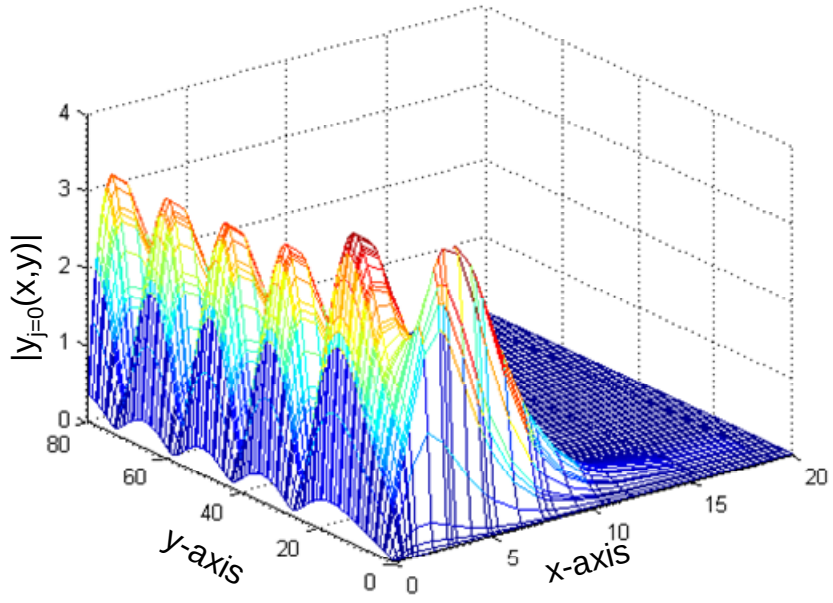

Figure 12a. Radial Wave Function (j=0) For First Y Knot = 0.5, k = 0.3 And 26.8^0 Y-Axis Azimuthal Shift.

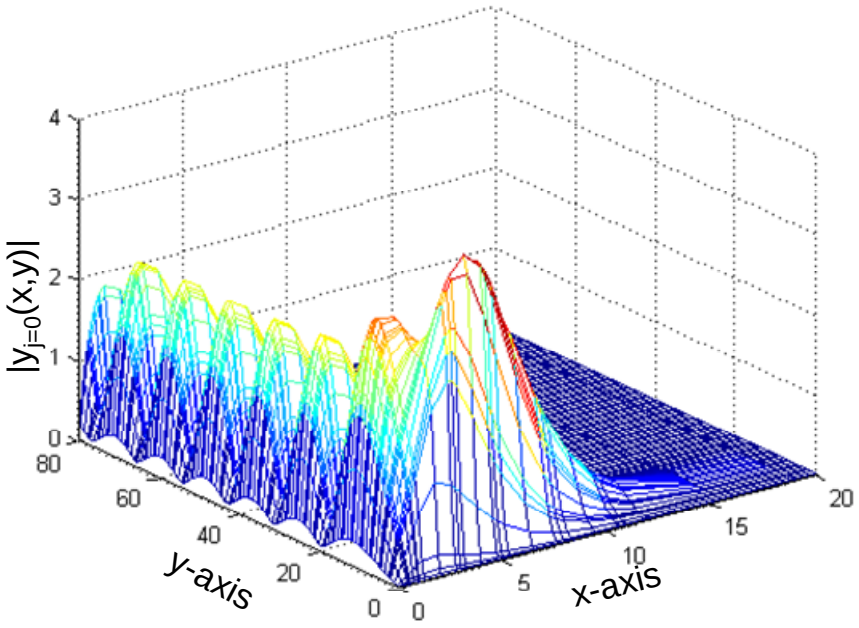

Figure 12b. Radial Wave Function (j=0) For First Y Knot = 0.5, k = 0.4 And 26.8^0 Y-Axis Azimuthal Shift.

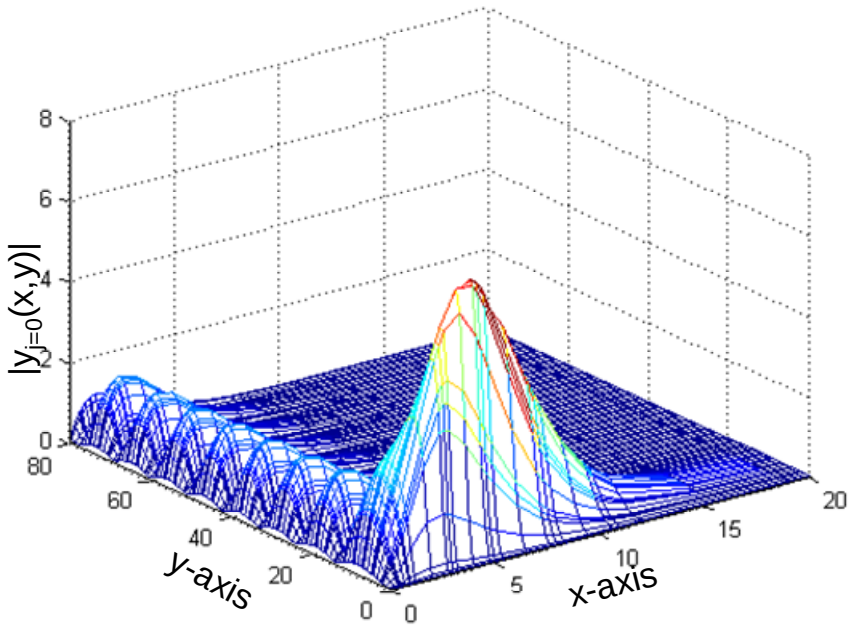

Figure 12c. Radial Wave Function (j=0) For First Y Knot = 0.5, k = 0.5 And 26.8^0 Y-Axis Azimuthal Shift.

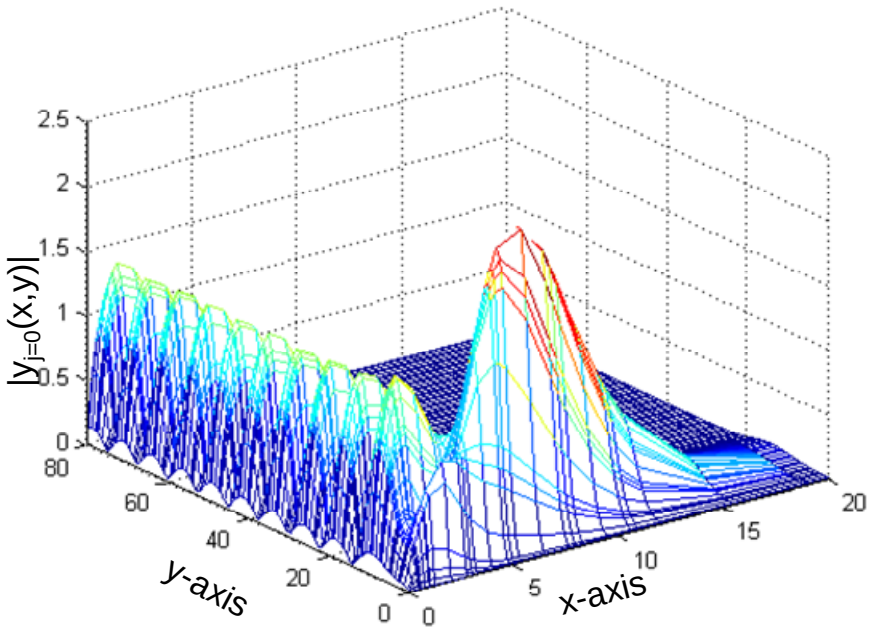

Figure 12d. Radial Wave Function (j=0) For First Y Knot = 0.5, k = 0.6 And 26.8^0 Y-Axis Azimuthal Shift.

Figures 12a and 12b show a smoother transition between the interaction region near zero than 11a and 11b where the interaction is significantly nullified by the numerical instability caused by the high potential in the Schrodinger equation.

Figures 12c and 12d also show a smoother transition, although they also show some bonding between the hydrogen electron and the positron in the form of positronium due to the higher energies. As the energy increases, more degradation results as explained previously.

Figures 13a to 13d, 14a to 14d and 15a to 15d show the radial wave function for a shift of 10^0, 20^0 and 30^0 respectively.

At the 10^0 shift the numerical instability is decreased when compared to 0^0 shift, but a smooth wave function is still not obtained. At the 20^0 shift, the wave function is smoother and the interaction region is beginning to show. However at k = 0.6 there is still some significant numerical instability.

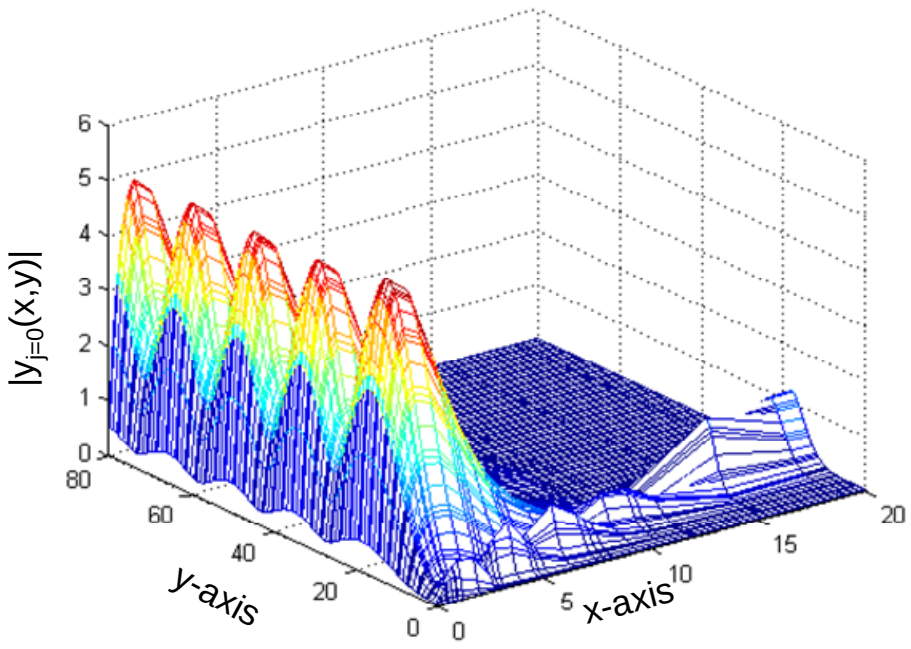

Figure 13a. Radial Wave Function (j=0) For First Y Knot = 0.5, k = 0.3 And 10^0 Y-Axis Azimuthal Shift.

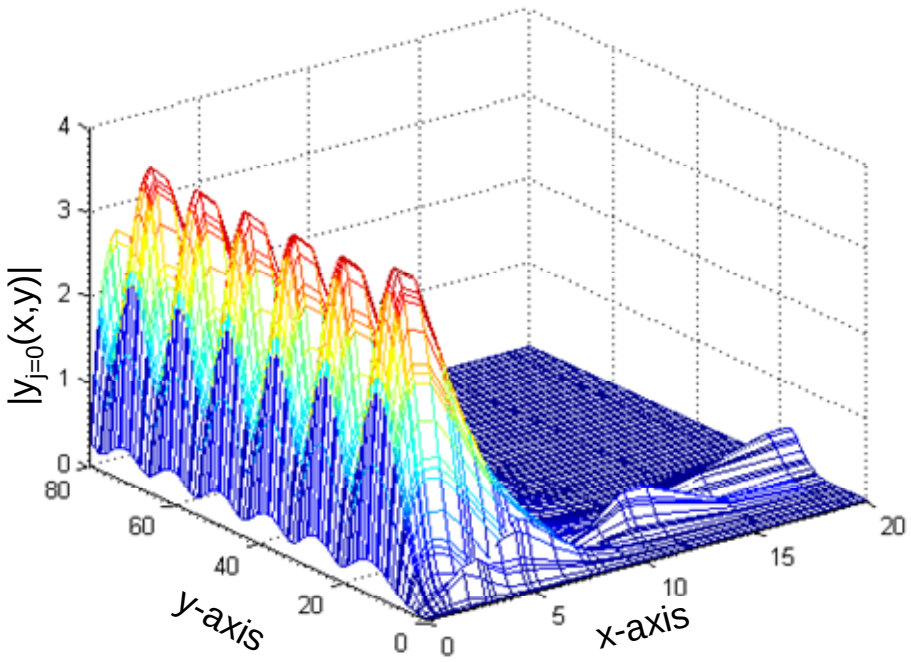

Figure 13b. Radial Wave Function (j=0) For First Y Knot = 0.5, k = 0.4 And 10^0 Y-Axis Azimuthal Shift.

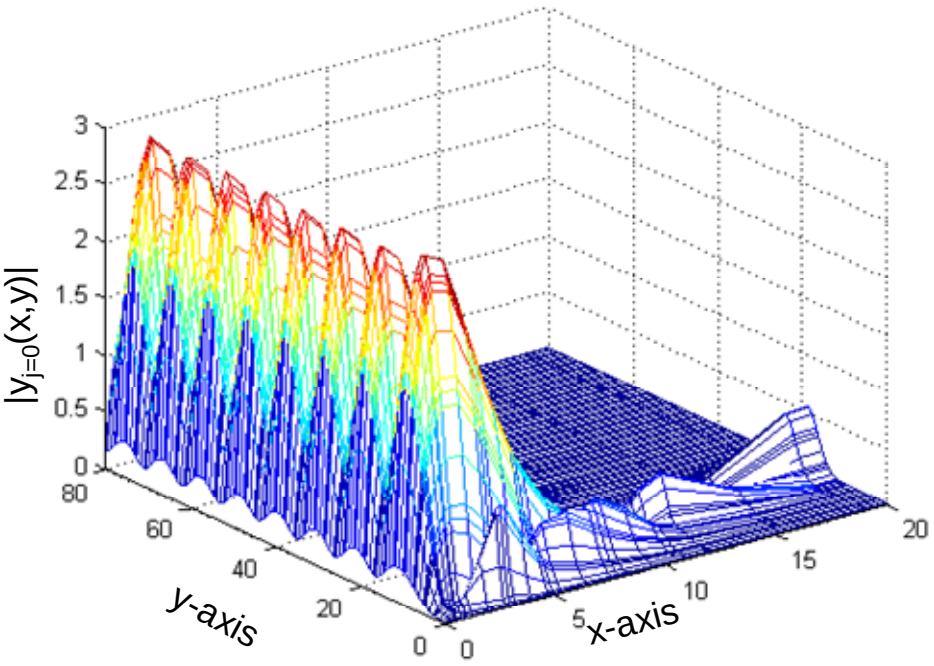

Figure 13c. Radial Wave Function (j=0) For First Y Knot = 0.5, k = 0.5 And 10^0 Y-Axis Azimuthal Shift.

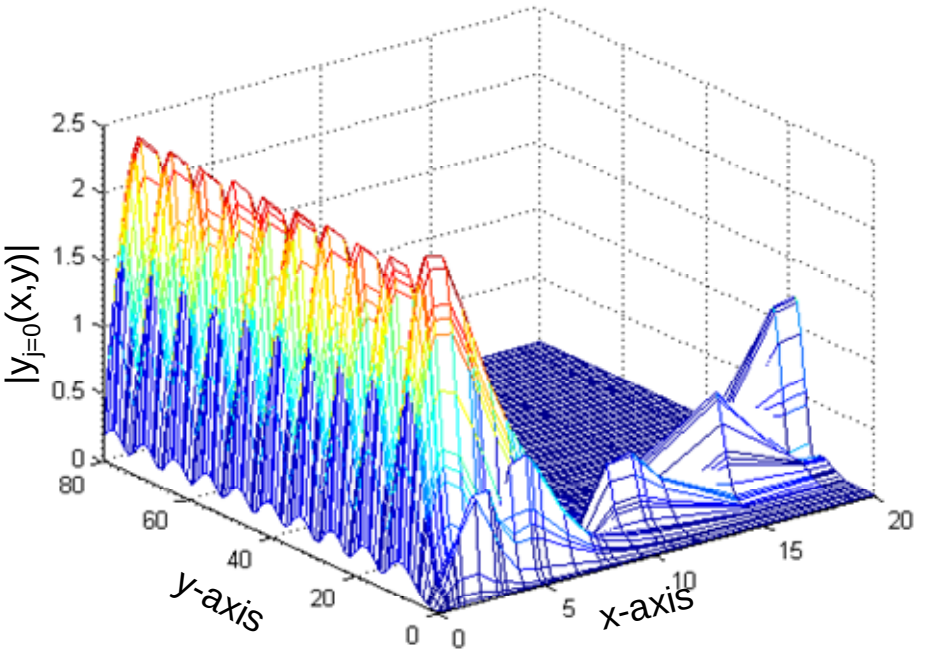

Figure 13d. Radial Wave Function (j=0) For First Y Knot = 0.5, k = 0.6 And 10^0 Y-Axis Azimuthal Shift.

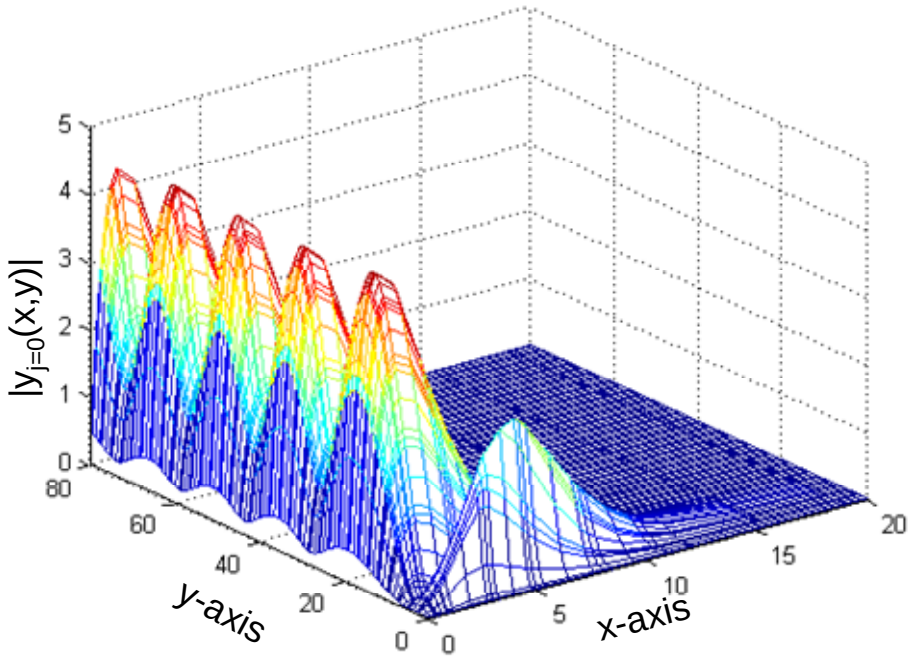

Figure 14a. Radial Wave Function (j=0) For First Y Knot = 0.5, k = 0.3 And 20^0 Y-Axis Azimuthal Shift.

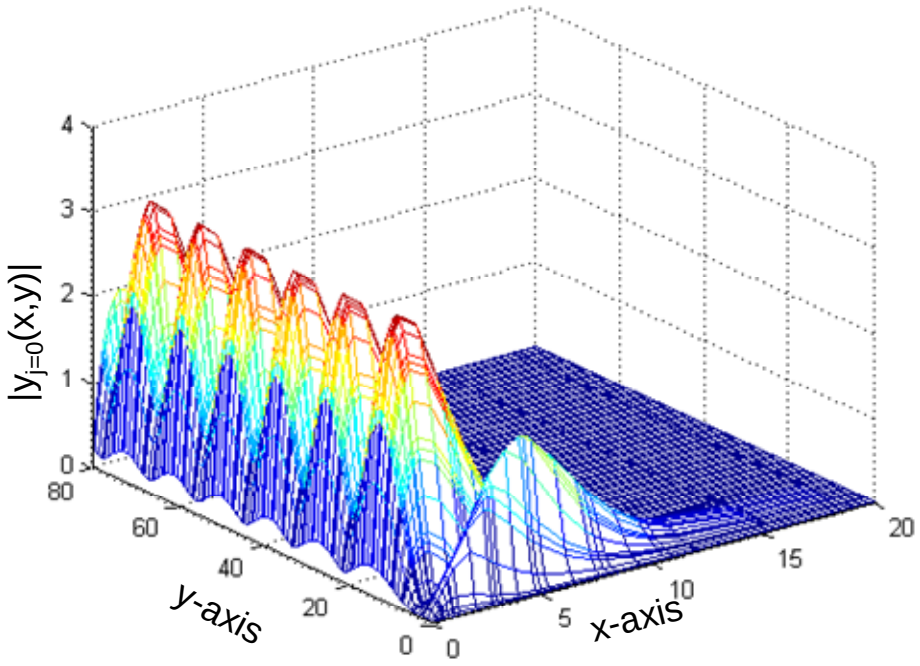

Figure 14b. Radial Wave Function (j=0) For First Y Knot = 0.5, k = 0.4 And 20^0 Y-Axis Azimuthal Shift.

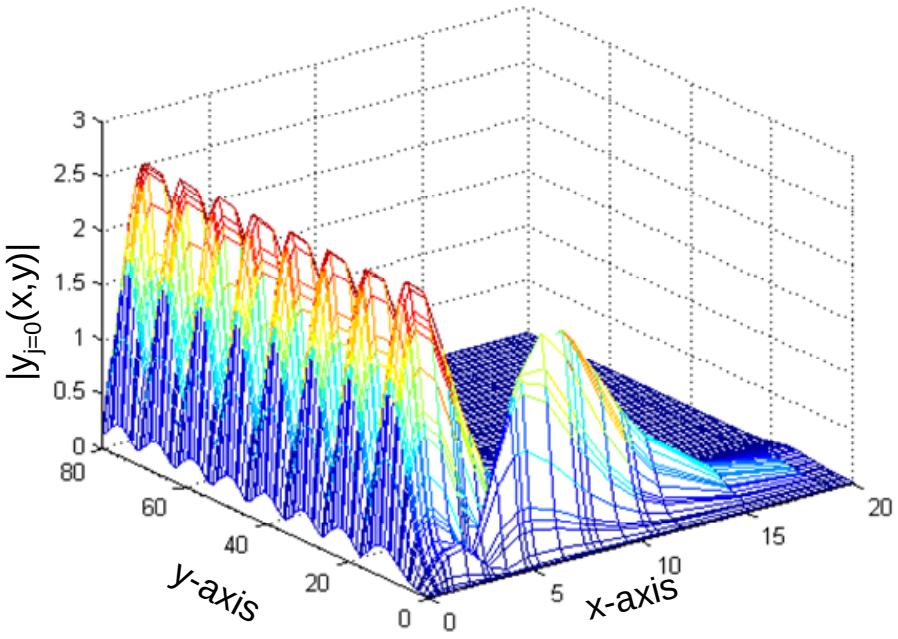

Figure 14c. Radial Wave Function (j=0) For First Y Knot = 0.5, k = 0.5 And 20^0 Y-Axis Azimuthal Shift.

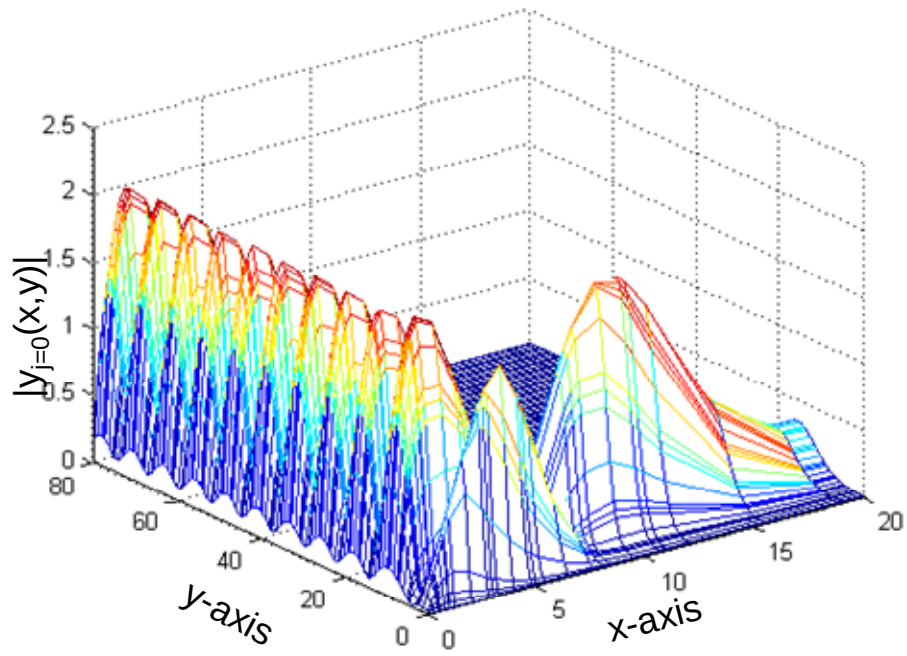

Figure 14d. Radial Wave Function (j=0) For First Y Knot = 0.5, k = 0.6 And 20^0 Y-Axis Azimuthal Shift.

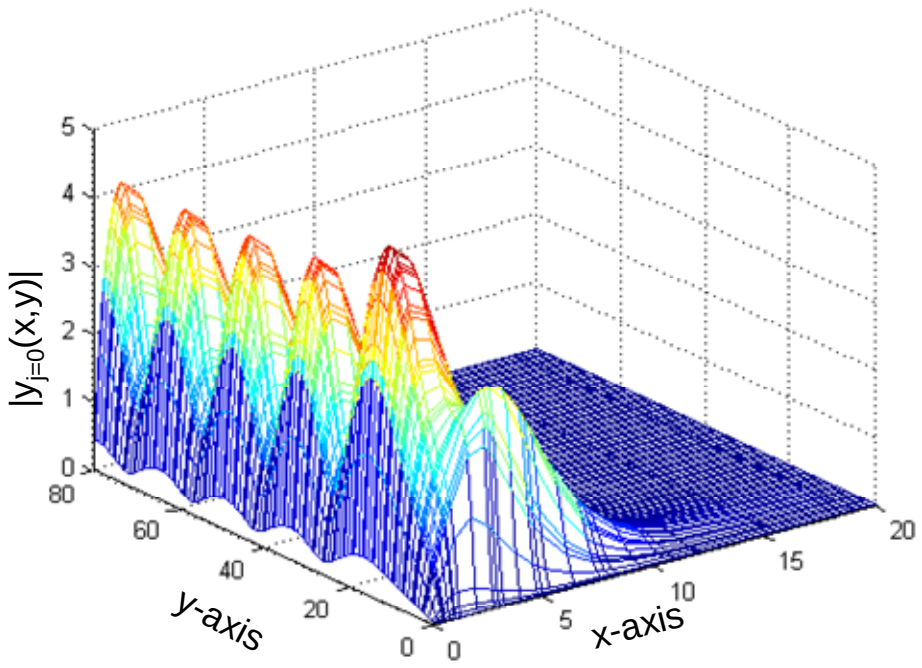

Figure 15a. Radial Wave Function (j=0) For First Y Knot = 0.5, k = 0.3 And 30^0 Y-Axis Azimuthal Shift.

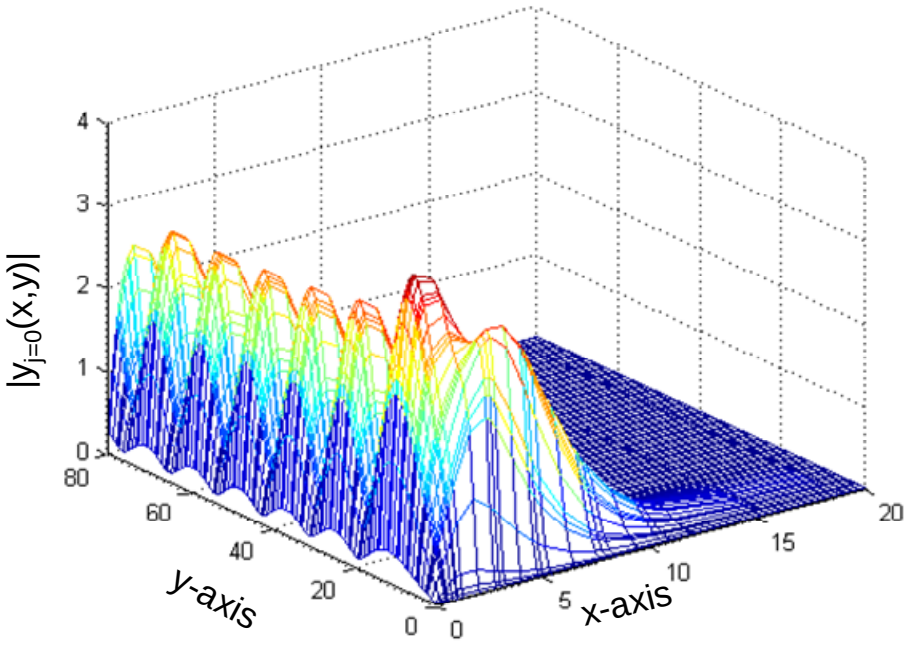

Figure 15b. Radial Wave Function (j=0) For First Y Knot = 0.5, k = 0.4 And 30^0 Y-Axis Azimuthal Shift.

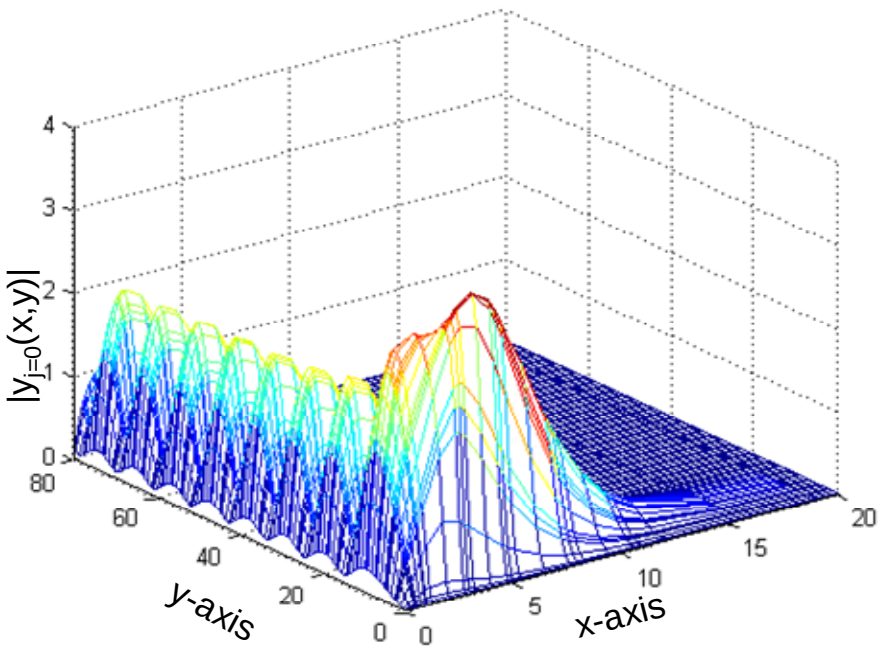

Figure 15c. Radial Wave Function (j=0) For First Y Knot = 0.5, k = 0.5 And 30^0 Y-Axis Azimuthal Shift.

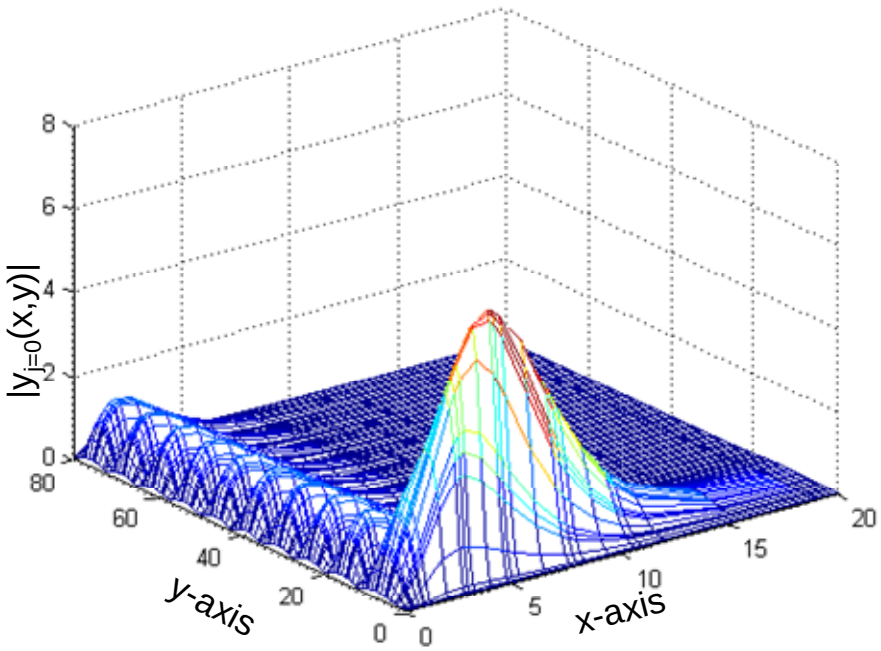

Figure 15d. Radial Wave Function (j=0) For First Y Knot = 0.5, k = 0.6 And 30^0 Y-Axis Azimuthal Shift.

The graphs of 28.6^0 and 30^0 show some larger differences in the interaction region at the higher energies indicating that the electron and positron bonding is having some effect on the wave function. However, as shown in Figures 21 and 22 these wave functions produce results that are in good agreement with the reference plot, with the 30^0 shift having less bias than that of the 26.8^0 shift.

An obvious improvement to the numerical calculations is to move the first y-axis knot location. Analysis of the position of the first knot and comparing the first collocation points to that of the x-axis yielded a knot location of 0.8 that gives a maximal distance between the closest two collocation point values of the x-axis and y-axis of 0.034 versus at least 3 points with identical distance of 0.0 when the knot is at 0.5. Using this knot location lessens the numerical instability near zero. However, it may increase some instability at the higher collocation locations if the numerical values for the y-axis approach that of the x-axis as all the y knots are adjusted for this first knot location.

Figures 16a to 20d show the wave function plots for the first knot location at 0.8 for the same energies and shifts as the previous figures.

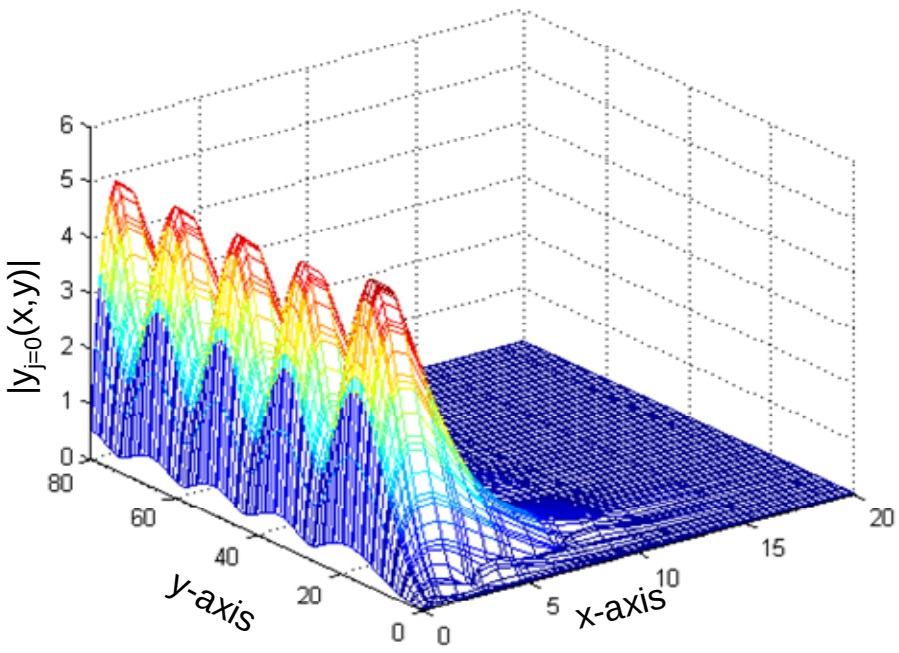

Figure 16a. Radial Wave Function (j=0) For First Y Knot = 0.8, k = 0.3 And 0^0 Y-Axis Azimuthal Shift.

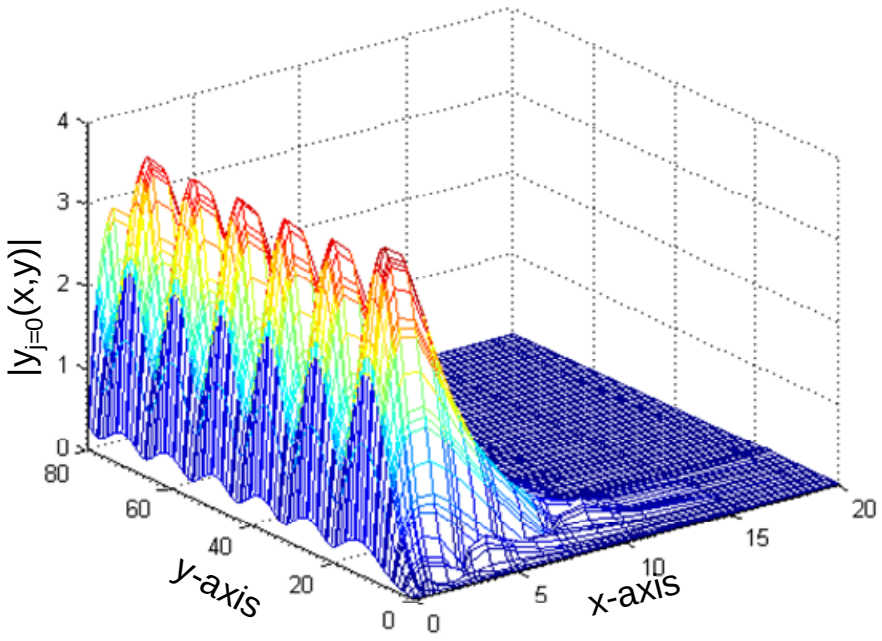

Figure 16b. Radial Wave Function (j=0) For First Y Knot = 0.8, k = 0.4 And 0^0 Y-Axis Azimuthal Shift.

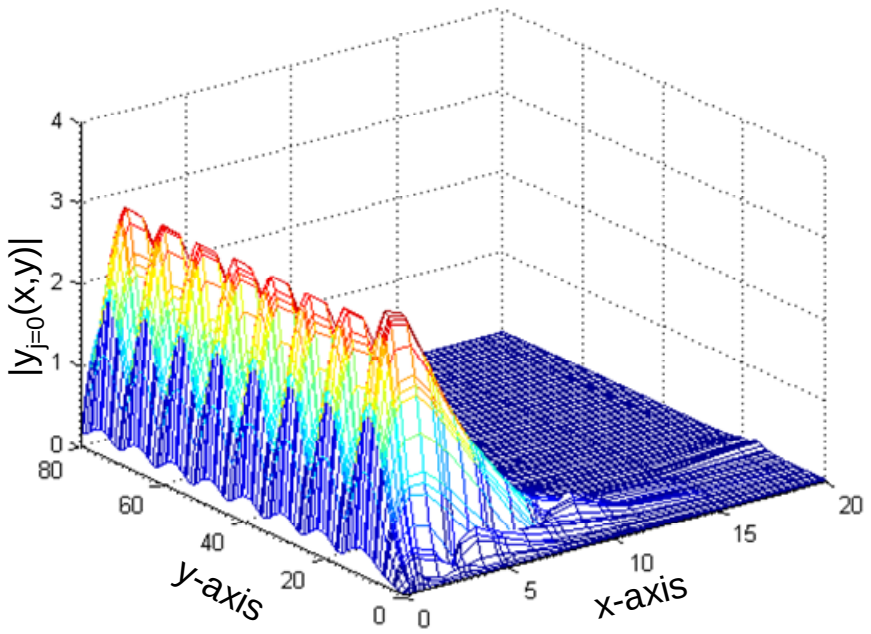

Figure 16c. Radial Wave Function (j=0) For First Y Knot = 0.8, k = 0.5 And 0^0 Y-Axis Azimuthal Shift.

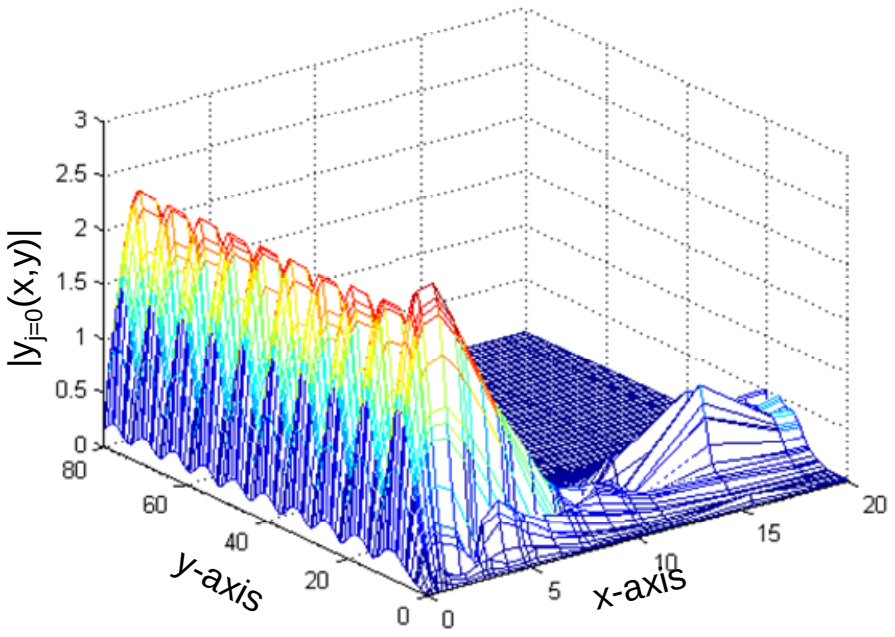

Figure 16d. Radial Wave Function (j=0) For First Y Knot = 0.8, k = 0.6 And 0^0 Y-Axis Azimuthal Shift.

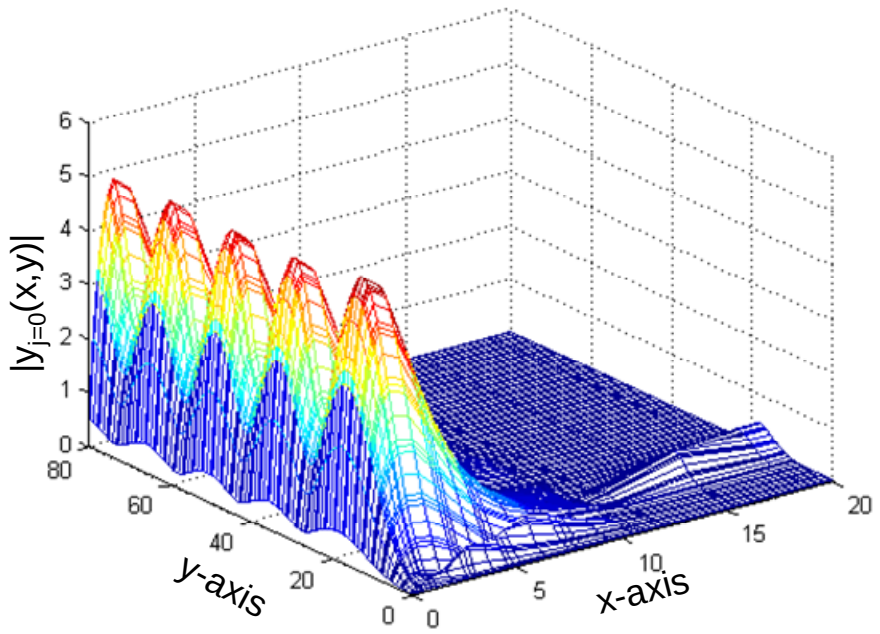

Figure 17a. Radial Wave Function (j=0) For First Y Knot = 0.8, k = 0.3 And 10^0 Y-Axis Azimuthal Shift.

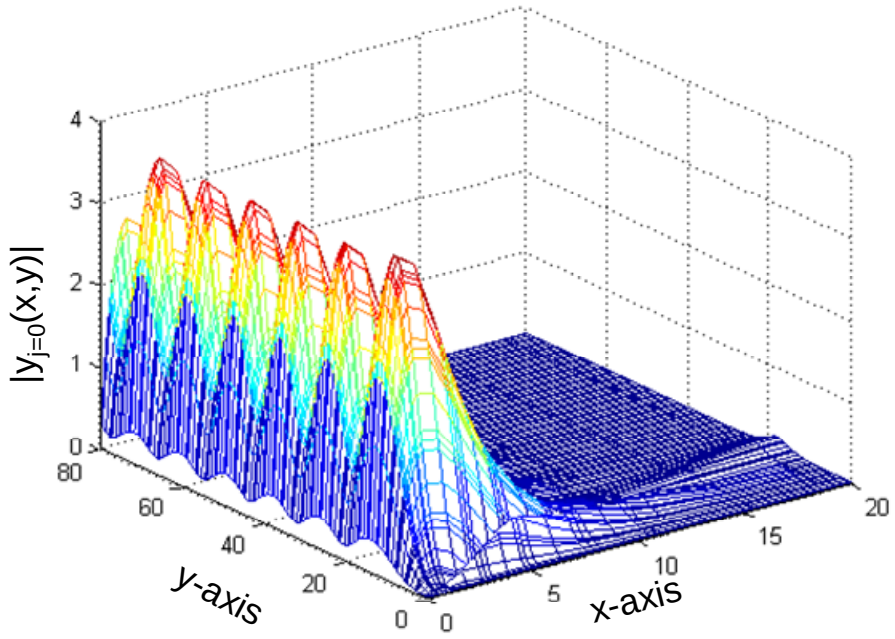

Figure 17b. Radial Wave Function (j=0) For First Y Knot = 0.8, k = 0.4 And 10^0 Y-Axis Azimuthal Shift.

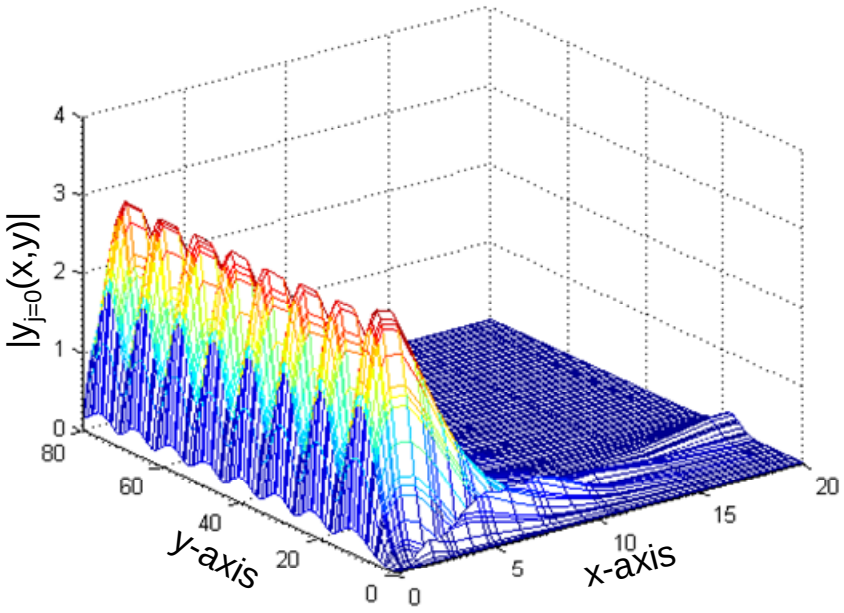

Figure 17c. Radial Wave Function (j=0) For First Y Knot = 0.8, k = 0.5 And 10^0 Y-Axis Azimuthal Shift.

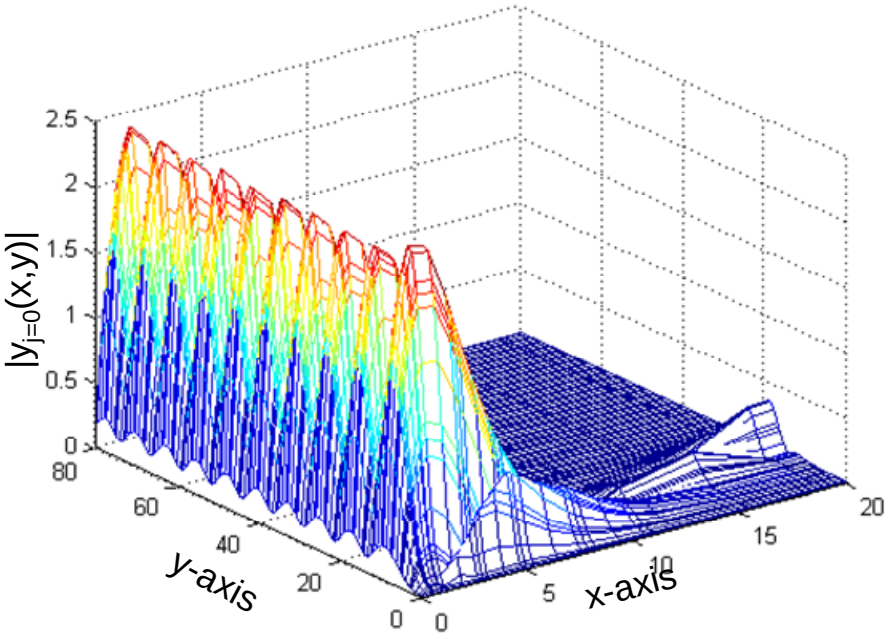

Figure 17d. Radial Wave Function (j=0) For First Y Knot = 0.8, k = 0.6 And 10^0 Y-Axis Azimuthal Shift.

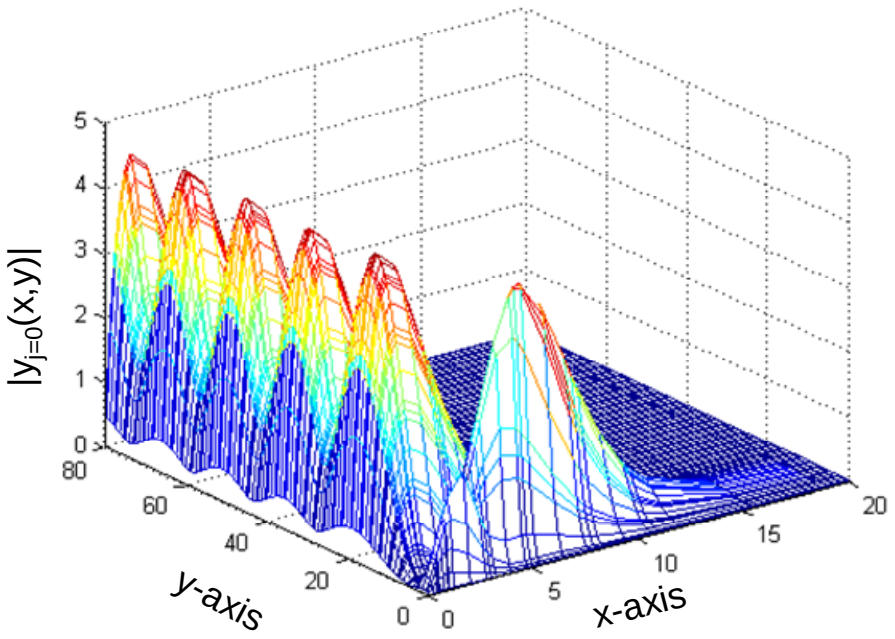

Figure 18a. Radial Wave Function (j=0) For First Y Knot = 0.8, k = 0.3 And 20^0 Y-Axis Azimuthal Shift.

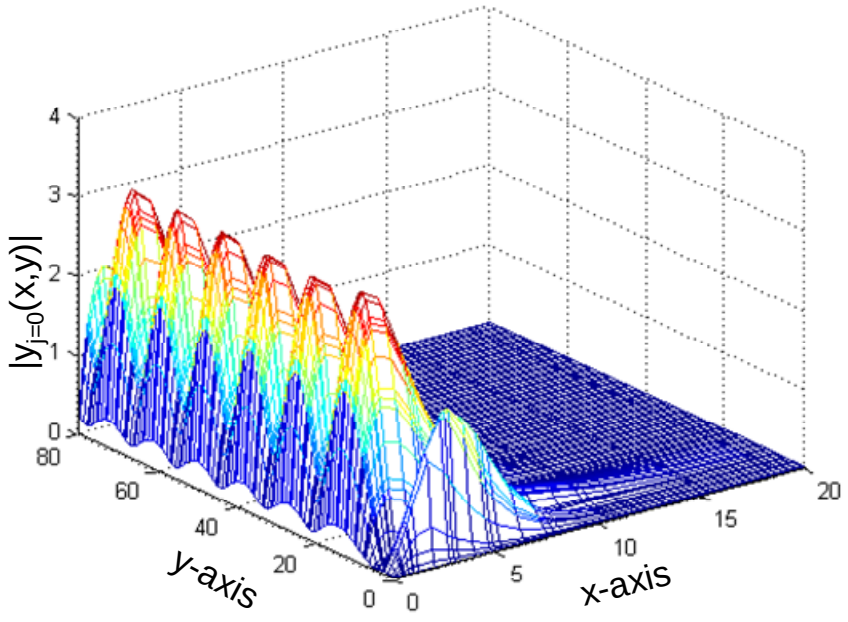

Figure 18b. Radial Wave Function (j=0) For First Y Knot = 0.8, k = 0.4 And 20^0 Y-Axis Azimuthal Shift.

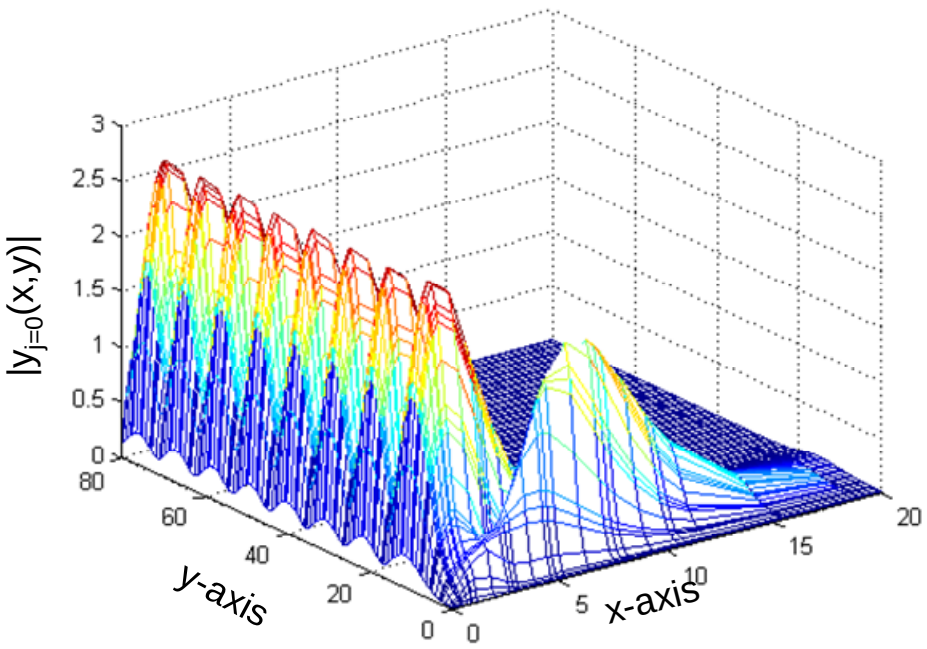

Figure 18c. Radial Wave Function (j=0) For First Y Knot = 0.8, k = 0.5 And 20^0 Y-Axis Azimuthal Shift.

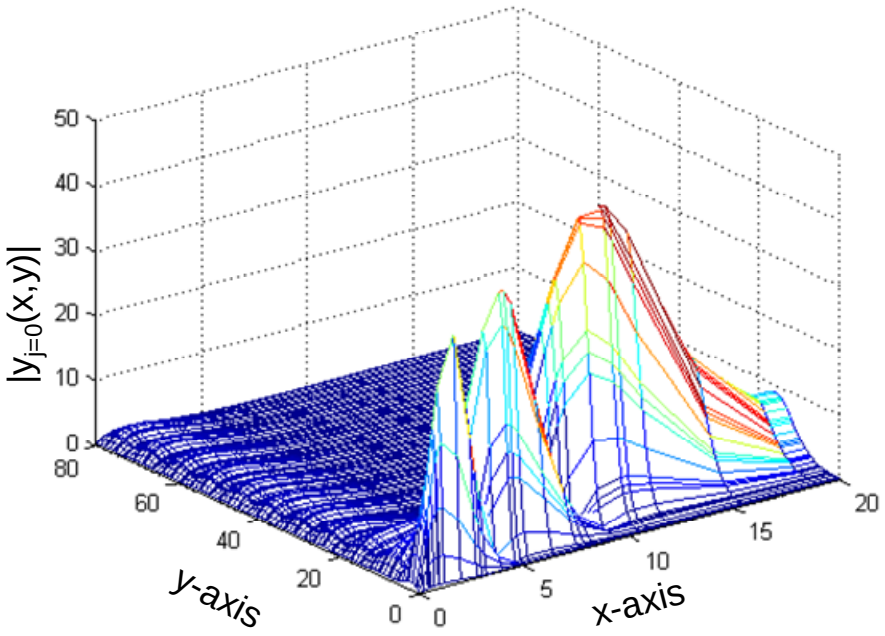

Figure 18d. Radial Wave Function (j=0) For First Y Knot = 0.8, k = 0.6 And 20^0 Y-Axis Azimuthal Shift.

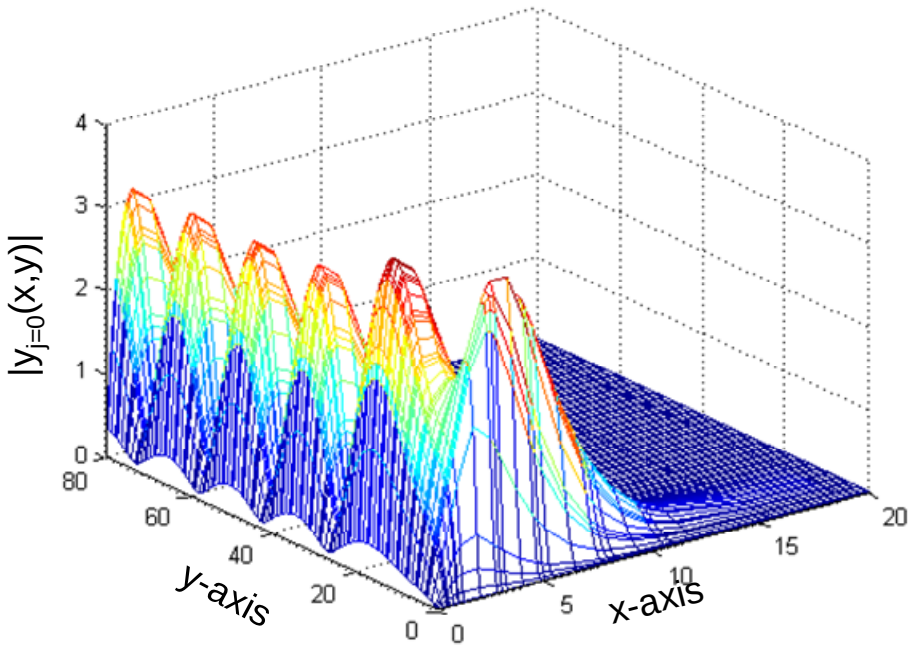

Figure 19a. Radial Wave Function (j=0) For First Y Knot = 0.8, k = 0.3 And 26.8^0 Y-Axis Azimuthal Shift.

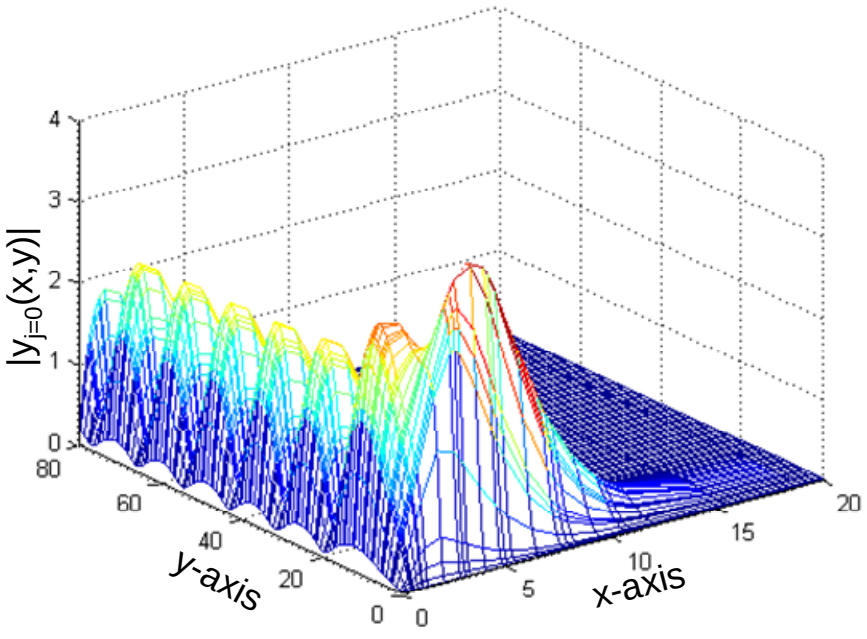

Figure 19b. Radial Wave Function (j=0) For First Y Knot = 0.8, k = 0.4 And 26.8^0 Y-Axis Azimuthal Shift.

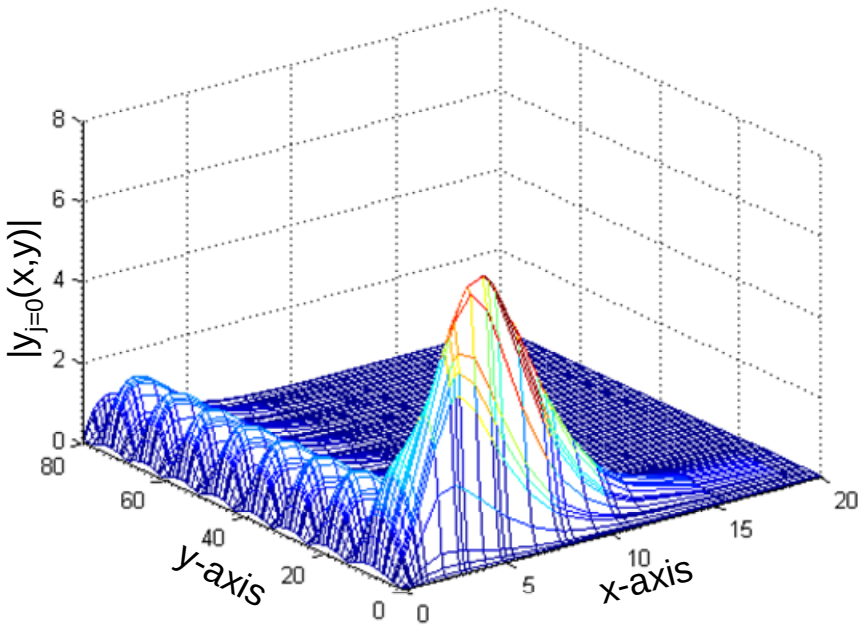

Figure 19c. Radial Wave Function (j=0) For First Y Knot = 0.8, k = 0.5 And 26.8^0 Y-Axis Azimuthal Shift.

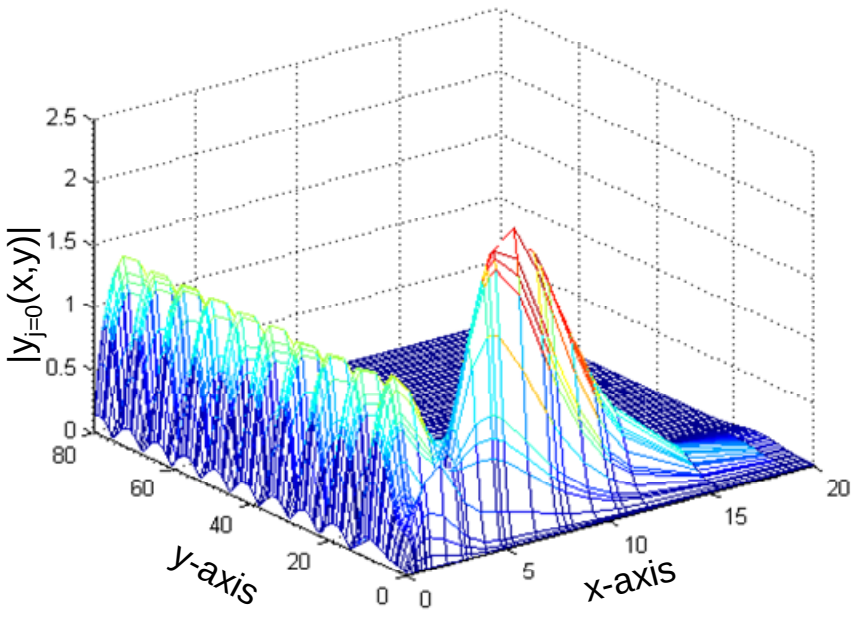

Figure 19d. Radial Wave Function (j=0) For First Y Knot = 0.8, k = 0.6 And 26.8^0 Y-Axis Azimuthal Shift.

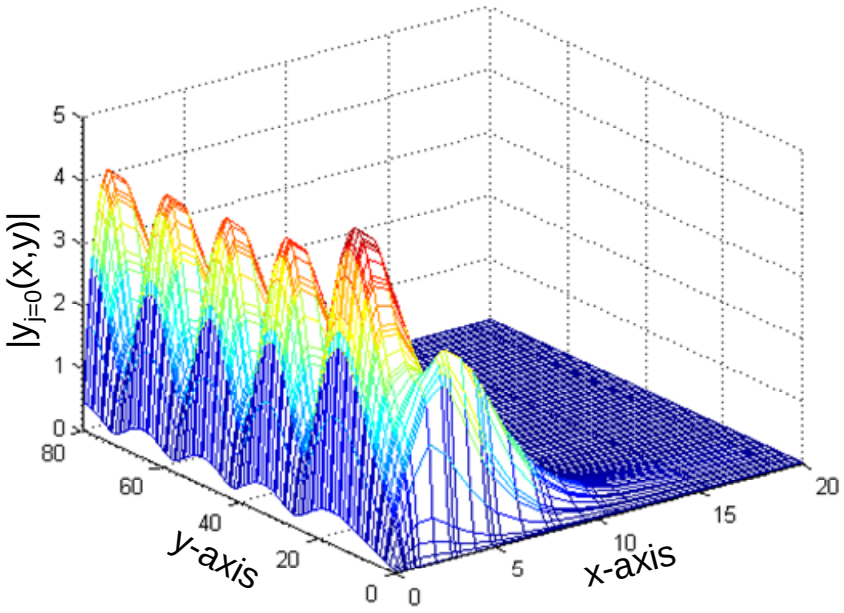

Figure 20a. Radial Wave Function (j=0) For First Y Knot = 0.8, k = 0.3 And 30^0 Y-Axis Azimuthal Shift.

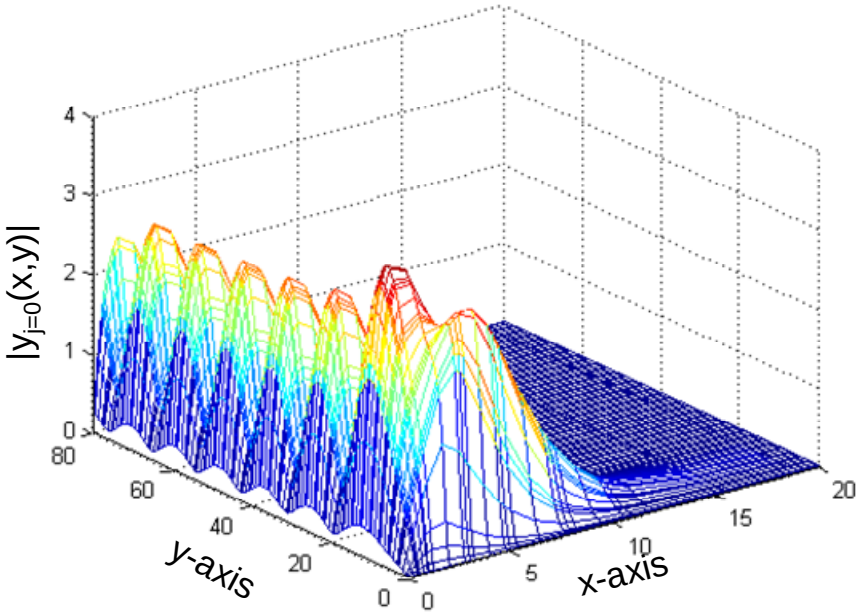

Figure 20b. Radial Wave Function (j=0) For First Y Knot = 0.8, k = 0.4 And 30^0 Y-Axis Azimuthal Shift.

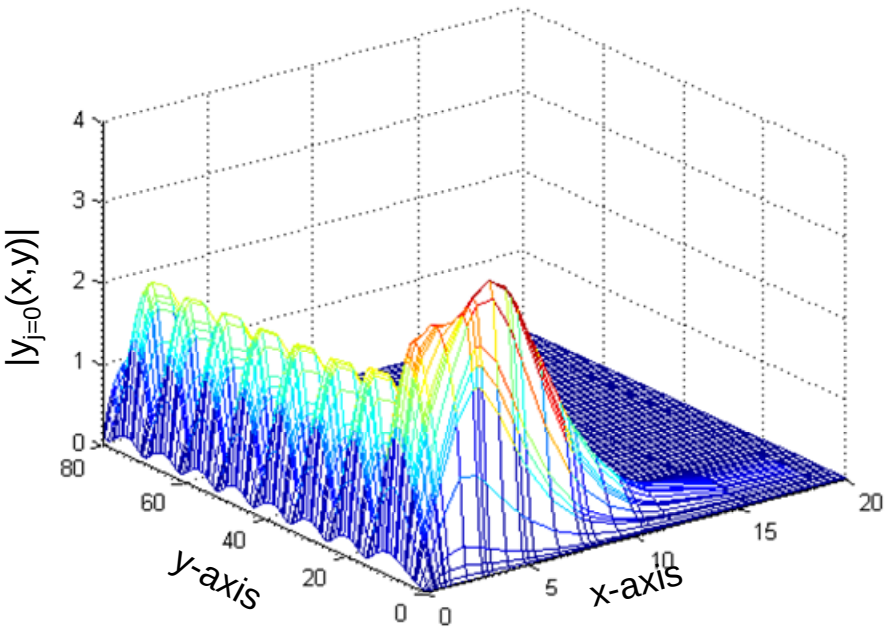

Figure 20c. Radial Wave Function (j=0) For First Y Knot = 0.8, k = 0.5 And 30^0 Y-Axis Azimuthal Shift.

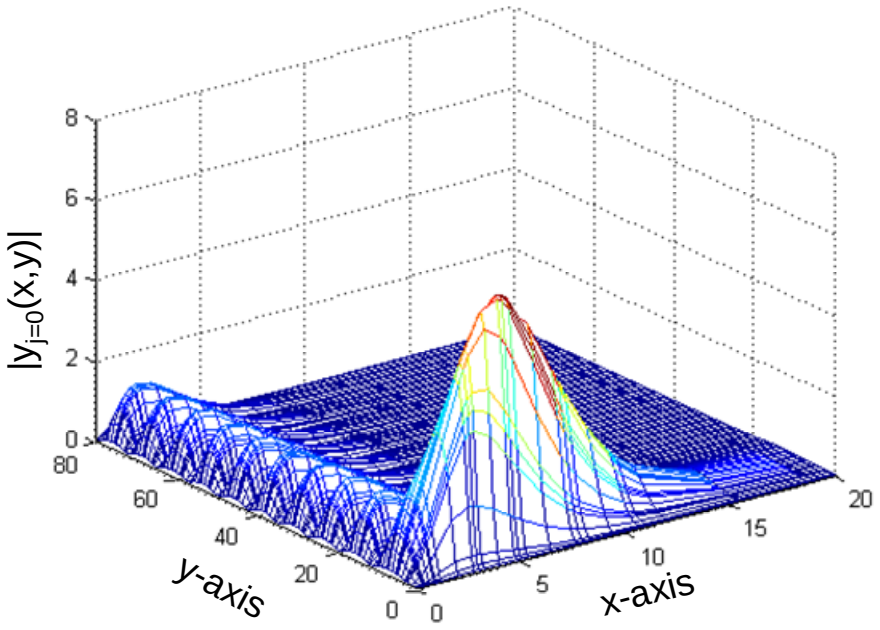

Figure 20d. Radial Wave Function (j=0) For First Y Knot = 0.8, k = 0.6 And 30^0 Y-Axis Azimuthal Shift.

Notice that there is an improvement in the shape of the wave function for 0^0 shift when the first knot is at 0.8 instead of 0.5. There is likely an optimal location for all the y-knots with respect to the x-knots and this is being investigated. Once found, the wave function convergence should improve for the 9x9 DVR case. In addition, the more optimal knot locations should also help the denser DVR cases as well, since the knot locations are not a function of the angles between the axis, but of the separation between the x and y knots values on their axes. This separation, however, does become more important when the angle between the axes is small since that forces the positron and electron along the same line.

The bonding affect is also degraded for the k = 0.5 and 0.6 cases where the first knot at 0.8 when compared to the case where the first knot is at 0.5. This is due to first knot being placed farther out than the 0.5 case. If Figure 5 is expanded to end at 0.8 (instead of ending at 0.6) one would see that the cumulative probability of the electron being at this distance from the proton is around eleven percent. This is more than three times the probability at a distance of 0.5. The positron basis

functions are being implemented in the region where the no electron interference assumption begins to break down.

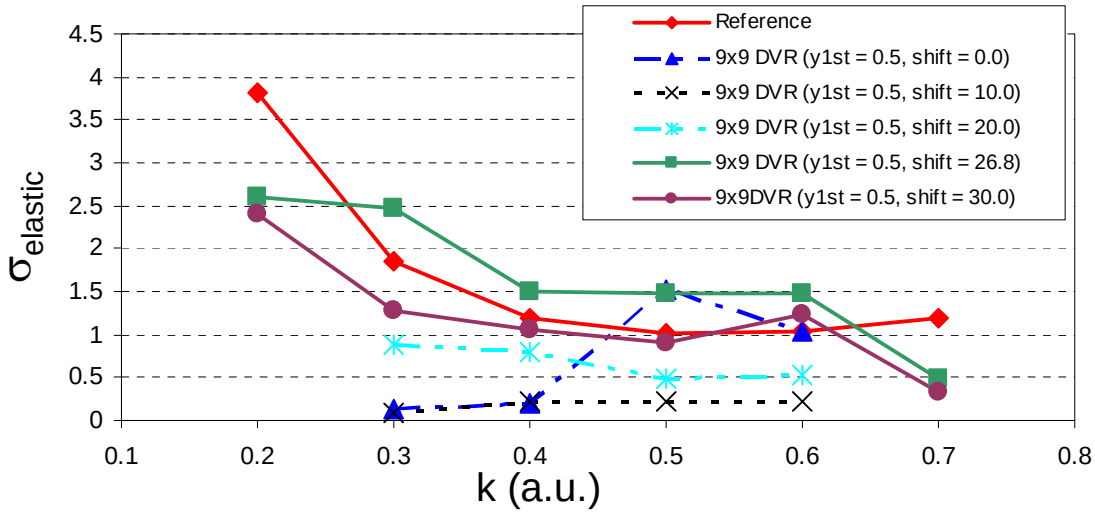

Figure 21. Elastic Cross Section Vs Incoming Momentum For First Knot Location 0.5.

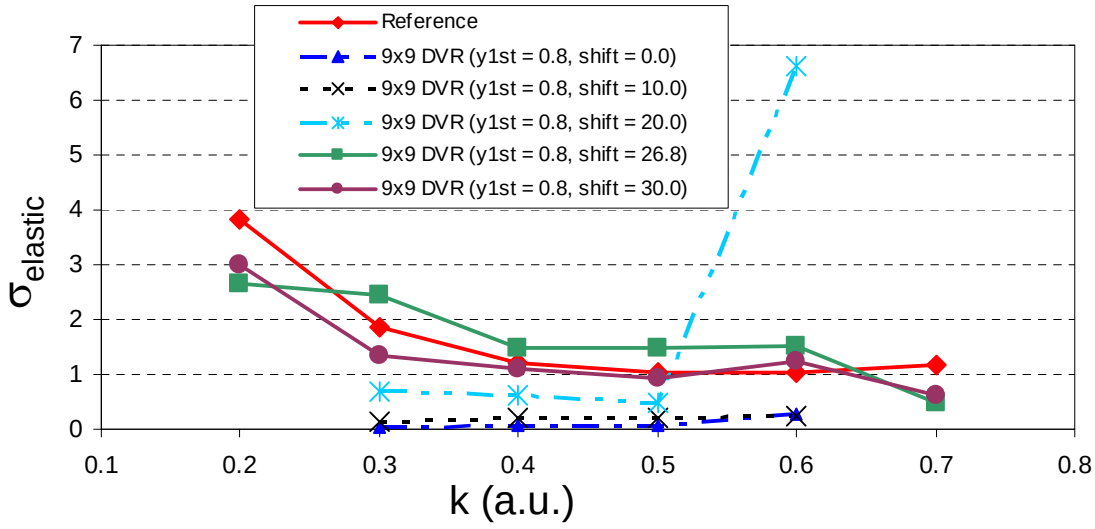

Figure 22. Elastic Cross Section Vs Incoming Momentum For First Knot Location 0.8.

The computed cross sections for all the azimuthal shift implementations and first knot locations are shown

in Figures 21 and 22. The 26.8^0 and 30^0 shifts yield results that best match the reference results. The results for the cases with lower angles between the x and y Jacobi axes yield degraded results as the angle decreases to 0^0, as expected when examining the wave functions. Also, as expected due to its wave function example, the k = 0.6 cross section when the first knot is at 0.8 and a shift angle of 20^0 deviated significantly from the ensemble results.

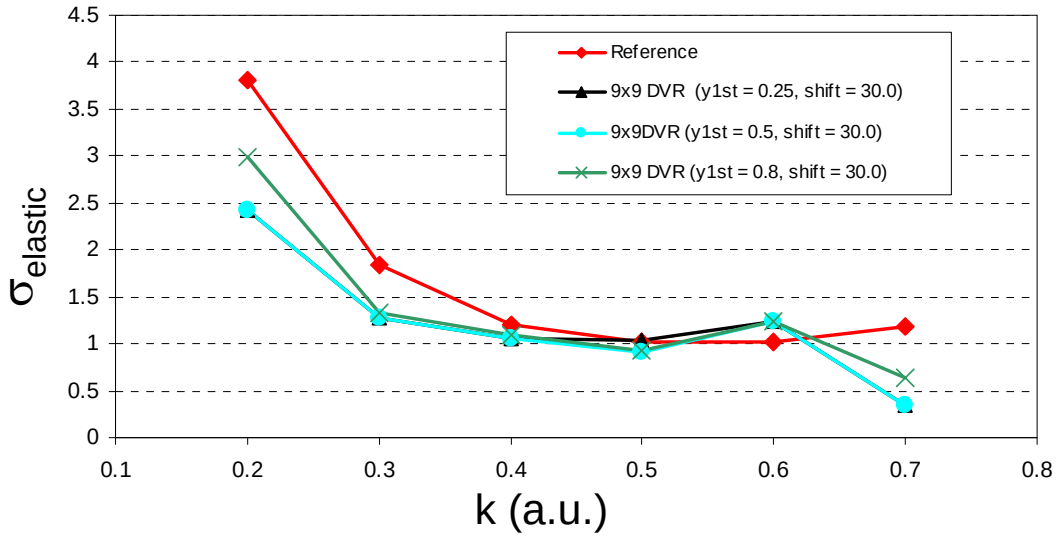

Figure 23. Elastic Cross Section Vs Incoming Momentum Using 30.0^0 y-axis Azimuthal Shift.

Figure 23 shows the results for a shift of 30^0. When compared to the results in Figure 10, a 30^0 shift yields cross sections that are closer to that of the reference. It is expected that using a higher density DVR basis set

will yield results that are less sensitive to the shift angle because, as the DVR density increases, more angular contributions will be included in the total cross section calculation.

CHAPTER 4

CONCLUSION

The 9x9 DVR results show the promise of the bipolar DVR technique for solving the scattering problem without partial waves. It has been shown, in the 9x9 DVR case, that one axis configuration tends to dominate the cross section results, while the other configurations tend to contribute little to the overall cross section as they represent the free particle cases. Only one configuration has a strong positron-electron interaction, while the other configurations have a small positron-electron interaction. When a higher density DVR basis set is implemented, there are additional axis configurations that also contribute to the overall result. Indeed there should be a set of configurations that represent a smooth transition from high interactions to lower interactions.

As this method evolves, using a larger number of DVR basis functions should yield a solution for the elastic-scattering problem with high accuracy. In addition, as more DVR basis functions are included, the amplitude function and cross section analysis may be performed beyond elastic-scattering into the multi-channel

scattering region. Also, additional potentials, including anisotropic potentials, can then be included into the Schrodinger equation for analysis of the various scattering effects.

Larger DVR basis should be implementable in the near future as computer processing continues to improve. Even with today's computer systems, larger DVR basis calculations should be possible if a sparse linear equation solver could be found that is capable of solving a large general NxN matrix with N greater than one million. Using present computer systems and software it is possible to use only a dense matrix solver. The computer resources required to use a dense matrix solver for larger DVR grids is prohibitive.

APPENDIX A

ATOMIC UNITS AND MASS-SCALED JACOBI COORDINATES

This appendix summarizes atomic units as used in the Schrodinger equation. This appendix also summarizes the formulas related to the Jacobi coordinates in scattering systems. More in depth details are found in references 1 to 9, 36, 37 and 38.

A.1 Introduction

To describe the three-body quantum-mechanical kinematics used in this paper, where each system is invariant under translation and rotation, it is most convenient to use the class of coordinates called mass-scaled Jacobi coordinates. In addition, to make numerical computations more convenient, atomic units are implemented in the equations described in this paper.

A.2 Electron Atomic Units

Some common physical constants that are used in quantum-mechanical calculations are listed in the following table

Table 4. Physical Constants.

Symbol	MKS value	Description
c	2.99785234×10^{8} M/s	Speed of light
h	$6.625705334 \times 10^{-34}$ W-s^2 $6.625705334 \times 10^{-34}$ J-s	Plank's constant (units of angular momentum)
hc	$1.986288624 \times 10^{-25}$ W-M-s	Product of h and c
e	1.6021×10^{-19} C	Electron charge
m_e	$9.1093897 \times 10^{-31}$ K	Electron mass
eV	1.6021×10^{-19} J	Electron volt (Energy)
K	8.98755×10^{9} N-m^2/C^2	Boltzman constant
η	$1.054513755 \times 10^{-34}$ J-s	h divided by 2π
$m_e c^2$	$8.186716609 \times 10^{-14}$ J 5.10999×10^{5} eV 0.511 Mev	Electron energy

To make numerical calculations convenient, non-dimensionalization is implemented in the equations by using electron atomic units. Electron atomic units are implemented by defining a set of units such that $\eta^a = e^a = m_e^a = K^a = 1$, where the superscript a, denotes atomic units. Using these sets of units, the unit of length is the electron Bohr radius $a^a = 1$ with the corresponding length in MKS units of $a = \eta^2 / K m_e e^2 = 0.529169 \times 10^{-10}$ M

Similarly the unit of energy is $E^a = 1$, and the corresponding electron Bohr energy $E_B^a = -½$ with $E_B = -\eta^2 / 2a^2 m_e = -2.179698535 \times 10^{-18}$ J = -13.623 eV.

As an example of the use of atomic units, the radial portion of the Schrodinger equation is typically given by the following form

$$\left(\frac{-\eta^{(mks)2}}{2M^{mks}}\frac{\partial^2}{\partial r^2}+V+\frac{l(l+1)\eta^{(mks)2}}{2M^{(mks)}r^2}\right)\psi=E^{mks}\psi=\frac{\eta^{(mks)2}k^{(mks)2}}{2M^{(mks)}}\psi \qquad \text{Eq. 101}$$

Substituting atomic units yields

$$\left(\frac{-1}{2M^{a}}\frac{\partial^2}{\partial r^{(a)2}}+V+\frac{l(l+1)}{2M^{a}r^{(a)2}}\right)\psi=E^{a}\psi=\frac{k^{(a)2}}{2M^{a}}\psi \qquad \text{Eq. 102}$$

or, dropping the notation for atomic units (a)

$$\left(\frac{-1}{2M}\frac{\partial^2}{\partial r^2}+V+\frac{l(l+1)}{2Mr^2}\right)\psi=\frac{k^2}{2M}\psi \qquad \text{Eq. 103}$$

and then simplifying the equation in atomic units becomes

$$\left(-\frac{\partial^2}{\partial r^2}+2MV+\frac{l(l+1)}{r^2}\right)\psi=k^2\psi \qquad \text{Eq. 104}$$

Note that if the electron-atomic units are not convenient for numerical calculations then another set of atomic units may be better suited for the calculations. For example muonic-atomic units would have $\eta^m=e^m=m_\mu^m=K^m=1$ where m_μ is the mass of the muon and the superscript, m, denotes muonic atomic units (this superscript notation would, generally, be left out of equations with the understanding that all units are muonic atomic).

The Rydberg constant is a unit of energy equal to 13.6056923 eV. The previous equations have shown that in

electron atomic units (a.u.) 1 unit of energy is equal to 27.246 eV. Thus 1 a.u. = 2.00254 Ryd. This conversion allows for a convenient representation of energy in the standard form Rydberg rather than the convenient computational form a.u.

A.3. Jacobi Coordinates

This paper discusses the kinematics of a three-body system. The three-body kinematics is conveniently described using the Jacobi vectors.

To describe the motion of a cluster of particles, one must first set up a convenient coordinate system. For the three-body system let r_i denote the position of each particle in the system, i = 1, 2, 3.

After separation of the center of mass motion, the Jacobi coordinates for the relative motions are defined as (x_α, y_α) where α = (1, 2, 3) labels the pairs of particles with members $\beta \neq \alpha$ (e.g. pair 1 consists of particles 2 and 3). The coordinates for each pair of particles are given in the following figure.

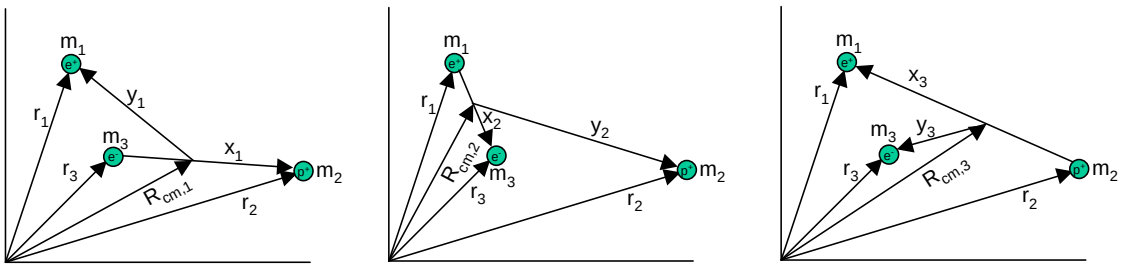

Rules:
1. (x_i, y_i) coordinates reflect that m_i is the free particle (y_i always points to m_i)
2. x_i points from m_{i-1} to m_{i+1} (cyclically, x_α points from m_γ to m_β).
3. y_i originates from CM of m_{i-1} and m_{i+1} (cyclically, y_α originates from CM of m_γ and m_β).

Figure 24. Jacobi Coordinates For A Three Particle System.

From Figure 24

$$\bar{x}_\alpha = \bar{r}_\beta - \bar{r}_\gamma \qquad \text{Eq. 105}$$

$$\bar{y}_\alpha = \bar{r}_\alpha - \bar{R}_{CM,\alpha} = \bar{r}_\alpha - \frac{m_\beta \bar{r}_\beta + m_\gamma \bar{r}_\beta}{m_\beta + m_\gamma} \qquad \text{Eq. 106}$$

where (α,β,γ) = cyclic (1,2,3).

These three sets of coordinates form the three-body Jacobi coordinates. $\bar{y}_\alpha$ is the scattering coordinate, which corresponds to the distance the α particle is from the center of mass of the particle pair (β, γ). $\bar{x}_\alpha$ is the bound coordinate, which corresponds to the bound particles (β, γ).

Any one pair of Jacobi coordinates completely describes the relative motions. The other two pairs of coordinates can be expressed linearly in terms of the first pair.

To compute the transformation between each Jacobi coordinates one must analyze Figure 25.

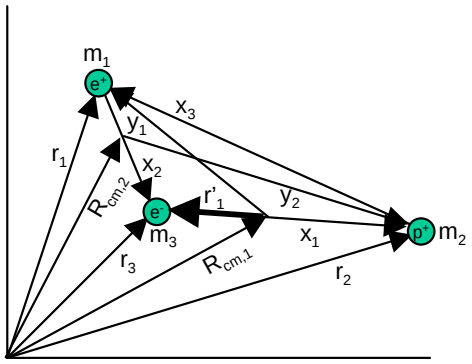

Figure 25. Jacobi Coordinates.

To find $\bar{x}_2$ given $(\bar{x}_1, \bar{y}_1)$, note that $\bar{r}'_1 = \bar{y}_1 + \bar{x}_2$. Thus $\bar{x}_2 = \bar{r}'_1 - \bar{y}_1$. But $\bar{r}'_1 + \bar{R}_{CM,1} = \bar{r}_3$, so that

$$\bar{r}'_1 = \bar{r}_3 - \frac{m_2\bar{r}_2 + m_3\bar{r}_3}{m_2 + m_3} = \frac{m_2(\bar{r}_3 - \bar{r}_2)}{m_2 + m_3} = \frac{-\bar{x}_1 m_2}{m_2 + m_3} \qquad \text{Eq. 107}$$

Thus,

$$\bar{x}_2 = \frac{-m_2}{m_2 + m_3}\bar{x}_1 - \bar{y}_1 \qquad \text{Eq. 108}$$

To find $\bar{y}_2$ given $(\bar{x}_1, \bar{y}_1)$, note that

$$\bar{y}_2 = \bar{r}_2 - \frac{m_1\bar{r}_1 + m_3\bar{r}_3}{m_1 + m_3} = \frac{m_3\bar{x}_1 - m_1\bar{x}_3}{m_1 + m_3} \qquad \text{Eq. 109}$$

which with $-\bar{x}_3 = \bar{x}_1 + \bar{x}_2$ gives

$$\bar{y}_2 = \frac{m_3\bar{x}_1 + m_1(\bar{x}_1 + \bar{x}_2)}{m_1 + m_3} = \bar{x}_1 + \frac{m_1\bar{x}_2}{m_1 + m_3} \qquad \text{Eq. 110}$$

or

$$\bar{y}_2 = \frac{m_3(m_1+m_2+m_3)}{(m_1+m_3)(m_2+m_3)}\bar{x}_1 - \frac{m_1}{(m_1+m_3)}\bar{y}_1 \qquad \text{Eq. 111}$$

It can be shown that, in general, the forward transformations $(\bar{x}_\beta, \bar{y}_\beta)$ β = cyclic (2,3,1) given $(\bar{x}_\alpha, \bar{y}_\alpha)$ α = cyclic (1,2,3) is given by

$$\bar{x}_\beta = \frac{-m_\beta}{m_\beta+m_\gamma}\bar{x}_\alpha - \bar{y}_\alpha \qquad \text{Eq. 112}$$

$$\bar{y}_\beta = \frac{m_\gamma M}{(m_\alpha+m_\gamma)(m_\beta+m_\gamma)}\bar{x}_\alpha - \frac{m_\alpha}{(m_\alpha+m_\gamma)}\bar{y}_\alpha \qquad \text{Eq. 113}$$

where $M = m_1 + m_2 + m_3$.

Similarly, in general the reverse transformations $(\bar{x}_\alpha, \bar{y}_\alpha)$ α = cyclic (1,2,3) given $(\bar{x}_\beta, \bar{y}_\beta)$ β = cyclic (2,3,1) is given by

$$\bar{x}_\alpha = \frac{-m_\alpha}{m_\alpha+m_\gamma}\bar{x}_\beta + \bar{y}_\beta \qquad \text{Eq. 114}$$

$$\bar{y}_\alpha = -\frac{m_\gamma M}{(m_\alpha+m_\gamma)(m_\beta+m_\gamma)}\bar{x}_\beta - \frac{m_\beta}{(m_\beta+m_\gamma)}\bar{y}_\beta \qquad \text{Eq. 115}$$

A.4 Mass-scaled Jacobi Coordinates

Denote the Jacobi coordinates previously described as $\bar{x}_\alpha^J$ and $\bar{y}_\alpha^J$.

Mass-scaled Jacobi coordinates are implemented to make the numerical calculations more convenient. These

coordinates yield a simple form for the kinetic energy operator and the transformations between coordinates is in the form of a simple rotation.

In the mass-scaled Jacobi coordinates $\bar{x}_\alpha$ and $\bar{y}_\alpha$, the Jacobi $\bar{x}_\alpha^J$-coordinate is scaled by t_α ($\bar{x}_\alpha = t_\alpha \bar{x}_\alpha^J$) and the $\bar{y}_\alpha^J$-coordinate is scaled by u_α ($\bar{y}_\alpha = u_\alpha \bar{y}_\alpha^J$) where

$$t_\alpha = \sqrt{\frac{2m_\beta m_\gamma}{m_\beta + m_\gamma}} \qquad \text{Eq. 116}$$

and

$$u_\alpha = \sqrt{\frac{2m_\alpha (m_\beta + m_\gamma)}{M}} \qquad \text{Eq. 117}$$

Note that $t_\alpha^2/2$ is the reduced mass of the pair α, and $u_\alpha^2/2$ is the reduced mass of the particle α and the pair α.

Letting

$$F1 = \frac{-m_\beta}{m_\beta + m_\gamma} \qquad \text{Eq. 118}$$

$$F2 = -1 \qquad \text{Eq. 119}$$

$$F3 = \frac{m_\gamma M}{(m_\alpha + m_\gamma)(m_\beta + m_\gamma)} \qquad \text{Eq. 120}$$

$$F4 = -\frac{m_\alpha}{(m_\alpha + m_\gamma)} \qquad \text{Eq. 121}$$

the transformation equations, before mass scaling, are written as

$$\bar{x}_\beta^J = F1\,\bar{x}_\alpha^J + F2\,\bar{y}_\alpha^J \qquad \text{Eq. 122}$$

$$\bar{y}_\beta^J = F3\,\bar{x}_\alpha^J + F4\,\bar{y}_\alpha^J \qquad \text{Eq. 123}$$

$$\bar{x}_\alpha^J = F4\,\bar{x}_\beta^J - F2\,\bar{y}_\beta^J \qquad \text{Eq. 124}$$

$$\bar{y}_\alpha^J = -F3\,\bar{x}_\beta^J + F1\,\bar{y}_\beta^J \qquad \text{Eq. 125}$$

so that the mass-scaled coordinate transformation equations become:

$$\bar{x}_\beta = t_\beta F1\,\bar{x}_\alpha / t_\alpha + t_\beta F2\,\bar{y}_\alpha / u_\alpha \qquad \text{Eq. 126}$$

$$\bar{y}_\beta = u_\beta F3\,\bar{x}_\alpha / t_\alpha + u_\beta F4\,\bar{y}_\alpha / u_\alpha \qquad \text{Eq. 127}$$

$$\bar{x}_\alpha = t_\alpha F4\,\bar{x}_\beta / t_\beta - t_\alpha F2\,\bar{y}_\beta / u_\beta \qquad \text{Eq. 128}$$

$$\bar{y}_\alpha = -u_\alpha F3\,\bar{x}_\beta / t_\beta + u_\alpha F1\,\bar{y}_\beta / u_\beta \qquad \text{Eq. 129}$$

or

$$\bar{x}_\beta = -\sqrt{\frac{m_\alpha m_\beta}{(m_\alpha + m_\gamma)(m_\beta + m_\gamma)}}\,\bar{x}_\alpha - \sqrt{\frac{m_\gamma M}{(m_\alpha + m_\gamma)(m_\beta + m_\gamma)}}\,\bar{y}_\alpha \qquad \text{Eq. 130}$$

$$\bar{y}_\beta = \sqrt{\frac{m_\gamma M}{(m_\alpha + m_\gamma)(m_\beta + m_\gamma)}}\,\bar{x}_\alpha - \sqrt{\frac{m_\alpha m_\beta}{(m_\alpha + m_\gamma)(m_\beta + m_\gamma)}}\,\bar{y}_\alpha \qquad \text{Eq. 131}$$

$$\bar{x}_\alpha = -\sqrt{\frac{m_\alpha m_\beta}{(m_\alpha + m_\gamma)(m_\beta + m_\gamma)}}\,\bar{x}_\beta + \sqrt{\frac{m_\gamma M}{(m_\alpha + m_\gamma)(m_\beta + m_\gamma)}}\,\bar{y}_\beta \qquad \text{Eq. 132}$$

$$\bar{y}_\alpha = -\sqrt{\frac{m_\gamma M}{(m_\alpha + m_\gamma)(m_\beta + m_\gamma)}}\,\bar{x}_\beta - \sqrt{\frac{m_\alpha m_\beta}{(m_\alpha + m_\gamma)(m_\beta + m_\gamma)}}\,\bar{y}_\beta \qquad \text{Eq. 133}$$

Let

$$c_{\beta\alpha} = -\sqrt{\frac{m_\alpha m_\beta}{(m_\alpha + m_\gamma)(m_\beta + m_\gamma)}} \qquad \text{Eq. 134}$$

$$w_{\beta\alpha} = -\sqrt{\frac{m_\gamma M}{(m_\alpha + m_\gamma)(m_\beta + m_\gamma)}} \qquad \text{Eq. 135}$$

Then, for the mass-scaled Jacobi coordinates the coordinate transformation equations are written as:

$$\bar{x}_\beta = c_{\beta\alpha}\bar{x}_\alpha + w_{\beta\alpha}\bar{y}_\alpha \qquad \text{Eq. 136}$$

$$\bar{y}_\beta = -w_{\beta\alpha}\bar{x}_\alpha + c_{\beta\alpha}\bar{y}_\alpha \qquad \text{Eq. 137}$$

$$\bar{x}_\alpha = c_{\beta\alpha}\bar{x}_\beta - w_{\beta\alpha}\bar{y}_\beta \qquad \text{Eq. 138}$$

$$\bar{y}_\alpha = w_{\beta\alpha}\bar{x}_\beta + c_{\beta\alpha}\bar{y}_\beta \qquad \text{Eq. 139}$$

Note that $c_{\beta\alpha} = c_{\alpha\beta}$, $w_{\beta\alpha} = w_{\alpha\beta}$ and $w_{\beta\alpha} = \sqrt{1-c_{\beta\alpha}^2}$. The above forward and reverse equations are combined into one set of equations,

$$\bar{x}_\beta = c_{\beta\alpha}\bar{x}_\alpha + u_{\beta\alpha}w_{\beta\alpha}\bar{y}_\alpha \qquad \text{Eq. 140}$$

$$\bar{y}_\beta = -u_{\beta\alpha}w_{\beta\alpha}\bar{x}_\alpha + c_{\beta\alpha}\bar{y}_\alpha \qquad \text{Eq. 141}$$

where $\alpha, \beta = (1, 2, 3)$, $\alpha \neq \beta$ and

$$u_{\beta\alpha} = (-1)^{\beta-\alpha}\mathrm{sgn}(\alpha-\beta) \qquad \text{Eq. 142}$$

Or by letting

$$s_{\beta\alpha} = u_{\beta\alpha}w_{\beta\alpha} = (-1)^{\beta-\alpha}\mathrm{sgn}(\alpha-\beta)\sqrt{1-c_{\beta\alpha}^2} \qquad \text{Eq. 143}$$

the transformation equations between different mass-scaled Jacobi coordinates take the shape of the more familiar orthogonal transformations

$$\bar{x}_\beta = c_{\beta\alpha}\bar{x}_\alpha + s_{\beta\alpha}\bar{y}_\alpha \qquad \text{Eq. 144}$$

$$\bar{y}_\beta = -s_{\beta\alpha}\bar{x}_\alpha + c_{\beta\alpha}\bar{y}_\alpha \qquad \text{Eq. 145}$$

For scattering problems, a more convenient set of local coordinates is the lengths of the mass-scaled Jacobi vectors and the angle between them[4].

$$x_\alpha = |\bar{x}_\alpha| \qquad \text{Eq. 146}$$

$$y_\alpha = |\bar{y}_\alpha| \qquad \text{Eq. 147}$$

$$z_\alpha = \cos(\theta_\alpha) = \frac{\bar{x}_\alpha \bullet \bar{y}_\alpha}{x_\alpha y_\alpha} \qquad \text{Eq. 148}$$

The coordinate transformation for the lengths becomes

$$x_\beta^2 = c_{\beta\alpha}^2 x_\alpha^2 + s_{\beta\alpha}^2 y_\alpha^2 + 2 s_{\beta\alpha} c_{\beta\alpha} x_\alpha y_\alpha z_\alpha \qquad \text{Eq. 149}$$

$$y_\beta^2 = s_{\beta\alpha}^2 x_\alpha^2 + c_{\beta\alpha}^2 y_\alpha^2 - 2 s_{\beta\alpha} c_{\beta\alpha} x_\alpha y_\alpha z_\alpha \qquad \text{Eq. 150}$$

$$z_\beta = \frac{(c_{\beta\alpha}^2 - s_{\beta\alpha}^2) x_\alpha y_\alpha z_\alpha - s_{\beta\alpha} c_{\beta\alpha}(x_\alpha^2 - y_\alpha^2)}{x_\beta y_\beta} \qquad \text{Eq. 151}$$

A.5 The Coulomb Potential In Mass-scaled Jacobi Coordinates

In atomic units the Coulomb potential, V_α, for the α particle pair is given by

$$V_\alpha = e_\beta e_\gamma / r_{\beta\gamma} = t_\alpha e_\beta e_\gamma / t_\alpha \bar{x}_\alpha \qquad \text{Eq. 152}$$

In mass-scaled coordinates this becomes

$V_\alpha = t_\alpha e_\beta e_\gamma / x_\alpha$ Eq. 153

Defining $q_\alpha = t_\alpha e_\beta e_\gamma$ as the mass-scaled charge, the Coulomb potential for the pair $\alpha = (\beta,\gamma)$ then becomes

$V_\alpha(x_\alpha) = q_\alpha / x_\alpha$ Eq. 154

A.6 The Two-Particle Schrodinger Equation In Mass-scaled Jacobi Coordinates

The two-particle Schrodinger Equation is given by

$$\left(\frac{p_1^2}{2m_1} + \frac{p_2^2}{2m_2} + V(\bar{r}_1, \bar{r}_2)\right)\Psi = E\Psi$$ Eq. 155

However, when dealing with two-particle systems it is convenient to separate the motion into that of the center of mass and the motion relative to the center of mass. The Hamiltonian is separated into a sum of two parts; one part H_{CM} involving the center of mass coordinates and another part H_{rel} containing coordinates relative to the center of mass.

When the potential is a function only of the radial distance between the two-particles the Hamiltonian is written as

$$\frac{p_1^2}{2m_1} + \frac{p_2^2}{2m_2} + V(\bar{r}_2 - \bar{r}_1)$$ Eq. 156

Separating the Hamiltonian into H_{CM} + H_{rel} is performed via the coordinate transformation

$$\bar{r} = \bar{r}_2 - \bar{r}_1 \qquad \text{Eq. 157}$$

$$\bar{p} = u\dot{\bar{r}} \qquad \text{Eq. 158}$$

$$\bar{R}_{CM} = \frac{m_1\bar{r}_1 + m_2\bar{r}_2}{m_1 + m_2} \qquad \text{Eq. 159}$$

$$\bar{P}_{CM} = \bar{p}_1 + \bar{p}_2 \qquad \text{Eq. 160}$$

$$u = \frac{m_1 m_2}{M} \qquad \text{Eq. 161}$$

$$M = m_1 + m_2 \qquad \text{Eq. 162}$$

where u is the reduced mass, $\bar{R}_{CM}$ is the center of mass vector, and $\bar{r}$ is the relative motion vector.

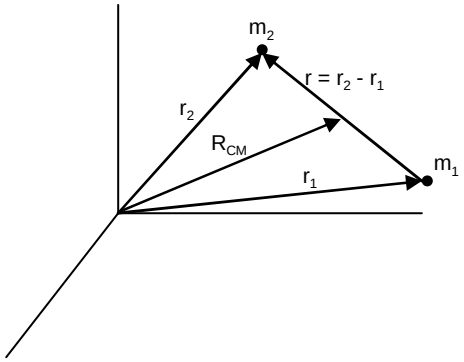

Figure 26. Two-particle Coordinate Reduction.

The Hamiltonian is rewritten as

$$H_{cm} + H_{rel} = \left(\frac{\bar{P}_{CM}^2}{2M}\right) + \left(\frac{\bar{p}^2}{2u} + V(\bar{r})\right) \qquad \text{Eq. 163}$$

The Hamiltonian for the center of mass motion is $\bar{P}_{CM}^2/2M$. The center of mass motion is cyclic, since its

Hamiltonian does not depend on the center of mass vector, R_{CM}. Thus the center of mass momentum is constant. Since the center of mass coordinates and the relative coordinates are independent of each other, the full wave function is just the product of the center of mass motion wave function (a free particle) and the relative motion wave function.

The wave function of the relative coordinates provides the details required to determine the scattering cross section. The equation for the relative wave function is given by

$$\left(\frac{\bar{p}^2}{2u} + V(\bar{r})\right)\Psi = E_{rel}\Psi \qquad \text{Eq. 164}$$

where E_{rel} is the energy of the relative energy: $E = E_{cm}+E_{rel}$. Since the center of mass results will not be further resolved, it is understood that E represents the relative energy in all subsequent equations.

To make computations more convenient, mass-scaled coordinates are used on the relative coordinates. For the two-particle case, the radial vector, now denoted by r^n, is scaled by a reduced mass factor to obtain the reduced mass radial vector r.

$$\bar{r} = \sqrt{2u}\bar{r}^n \qquad \text{Eq. 165}$$

$$\bar{p} = \frac{1}{\sqrt{2u}}\bar{p}^{n} \qquad \text{Eq. 166}$$

which yields the following Schrodinger equation for the relative motion mass-scaled coordinates:

$$(\bar{p}^2 + V(\bar{r}))\Psi = E\Psi \qquad \text{Eq. 167}$$

Notice that the energy parameter is unchanged and remains in its original units (e.g. a.u.).

The three-particle Schrodinger Equation, assuming pairwise interactions, is given by

$$\left(\frac{p_1^2}{2m_1} + \frac{p_2^2}{2m_2} + \frac{p_3^2}{2m_3} + V(\bar{r}_1,\bar{r}_2) + V(\bar{r}_2,\bar{r}_3) + V(\bar{r}_3,\bar{r}_1)\right)\Psi = E\Psi \qquad \text{Eq. 168}$$

When dealing with three particle systems it is again convenient to separate the motion into that of the center of mass and the relative motion as given by the Jacobi coordinates. The Hamiltonian is separated into a part H_{CM} involving the center of mass coordinates and H_{rel} containing Jacobi coordinates.

Using the α three-body Jacobi coordinates, the three-body Hamiltonian (with the center of mass Hamiltonian subtracted out) becomes

$$\frac{p_{x_\alpha}^2}{t_\alpha^2} + \frac{p_{y_\alpha}^2}{u_\alpha^2} + V(x_\alpha) + V(x_\beta) + V(x_\gamma) \qquad \text{Eq. 169}$$

or in mass-scaled coordinates

$$p_{x_\alpha}^2 + p_{y_\alpha}^2 + V(x_\alpha) + V(x_\beta) + V(x_\gamma) \qquad \text{Eq. 170}$$

so that the mass-scaled Schrodinger equation in the α three-body Jacobi coordinates is given by

$$\left(p_{x_\alpha}^2 + p_{y_\alpha}^2 + V(x_\alpha) + V(x_\beta) + V(x_\gamma)\right)\Psi = E\Psi \qquad \text{Eq. 171}$$

In terms of the rotational angular momentum of the bound pair, given by the operator $\hat{l}_{x_\alpha}$, and of the orbital angular momentum of the free particle about the bound pair, $\hat{l}_{y_\alpha}$, the quantum-mechanical form of the mass-scaled Schrodinger equation, with pairwise Coulomb potentials, is thus

$$\left(-\frac{1}{x_\alpha}\frac{\partial}{\partial x_\alpha^2}x_\alpha - \frac{1}{y_\alpha}\frac{\partial}{\partial y_\alpha^2}y_\alpha + \frac{\hat{l}_{x_\alpha}^2}{x_\alpha^2} + \frac{\hat{l}_{y_\alpha}^2}{y_\alpha^2} + \frac{q_\alpha}{x_\alpha} + \frac{q_\beta}{x_\beta} + \frac{q_\gamma}{x_\gamma}\right)\Psi = E\Psi \qquad \text{Eq. 172}$$

where the coordinates x_β and x_γ are found via the previously derived mass-scaled Jacobi coordinate transformation equations with inputs (x_α, y_α).

Each term in the above equation has units of energy in atomic units.

APPENDIX B

DISCRETE VARIABLE REPRESENTATION (DVR)

This appendix summarizes the Discrete Variable Representation expansion of wave functions in scattering systems. More in-depth details are found in references 22 to 35.

B.1 Introduction

If the Schrodinger equation is in the form $H\Psi+V\Psi = E\Psi$, and if the solution to $H\Psi = E\Psi$ is known, then the Hamiltonian, H, possesses a complete set of orthonormal Eigen functions, $\psi_v(x)$. A differential method to solve the time-independent Schrodinger equation is to use the Hamiltonian basis where one expands the wave function

$$\Psi(x) = \sum_{\nu=1}^{\infty} c_\nu \psi_\nu(x) \qquad \text{Eq. 173}$$

and this expansion is substituted into the full Schrodinger equation to find the expansion coefficients and hence the wave function.

If the expansion is truncated so that only a finite number of basis functions are implemented, then the time-independent Schrodinger equation is solved using the

finite basis representation, FBR. Using any basis that consists of orthogonal polynomials is equivalent to using Gaussian quadratures since quadrature points and weights can be selected such that the overlap integral is exact. Using this method the potential energy matrix is also equivalent to using Gaussian quadratures. The potential energy matrix may be diagonalized using a unitary transformation.

A set of basis functions, $\psi_v(x)$, are orthogonal and complete if they satisfy the following relations

$$<\psi_\nu \mid \psi_{\nu'}>=\int (\psi_\nu(x))^* \psi_{\nu'}(x)dx = \delta_{\nu\nu'} \quad \text{(orthogonality)} \qquad \text{Eq. 174}$$

$$<x \mid x'>=\sum_{\nu=1}^{\infty} (\psi_\nu(x))^* \psi_\nu(x') = \delta(x-x') \quad \text{(completeness)} \qquad \text{Eq. 175}$$

If there exists a set of basis functions such that the N-point Gaussian quadrature approximation to Eq. 174 is exact for the first N orthogonalities, then for those finite sets of basis functions (hence FBR), the orthogonality and completeness relations become

$$<\nu \mid \nu'>=\sum_{i=1}^{N} (\psi_\nu(x_i))^* \psi_{\nu'}(x_i) w_i = \delta_{\nu\nu'} \quad \text{(orthogonality)} \qquad \text{Eq. 176}$$

$$<i \mid i'>=\sum_{k=1}^{N} (\psi_\nu(x_i))^* \psi_\nu(x_{i'}) \sqrt{w_i w_{i'}} = \delta_{ii'} \quad \text{(completeness)} \qquad \text{Eq. 177}$$

where

ν = index of basis functions

i = index of Gaussian quadrature point

x_i = Gaussian quadrature point

w_i = Gaussian quadrature weight associated with the point x_i

$()^*$ = represents the complex conjugate

The elements of the potential energy matrix are given by

$$<\nu|V(x)|\nu'>=\sum_i \psi_\nu(x_i)V(x_i)\psi_{\nu'}(x_i)w_i$$

This matrix may be diagonalized using a diagonalization algorithm or equivalently by using a unitary transformation.

However, using an orthogonal and complete set of N basis functions, the DVR method associates the basis functions with quadrature points and the potential energy operator is automatically represented by a diagonal matrix.

The diagonal elements are the values of the potential at the quadrature points. This set of basis functions yields a discrete orthogonal system. The approximation involved in the DVR is identical to the approximation

involved with FBR. As the number of quadrature points and basis functions approach infinity the DVR and FBR results approach the exact solution.

The FBR basis functions, ψ_ν, ν = 1 to N, and DVR basis functions, ϕ_i, i = 1 to N, are related by a unitary transformation, the same unitary transformation that diagonalizes the potential energy matrix obtained using the FBR method.

$$\phi_i(x) = \sum_{\nu=1}^{N} (A_{i\nu})^* \psi_\nu(x) = \sum_{\nu=1}^{N} (A^+)_{\nu i} \psi_\nu(x) \qquad \text{Eq. 178}$$

where the unitary matrix element $A_{i\nu}$ is given by the FBR basis function evaluated at a quadrature point x_i multiplied by the square root of the Gaussian weight for that quadrature point. A^+ is the Hermitian adjoint of A.

$$A_{i\nu} = \sqrt{w_i}\,\psi_\nu(x_i) \qquad \text{Eq. 179}$$

A is unitary since

$$(A^+A)_{\nu\nu'} = \sum_{i=1}^{N} (A^+)_{\nu i} A_{i\nu'} = \sum_{i=1}^{N} (A_{i\nu})^* A_{i\nu'}$$
$$= \sum_{i=1}^{N} \sqrt{w_i}\,(\psi_\nu(x_i))^* \sqrt{w_i}\,\psi_{\nu'}(x_i) = \delta_{\nu\nu'} \qquad \text{(orthogonal)} \qquad \text{Eq. 180}$$

and

$$(AA^{+})_{ii'} = \sum_{\nu=1}^{N} A_{i\nu}(A^{+})_{\nu i'} = \sum_{\nu=1}^{N} A_{i\nu}(A_{i'\nu})^{*}$$
$$= \sum_{\nu=1}^{N} (\psi_{\nu}(x_{i'}))^{*}\psi_{\nu}(x_i)\sqrt{w_{i'}w_i} = \delta_{ii'} \qquad \text{(completeness)} \quad \text{Eq. 181}$$

The diagonalization of V^{FBR} is given by

$$V^{diag} = AV^{FBR}A^{+} \qquad \text{Eq. 182}$$

Evaluating the DVR basis functions at the quadrature point, x_l, using the completeness property gives

$$\phi_{lk} \equiv \phi_k(x_l) = \sum_{\nu=1}^{N} (A_{k\nu})^{*}\psi_{\nu}(x_l) = \sum_{\nu=1}^{N} \frac{(A_{k\nu})^{*}A_{l\nu}}{\sqrt{w_l}} = \frac{\delta_{kl}}{\sqrt{w_l}} \qquad \text{Eq. 183}$$

It can be shown that, using the DVR basis functions, the potential energy matrix V is diagonal if V is a multiplicative operator.

$$< \phi_{\nu} \mid V \mid \phi_{\nu'} >= \sum_{k=1}^{N} w_k(\phi_{\nu}(x_k))^{*}V(x_k)\phi_{\nu'}(x_k) = \sum_{k=1}^{N} \delta_{\nu k}V(x_k)\delta_{\nu' k} = V(x_{\nu})\delta_{\nu\nu'} \qquad \text{Eq. 184}$$

Approximating a function $\Psi(x)$ using the DVR basis by $\Psi(x) = \sum_j a_j \phi_j(x)$ with $\Psi(x_l) = a_l / \sqrt{w_l}$ the coefficient is derived by

$$a_l(r) = \int \phi_l(x)\tilde{\Psi}(x)dx$$
$$\approx \sum_k \phi_l(x_k)\tilde{\Psi}(x_k)w_k$$
$$= \sum_k \frac{\delta_{lk}}{\sqrt{w_k}}\tilde{\Psi}(x_k)w_k \qquad \text{Eq. 185}$$
$$= \Psi(x_j)\sqrt{w_j}$$

B.2 Two-Dimensional FBR Basis Functions

For the problems that are discussed in this paper, the two-dimensional FBR orthogonal basis functions are the spherical harmonics.

$$J_l^m(\theta,\phi) = \sqrt{\frac{2l+1}{4\pi}\frac{(l-m)!}{(l+m)!}} P_l^m(\cos(\theta)) e^{im\phi} \qquad \text{Eq. 186}$$

The spherical harmonics have the orthogonality property

$$\int_0^{2\pi}\int_0^{\pi} (J_l^m(\theta,\phi))^* J_{l'}^{m'}(\theta,\phi)\sin(\theta)d\theta d\phi = \delta_{ll'}\delta_{mm'} \qquad \text{Eq. 187}$$

The Gaussian quadrature approximation to this integral is given by

$$\sum_{i_\phi=1}^{N_\phi}\sum_{i_\theta=1}^{N_\theta} (J_l^m(\theta_{i_\theta},\phi_{i_\phi}))^* J_{l'}^{m'}(\theta_{i_\theta},\phi_{i_\phi}) w_{i_\theta} w_{i_\phi} \qquad \text{Eq. 188}$$

where

l = total angular momentum quantum number (eigenvalue of the total angular momentum operator)

m = z-component angular momentum quantum number (eigenvalue of the z-component angular momentum operator)

i_θ = index to θ Gaussian quadrature point

i_ϕ = index to ϕ Gaussian quadrature point

θ_{i_θ} = an angular θ Gaussian quadrature point indexed by i_θ

ϕ_{i_ϕ} = an angular ϕ Gaussian quadrature point indexed by i_ϕ

w_{i_θ} = weight associated with the point indexed by i_θ

w_{i_ϕ} = weight associated with the point indexed by i_ϕ

N_θ = number of angular θ Gaussian quadrature points

N_ϕ = number of angular ϕ Gaussian quadrature points

The two-dimensional spherical harmonic functions are a product of two one-dimensional functions, the modified Legendre polynomials (function of θ) and a complex exponential (function of ϕ).

To reduce these equations to a convenient one-dimensional form the following notation is implemented

ν = index representing the pair of quantum numbers (l,m)

i = index representing the pair of indices (i_θ,i_ϕ)

Ω = angle representation of the pair of angles (θ,ϕ)

N = number of Ω Gaussian quadrature points, $N = N_\theta * N_\phi$

Ω_i = angular Ω Gaussian quadrature point indexed by i

w_i = weight associated with the quadrature point indexed by i and given by $w_i = w_{i_\theta} * w_{i_\phi}$

The Gaussian quadrature approximation is rewritten as

$$\sum_{i=1}^{N} (J_{\nu}(\Omega_i))^{*} J_{\nu'}(\Omega_i) w_i \qquad \text{Eq. 189}$$

Note that, while not a requirement on the DVR basis functions, for this paper the number of angular quadrature grid points is equal to the number of angular momentum quantum number pairs. The number of angular quadrature grid points is also restricted to odd numbers so that the basis functions are linearly independent on the DVR grid.

Discrete orthogonality and completeness are given by

$$<\nu|\nu'>= \sum_{i=1}^{N} (J_{\nu}(\Omega_i))^{*} J_{\nu'}(\Omega_i) W_i = \sum_{i=1}^{N} (J_{i\nu})^{*} J_{i\nu'} w_i \qquad \text{Eq. 190}$$

$$<i|i'>= \sum_{\nu=1}^{N} (J_{\nu}(\Omega_i))^{*} J_{\nu}(\Omega_{i'}) \sqrt{w_i w_{i'}} = \sum_{\nu=1}^{N} (J_{i\nu})^{*} J_{i'\nu} \sqrt{w_i w_{i'}} \qquad \text{Eq. 191}$$

Let $J_{i\nu}$ be a matrix element of the matrix J: $J_{i\nu} = J_{\nu}(\Omega_i)$. Let the matrix J^{-1} have matrix elements $(J^{-1})_{\nu i} = (J^{+})_{\nu i} = (J_{i\nu})^{*}$, where J^{+} is the Hermitian adjoint of the matrix J. The previous equations are also written as

$$<\nu|\nu'>= \sum_{i=1}^{N} (J^{-1})_{\nu i} J_{i\nu'} w_i \qquad \text{Eq. 192}$$

$$<i|i'>= \sum_{\nu=1}^{N} (J^{-1})_{\nu i} J_{i'\nu} \sqrt{w_i w_{i'}} \qquad \text{Eq. 193}$$

B.3 Angular Grid Gaussian Quadrature Points And Weights

The selection of the pairs of angular grid quadrature points and corresponding weights are not unique. However, for a given set of quadrature grid points the corresponding weights are unique. This section describes a mathematically convenient method of obtaining the angular grid quadrature points and weights. For the purposes of this paper, this method is arbitrarily referred to as the "traditional method". This method is used for this paper and follows that of reference 29.

N_θ and N_ϕ are equal and each is an odd number.

The θ angular quadrature points, θ_{i_θ}, are found by obtaining the roots of the N_θ^{th} order Legendre polynomial.

$$P_{N_\theta}(\cos(\theta_{i_\theta})) = 0 \qquad \text{Eq. 194}$$

The ϕ angular quadrature points, ϕ_{i_ϕ}, are found by evenly spacing each point over the interval [0, 2π] in the following manner

$$\phi_{i_\phi} = \pi(2i_\phi - 1)/N_\phi \qquad \text{Eq. 195}$$

The θ angular weights are given by the Gauss-Legendre weights

$$w_{i_\theta} = \left(\frac{\sqrt{2}}{\sin(\theta_{i_\theta}) P'_{N_\theta}(\cos(\theta_{i_\theta}))} \right)^2 \qquad \text{Eq. 196}$$

The ϕ angular weights are given by the Gauss-Fourier weights

$$w_{i_\phi} = 2\pi / N_\phi \qquad \text{Eq. 197}$$

Figure 27 shows an example of the traditional angular grid for $N_\theta = N_\phi = 3$. See also Figure 3 of Chapter 2 for a three-dimensional representation.

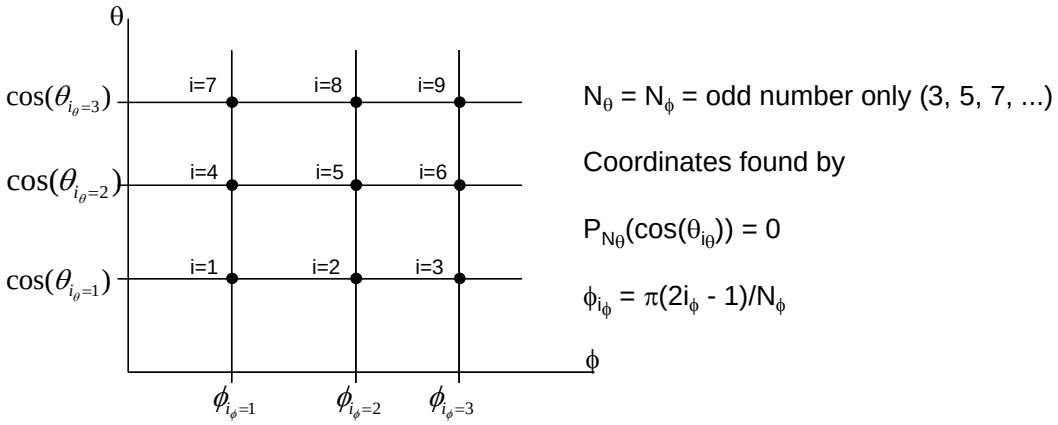

Figure 27. Traditional Angular Grid Example.

Evaluating finds $\theta_1 = 140.718^0$, $\theta_2 = 90^0$, $\theta_3 = 39.2315^0$ and $\phi_1 = 60^0$, $\phi_2 = 180^0$, $\phi_3 = 300^0$.

B.4 Angular Momentum Quantum Numbers

The selection of the angular momentum quantum numbers is not unique. This section describes the "traditional" and "non-traditional" method of obtaining the angular

momentum quantum numbers. "Traditional" is used in the same sense as it was in the preceding section, referring to a method commonly in use. The non-traditional method described also follows that of reference 29.

In the non-traditional method the total angular momentum quantum number runs from 1 to $3(N_\theta-1)/2$ and all possible angular momentum quantum numbers (l,m) are used up to $l=(N_\theta-1)/2$. For $l > N_\theta$, the z-component angular momentum numbers, m, are used only up to $(N_\theta-1)/2$. For $l > (N_\theta-1)$ only the following z-component angular momentum numbers are used $(l-N_\theta) < m < (N_\theta-1)/2$.

An example of angular momentum quantum numbers for the non-traditional method are shown in Figure 28, for N_θ = 3, 5, and 7.

$N_\theta=3$ m	l	$N_\theta=5$ m	l	$N_\theta=7$ m	l
0	0	0	0	0	0
-1 0 1	1	-1 0 1	1	-1 0 1	1
-1 0 1	2	-2 -1 0 1 2	2	-2 -1 0 1 2	2
-1 1	3	-2 -1 0 1 2	3	-3 -2 -1 0 1 2 3	3
		-2 -1 0 1 2	4	-3 -2 -1 0 1 2 3	4
		-2 -1 1 2	5	-3 -2 -1 0 1 2 3	5
		-2 2	6	-3 -2 -1 0 1 2 3	6
				-3 -2 -1 1 2 3	7
				-3 -2 2 3	8
				-3 3	9

Figure 28. Non-Traditional Quantum Numbers Example.

For this paper the correlation between the index ν and the angular momentum number pair (l,m) is such that the

lowest available index ν corresponds to the lowest remaining available total angular momentum l and its lowest available remaining z-component m. The relation between ν and (l,m) for N_θ = 3 is as follows

ν	0	1	2	3	4	5	6	7	8
(l,m)	(0,0)	(1,-1)	(1,0)	(1,1)	(1,-1)	(1,0)	(1,1)	(1,-1)	(1,1)

In the traditional method the total angular momentum quantum number runs from 1 to (N_θ-1) and all possible angular momentum quantum numbers (l,m) are used for each l.

An example of angular momentum quantum numbers for the traditional method are shown in Figure 29, for N_θ = 3, 5, and 7.

N_θ = 3					N_θ = 5									N_θ = 7												
	m				l	m								l	m											l
		0			0					0				0											0
	-1	0	1		1				-1	0	1			1				-1	0	1					1
-2	-1	0	1	2	2			-2	-1	0	1	2		2			-2	-1	0	1	2				2
							-3	-2	-1	0	1	2	3	3			-3	-2	-1	0	1	2	3			3
						-4	-3	-2	-1	0	1	2	3	4	4		-4	-3	-2	-1	0	1	2	3	4		4
																-5	-4	-3	-2	-1	0	1	2	3	4	5	5
															-6	-5	-4	-3	-2	-1	0	1	2	3	4	5	6	6

Figure 29. Traditional Quantum Numbers Example.

The correlation between ν and (l,m) follows the same pattern as the non-traditional case. The relation between ν and (l,m) for N_θ = 3 is as follows

ν	0	1	2	3	4	5	6	7	8
(l,m)	(0,0)	(1,-1)	(1,0)	(1,1)	(2,-2)	(2,-1)	(2,0)	(2,1)	(2,2)

B.5 Gram-Schmidt Orthogonally And Completeness

Let $\{u_i\}$ be a set of linearly independent basis functions on a set U where the inner product $\langle u_i | u_{i'} \rangle$ is defined. Then an orthonormal set of functions $\{V_i\}$ are derived as follows

$$v_i = u_i + \sum_{j=0}^{i-1} a_{i,j} V_j \; ; \quad V_i = \frac{v_i}{< v_i \mid v_i >} \; ; \quad a_{i,j} = - < u_i | V_i > \qquad \text{Eq. 198}$$

Note that the orthonormal functions are written as a linear combination of the original set

$$V_i = \sum_{j=0}^{i} A_{i,j} v_j \qquad \text{Eq. 199}$$

where $A_{i,j}$ are elements of the upper triangular transformation matrix.

Using the spherical harmonics angular basis functions, if upon implementation on the computer $\langle \nu | \nu' \rangle = \delta_{\nu\nu'}$ for all (ν, ν') then the basis functions are orthogonal. If $\langle i | i' \rangle = \delta_{ii'}$ for all (i, i') then the basis functions are complete.

The angular FBR basis functions must satisfy orthogonality and completeness for all ν, ν' up to N and for all i, i' up to to N so that the unitary transformation matrix may be obtained.

Using the angular FBR basis functions with the traditional angular grid and non-traditional quantum numbers finds orthogonality satisfied for l, l' < N_θ and m = m' (assuming negligible numerical precision error). However for other l, l', m, m' combinations orthogonality may not be satisfied (precision error may also void orthogonality for some cases where it should be exact). For these cases, the basis functions are orthogonalized with the Gram-Schmidt algorithm based on the orthogonality overlap $\langle \nu | \nu' \rangle$.

The Gram-Schmidt method forms an orthogonal and complete set of basis functions by obtaining new basis functions that are a linear combination of the spherical harmonic basis functions.

Denote this set of basis functions by

$$S_\nu(\Omega) = \sum_{\nu'=1}^{N} C_{\nu\nu'} J_{\nu'}(\Omega) \qquad \text{Eq. 200}$$

where $C_{\nu\nu'}$ are the Gram-Schmidt coefficients.

An example of an implementation of the modified Gram-Schmidt algorithm and coefficient extraction using the angular and momentum grid is shown in the following pseudo code example.

S = J

```
S+ = J+
C = I

for ν=1 to MatrixSize step 1
  Rνν = √<Sν|Sν>
  for j=1 to MatrixSize step 1
    Sjν     = Sjν/Rνν
    (S+)νj  = (Sjν)+
  end do
  for c=1 to n step 1
    Cνc = Cνc/Rνν
  enddo

  for ν'=ν+1 to MatrixSize step 1
    Rνν' =<Sν|Sν'>
    for j=1 to MatrixSize step 1
      Sjν'    = Sjν' - Sjν*Rνν'
      (S+)ν'j = (Sjν')+
    end do
    Cν'ν = -Rνν'
  end do
  for c=ν-1 to 1 step -1
    for r=ν+1 to MatrixSize step 1
      Crc = Crc + Cνc*Crν
    end do
  end do
  for r=ν+1 to MatrixSize step 1
    Crν = Crν/Rνν
  end do
end do

C = CT

where

J = original FBR basis function matrix

S = Gram-Schmidt FBR basis function matrix

C = Gram-Schmidt linear expansion coefficients

I = Identity matrix
```

C^T = Transpose of C

If the original set of basis functions are complete and orthogonal then C is the identity matrix. $S_\nu(\Omega)$, with $(S^{-1})_{\nu i} = (S^+)_{\nu i} = (S_{i\nu})^*$ denote a set of FBR basis functions that are guaranteed to be orthogonal and complete for all ν, ν' up to N and for all i, i' up to to N.

$$<\nu|\nu'>=\sum_{i=1}^{N}(S^{-1})_{\nu i}S_{i\nu'}w_i=\delta_{\nu\nu'} \qquad \text{(orthogonality)} \qquad \text{Eq. 201}$$

$$<i|i'>=\sum_{\nu=1}^{N}(S^{-1})_{\nu i}S_{i'\nu}\sqrt{w_i w_{i'}}=\delta_{ii'} \qquad \text{(Completeness)} \qquad \text{Eq. 202}$$

For this thesis the total number of angular momentum quantum numbers, ν, is equal to the total number of angular quadrature points, j. The total number is also an odd number. This is not a strict requirement on the use of DVR functions. However, for the selection of angular basis functions, the selection of angular quantum grid points, and the selection of grid angles the Gram-Schmidt expansion fails when the total number of DVR basis functions is an even number since the basis functions are not linearly independent on the ν = (l, m) and Ω = (θ, ϕ) grid.

A graphical example of this is shown in Figures 30 and 31. Figure 30 shows the general form of the spherical

harmonic functions (real and imaginary parts) for l = N-1 and m = N/2 with N = 4. From the figure it is obvious that these two functions are not linearly dependent.

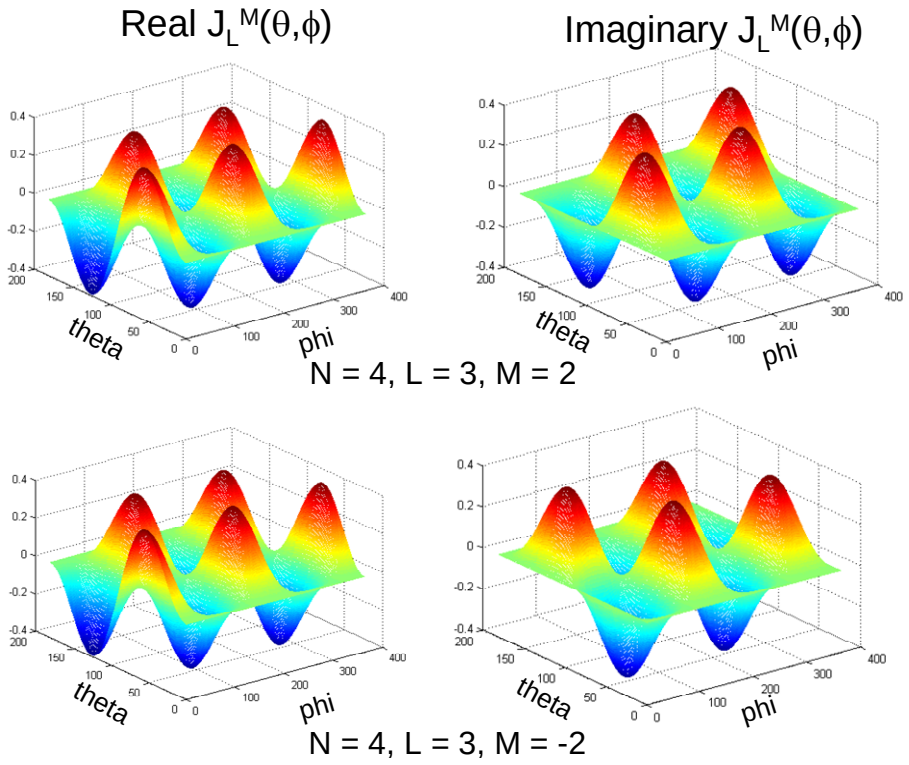

Figure 30. Plots of Spherical Harmonic Functions for N = 4, L = 3, and |M| = 2.

However, using a set of azimuthal grid angles, ϕ, of 45, 135, 225 and 315 degrees demonstrates that on this grid these two functions are linearly dependent. On this grid, independent of the polar angle, θ, the real part of each function is zero. And the imaginary parts are proportional to each other by minus one. This results in

the two functions being linearly dependent on the grid. This is visually demonstrated in Figure 31.

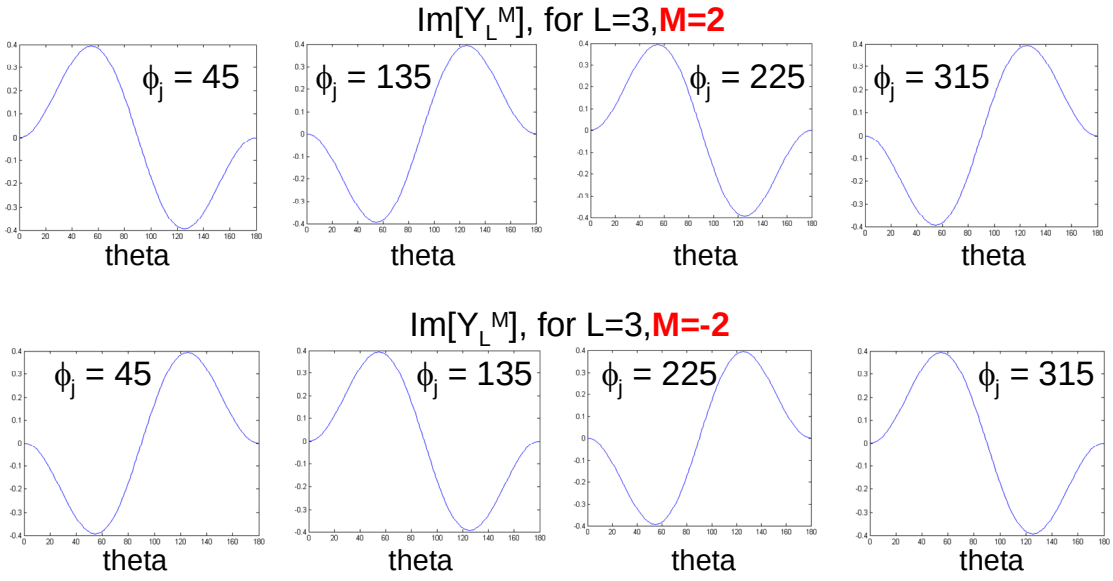

Figure 31. Imaginary Part of Spherical Harmonic Functions on Even Number Grid.

For a numerical example, suppose N is an even number. Let (l, m) be the angular grid point that has a value of (N-1, N/2). Then the sum of two basis functions is proportional to

$$J_{N-1}^{N/2}(\theta,\phi) + J_{N-1}^{-N/2}(\theta,\phi) \propto [1+(-1)^{N/2} e^{-2i\phi N/2}] \qquad \text{Eq. 203}$$

The azimuthal grid angle is given by $\phi_k = (2k-1)\pi/N$, k = 1, ..., N. The exponent can be rewritten as $-i(2k-1)\pi$, which is always an odd multiple of $i\pi$. The term $(-1)^{N/2}$ is -1 if

N/2 is odd and +1 if N/2 is even. The basis functions are equal if N/2 is odd and are of opposite sign if N/2 is even. This is true for all the grid angles. Thus, on the grid, these functions are not linearly independent if N is even, and the Gram-Schmidt algorithm does not orthogonalize this set of basis functions.

B.6 Two-Dimensional DVR

The two-dimensional or two-variable DVR basis functions are constructed from the FBR basis functions as described previously. For the case of spherical harmonic basis functions the DVR basis functions are given by

$$\phi_j(\Omega) = \sum_{\nu=1}^{N} (A_{j\nu})^* S_\nu(\Omega) = \sum_{\nu=1}^{N} (A^+)_{\nu j} S_\nu(\Omega) \qquad \text{Eq. 204}$$

with

$$A_{j\nu} = \sqrt{w_j} S_\nu(\Omega_j) = \sqrt{w_j} S_{j\nu} \qquad \text{Eq. 205}$$

and

$$(A^+)_{\nu j} = (A_{j\nu})^* = \sqrt{w_j} (S_{j\nu})^* = \sqrt{w_j} (S^+)_{\nu j} \qquad \text{Eq. 206}$$

so that the two-dimensional DVR is given by

$$\phi_j(\Omega) = \sqrt{w_j} \sum_{\nu=1}^{N} (S_{j\nu})^* S_\nu(\Omega) \qquad \text{Eq. 207}$$

A three-dimensional wave function $\Psi(r,\theta,\phi) = \Psi(r,\Omega)$ is approximated using the DVR functions as follows

$$\Psi(r,\Omega) \approx \sum_{j=1}^{N} \psi_j(r)\phi_j(\Omega) = \sum_{j=1}^{N}\sum_{\nu=1}^{N} \sqrt{w_j}\,(S_{j\nu})^* S_\nu(\Omega)\psi_j(r) \qquad \text{Eq. 208}$$

where $\psi_j(r)$ are the radial expansion coefficients.

When evaluated at the k^{th} angular grid point

$$\Psi(r,\Omega_k) = \sum_{j=1}^{N} \psi_j(r)\phi_j(\Omega_k) = \sum_{j=1}^{N} \psi_j(r)\frac{\delta_{jk}}{\sqrt{w_k}} = \frac{\psi_k(r)}{\sqrt{w_k}} \qquad \text{Eq. 209}$$

the wave function reduces to the corresponding expansion coefficient divided by the square root of the corresponding weight.

As an example, in DVR notation the ground state hydrogen wave function is written as

$$\phi^h(\bar{x}) = \sum_{j=1}^{N}\sum_{\nu=1}^{N} J_\nu(\hat{x})(J^{-1})_{\nu j}\sqrt{w_j}\,\psi_j(x) \qquad \text{Eq. 210}$$

with

$$\psi_j(x) = \phi^h(x)Y_0^0(\hat{x}_j)\sqrt{w_j} \qquad \text{Eq. 211}$$

so that when evaluated at the k^{th} two-dimensional DVR grid angle

$$\begin{aligned}
\phi^h(\bar{x})\Big|_{\hat{x}_k} &= \sum_{j=1}^{N}\sum_{\nu=1}^{N} J_\nu(\hat{x}_k)(J^{-1})_{\nu j}\sqrt{w_j}\,\psi_j(x) \\
&= \sum_{j=1}^{N}\Big(\sum_{\nu=1}^{N} J_\nu(\hat{x}_k)(J^{-1})_{\nu j}\sqrt{w_j}\sqrt{w_k}\Big)\phi^h(x)Y_0^0(\hat{x}_j)\sqrt{w_j}/\sqrt{w_k} \\
&= \sum_{j=1}^{N}\delta_{jk}\phi^h(x)Y_0^0(\hat{x}_j)\sqrt{w_j}/\sqrt{w_k} \\
&= \phi^h(x)Y_0^0(\hat{x}_k)
\end{aligned}$$

which is the normal ground state hydrogen wave function evaluated at $\hat{x}_k$.

B.7 Four-Dimensional FBR Basis Functions

Using spherical coordinates, adding three more degrees of freedom to a problem requires two additional angular degrees of freedom and one additional radial degree of freedom. Choosing an FBR for this system could be done by using a direct product of the two-dimensional FBR basis functions. However, for problems of the type that are discussed in this paper, which uses the Jacobi relative coordinates, the angular four-variable bipolar basis is a more convenient basis. Thus, the bipolar basis is chosen as the FBR basis functions. The bipolar basis are simultaneous eigenfunctions of the three-body total angular momentum $\bar{L}$, its z-axis projection M, rotational angular momentum of the bound pair $\bar{l}_x$ and the orbital angular momentum of the free particle about the bound pair $\bar{l}_y$.

The bipolar basis element is defined as

$$Y^{L,M}_{l_x,l_y}(\hat{x},\hat{y}) = \sum_{m_x+m_y=M} (Y^{m_x}_{l_x}(\theta_x\phi_x) Y^{m_y}_{l_y}(\theta_y\phi_y) C^{L,M}_{l_x,m_x,l_y,m_y}) = [Y^{m_x}_{l_x}(\hat{x}) \otimes Y^{m_y}_{l_y}(\hat{y})]^{L,M} \quad \text{Eq. 212}$$

where

L = total angular momentum quantum number, L = (l_x+l_y), (l_x+l_y-1), ..., $|l_x-l_y|$

M = total angular momentum projection

l_x = rotational angular momentum of the bound pair

l_y = the orbital angular momentum of the free particle about the bound pair

m_x = bound pair angular momentum projection along the relative coordinate x-axis

m_y = orbital angular momentum projection along the relative coordinate y-axis

$C^{L,M}_{l_x,m_x,l_y,m_y}$ = Clebsch-Gordon vector coupling coefficient, $\langle l_x, l_y, m_x, m_y | l_x, l_y, L, M \rangle$

$\hat{x}$ = angle representation of the pair of angles Ω_x = (θ_x, ϕ_x)

$\hat{y}$ = angle representation of the pair of angles Ω_y = (θ_y, ϕ_y)

To give the bipolar basis a convenient one-dimensional form the following notation is implemented

ν = index representing the quartet of quantum numbers (L, M, l_x, l_y)

Ω = angle representation of the quartet of angles ($\hat{x}$, $\hat{y}$) = (θ_x, ϕ_x, θ_y, ϕ_y)

The bipolar basis function is then rewritten as

$$Y_\nu(\Omega) = \sum_{m_x+m_y=M} (Y_{l_x}^{m_x}(\hat{x}) Y_{l_y}^{m_y}(\hat{y}) C_{l_x,m_x,l_y,m_y}^{L,M}) \qquad \text{Eq. 213}$$

Selection of the angular Gaussian quadrature points for the bipolar basis functions for this paper consists of the direct product of the two-dimensional angular quadrature points. Let

i = index representing the quartet of indices (i_{θ_x}, i_{ϕ_x}, i_{θ_y}, i_{ϕ_y})

Ω_i = angular Gaussian quadrature point indexed by i, ($\theta_{i_{\theta_x}}$, $\phi_{i_{\phi_x}}$, $\theta_{i_{\theta_y}}$, $\phi_{i_{\phi_y}}$)

N_x = number of Ω_x Gaussian quadrature points relative to the x-axis, $N_{\theta_x} * N_{\phi_x}$

N_y = number of Ω_y Gaussian quadrature points relative to the y-axis, $N_{\theta_y} * N_{\phi_y}$

N = total number of four-dimensional Gaussian quadrature points, $N_x * N_y$

The bipolar basis function evaluated at the i^{th} Gaussian quadrature grid point is denoted as $Y_\nu(\Omega_i)$ and is given by

$$Y_\nu(\Omega_i) = \sum_{m_x+m_y=M} (Y_{l_x}^{m_x}(\theta_{i_{\theta_x}}, \phi_{i_{\phi_x}}) Y_{l_y}^{m_y}(\theta_{i_{\theta_y}}, \phi_{i_{\phi_y}}) C_{l_x,m_x,l_y,m_y}^{L,M}) \qquad \text{Eq. 214}$$

Selection of the angular momentum quantum numbers for the bipolar basis functions for this paper consists of the (L, M, l_x, l_y) combinations resulting from the direct product of the two-dimensional angular momentum quantum numbers for the traditional method. Figure 32 shows an example of the result of a direct product of 2 N = 9 angular momentum grids.

N = 9 (2-D Angular Momentum Grid)

m					l
		0			0
	-1	0	1		1
-2	-1	0	1	2	2

$\nu = \nu_x \otimes \nu_y$ $N_x = 9$, $N_y = 9$ yields (3x3x3x3) = 81 (L, M, l_x, l_y) combinations

M									L	(l_x, l_y)	Possible (L, M, l_x, l_y)
				0					0	(0,0), (1,1),(2,2)	3*1
			-1	0	1				1	(0,1),(1,1),(1,2),(2,2) (1,0),(2,1)	6*3
		-2	-1	0	1	2			2	(0,2),(1,1),(1,2),(2,2) (2,0),(2,1)	6*5
	-3	-2	-1	0	1	2	3		3	(1,2),(2,2), (2,1)	3*7
-4	-3	-2	-1	0	1	2	3	4	4	(2,2)	1*9
											81

Figure 32. Four-Dimensional Angular Momentum Grid For N_x = 9, N_y = 9.

To obtain the ν = (L, M, l_x, l_y) combination given an l_x and an l_y one computes the next lowest available L =

$|l_x-l_y|$, $|l_x-l_y|+1$, ..., (l_x+l_y) and the next available M from -L <= M <= L.

The two-dimensional DVR angular grids need not be of the same size, thus the two-dimensional angular momentum grids also need not be of the same size. Figure 33 shows an example of the angular momentum results of a direct product of an N_x = 9 and an N_y = 25 set of grids.

2-D Angular Momentum Grids

N_x = 9 m	l	N_y = 25 m	l
0	0	0	0
-1 0 1	1	-1 0 1	1
-2 -1 0 1 2	2	-2 -1 0 1 2	2
		-3 -2 -1 0 1 2 3	3
		-4 -3 -2 -1 0 1 2 3 4	4

$\nu = \nu_x \otimes \nu_y$ N_x = 9, N_y = 25 yields (3x3x5x5) = 225 (L, M, l_x, l_y) combinations

M	L	(l_x, l_y)	Possible (L, M, l_x, l_y)
0	0	(0,0), (1,1),(2,2)	3*1
-1 0 1	1	(0,1),(1,1),(1,2),(2,2),(2,3) (1,0),(2,1),	7*3
-2 -1 0 1 2	2	(0,2),(1,1),(1,2),(1,3),(2,2),(2,3),(2,4) (2,0),(2,1)	9*5
-3 -2 -1 0 1 2 3	3	(0,3),(1,2),(1,3),(1,4),(2,2),(2,3),(2,4) (2,1)	8*7
-4 -3 -2 -1 0 1 2 3 4	4	(0,4),(1,3),(1,4),(2,2),(2,3),(2,4)	6*9
-5 -4 -3 -2 -1 0 1 2 3 4 5	5	(1,4),(2,3),(2,4)	3*11
-6 -5 -4 -3 -2 -1 0 1 2 3 4 5 6	6	(2,4)	1*13
			225

Figure 33. Four-Dimensional Angular Momentum Grid For N_x = 9, N_y = 25.

The maximum total angular momentum quantum number for an N_xxN_y grid is denoted by L_{max}. For a 9x9 grid L_{max} = 4, a 9x25 grid has L_{max} = 6, a 25x25 grid has L_{max} = 8, a 25x49 grid has L_{max} = 10 and for a 49x49 grid L_{max} = 12.

The corresponding quadrature weights are also a direct product of the two-dimensional quadrature weights.

$$W_i = w_{i_x} * w_{i_y} = w_{i_{\theta_x}} * w_{i_{\phi_x}} * w_{i_{\theta_y}} * w_{i_{\phi_y}} \quad \text{Eq. 215}$$

Using Gaussian quadratures the integral

$$<\nu \mid \nu'>= \int (Y_\nu(\Omega))^* Y_{\nu'}(\Omega) d\Omega \quad \text{Eq. 216}$$

is approximated by

$$<\nu \mid \nu'>= \sum_{i=1}^{N} (Y_\nu(\Omega_i))^* Y_{\nu'}(\Omega_i) W_i \quad \text{Eq. 217}$$

Also

$$<i \mid i'>= \sum_{i=1}^{N} (Y_\nu(\Omega_i))^* Y_\nu(\Omega_{i'}) \sqrt{W_i W_{i'}} \quad \text{Eq. 218}$$

As in the two-dimensional case, to guarantee orthogonality and completeness, the Gram-Schmidt method forms an orthogonal and complete set of basis functions by obtaining new basis functions that are a linear combination of the bipolar basis functions. The total number of grid points in each dimension must be odd so that the Gram-Schmidt method is successful using the bipolar basis functions on the angular grid.

$$S_\nu(\Omega) = \sum_{\nu'=1}^{N} C_{\nu\nu'} Y_{\nu'}(\Omega) \quad \text{Eq. 219}$$

with

$$<\nu \mid \nu'>= \sum_{i=1}^{N} (S_{i\nu})^* S_{i\nu'} W_i = \delta_{\nu\nu'} \quad \text{(orthogonality)} \quad \text{Eq. 220}$$

$$<i \mid i'>= \sum_{\nu=1}^{N} (S_{i\nu})^* S_{i'\nu} \sqrt{W_i W_{i'}} = \delta_{ii'} \quad \text{(completeness)} \quad \text{Eq. 221}$$

Using this set of basis functions the four-variable angular DVR basis functions are obtained and denoted in the same form as the two-dimensional case.

$$\phi_j(\Omega) = \sqrt{W_j}\sum_{\nu=1}^{N}(S_{j\nu})^* S_\nu(\Omega) \qquad \text{Eq. 222}$$

A six-dimensional wave function $\Psi(x,\theta_x,\phi_x,y,\theta_y,\phi_y)$ is approximated using the DVR functions as follows

$$\Psi(x,\hat{x},y,\hat{y}) \approx \sum_{j=1}^{N}\psi_j(x,y)\phi_j(\Omega) = \sum_{j=1}^{N}\sum_{\nu=1}^{N}\sqrt{W_j}(S_{j\nu})^* S_\nu(\Omega)\psi_j(x,y) \qquad \text{Eq. 223}$$

where $\psi_j(x,y)$ are the two-dimensional radial expansion coefficients.

When evaluated at the k^{th} angular grid point the wave function reduces to the corresponding expansion coefficient divided by the square root of the corresponding weight:

$$\Psi(x,y,\Omega_k) = \sum_{j=1}^{N}\psi_j(x,y)\phi_j(\Omega_k) = \sum_{j=1}^{N}\psi_j(x,y)\frac{\delta_{jk}}{\sqrt{W_k}} = \frac{\psi_k(x,y)}{\sqrt{W_k}} \qquad \text{Eq. 224}$$

To avoid possible numerical instabilities when using Jacobi coordinates or to add more distinct angles between axes it would be desirable to avoid overlap between the Jacobi x and y axis. That is, the x and y axis should have distinct angles such that the angle between the two axes is not zero. If the x and y axes were parallel, then

it is possible, depending on how the spatial grid points are chosen, to have the positron line up close to the same position as the electron in the Jacobi representation. This results in a strong interaction between the two-particles that creates a numerical instability when solving for the wave function.

The angle between Jacobi axes is given by

$$\cos(\theta_{xy}) = \cos(\theta_x)\cos(\theta_y) + \sin(\theta_x)\sin(\theta_y)\cos(\phi_x - \phi_y) \qquad \text{Eq. 225}$$

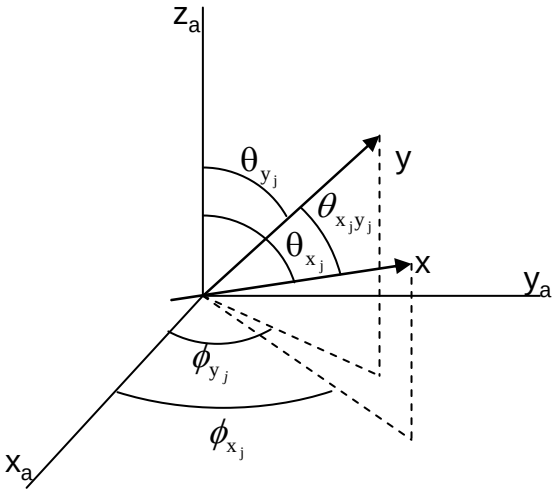

Figure 34. Jacobi Coordinates At The Four-Dimensional DVR Grid Point Indexed By j.

If the DVR quartet angles are a direct product of the two-dimensional DVR pair angles then for cases where $\theta_x = \theta_y$ and $\phi_x = \phi_y$ the angle between the axes is zero. For example for N = 81, $N_x = N_y = 9$, the axis polar angles are $\theta_1 = 140.718^0$, $\theta_2 = 90^0$, $\theta_3 = 39.2315^0$ and the axis azimuthal

angle are $\phi_1 = 60^0$, $\phi_2 = 180^0$, $\phi_3 = 300^0$ for both the x and y axis. This gives the angle between the Jacobi coordinate axes as $\theta = 0^0$, 50.77^0, 66.42^0, 101.54^0, 108.43^0 and 143.13^0, for a total of six distinct angles with one of them being 0^0.

In the general form the Jacobi x-axis and y-axis do not have their origins coaligned. The origin of the y-axis is at the center of mass of the x-axis particles. However in the case of e+ + H scattering, the proton's mass is very much greater than the electron's mass. The center of mass of the Hydrogen atom is nearly at the center of mass of the proton. This results in the x-axis and y-axis having nearly identical origin locations.

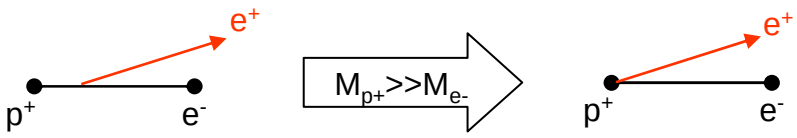

Figure 35. Jacobi Axis Origins Align.

If the angle between the axes is 0^0, then depending on how each axis collocation points are selected it is possible that the positron can line up with the electron causing numerical instability in the equations due to the potential energy between the two-particles.

Shifting the y-axis ϕ angle by $\Delta\phi$ is a convenient method to avoid parallel x and y axis. The resulting four-dimensional DVR is orthogonal and complete. This shift is illustrated in Figure 36 for N = 81, $N_x = N_y = 9$ and $\Delta\phi = 30^0$.

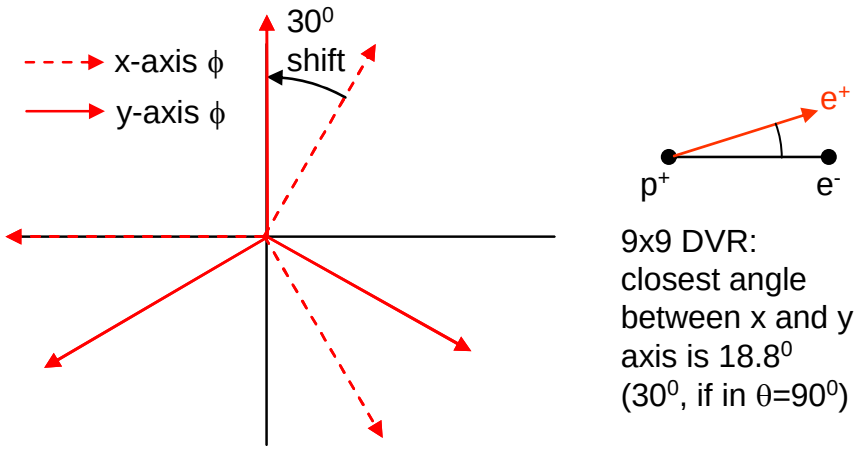

Figure 36. Example Of ϕ Shift For N = 81.

For the Jacobi y axis the angles are $\theta_1 = 140.718^0$, $\theta_2 = 90^0$, $\theta_3 = 39.2315^0$ and $\phi_1 = 90^0$, $\phi_2 = 210^0$, $\phi_3 = 330^0$. This gives the angle between Jacobi axes as $\theta = 18.8^0$, 30.0^0, 53.1^0, 56.8^0, 75.3^0, 90.0^0, 104.7^0, 123.2^0, 126.9^0, 150^0, and 161.2^0 for a total of eleven distinct angles and no overlapping x and y axis. Other shifts may be chosen to give a different set of angles between the axes.

Note that the angles between the individual y-axis vectors remain constant since the shift is the same for all y-axis vectors and therefore the shift is cancelled out in the cosine term.

APPENDIX C

SPLINE INTERPOLATION

This appendix summarizes the Hermite spline numerical technique implemented in this thesis to approximate the radial portion of the wave function. This appendix also discusses using a linear combination of basis functions in the region where they provide a better approximation to the wave function than Hermite splines.

This appendix explains how splines are used to approximate the wave function when given a linear differential equation involving the function. The result is a set of algebraic equations that are solved for the spline function coefficients.

More in depth details are found in references 10 to 21.

C.1 Introduction

This section describes the spline interpolation numerical technique implemented for this thesis. This technique uses well-defined polynomial functions to interpolate a complicated analytical function that is known at certain points called collocation points.

Using a single polynomial of high degree to interpolate a function, in general, does produce acceptable results. Polynomials tend to have an oscillation or "wiggle" problem. Interpolation requires that the interpolating polynomial to go through the points where the function values are known. This may create excessive fit oscillations between the collocation points.

As a remedy for this problem one might try to implement a polynomial of low degree. However, in general, this will not match the function for the entire set of collocation points due to the high frequencies of the function to be fitted.

However, if one groups the set of collocation points into contiguous subintervals and interpolates the function over each subinterval until the entire set is covered, the function may be interpolated using a set of low ordered polynomials.

Points called knots are used to separate each of the contiguous subintervals.

For a reasonable fit the function joints must be smooth where the separate polynomials meet to form a continuous interpolation of the continuous function.

Several techniques have been developed to piece polynomials together so that the total curve fit is an interpolation of the function. One such technique is the piecewise spline curve. In particular piecewise cubic and quintic Hermite polynomials may be implemented to interpolate the radial part of the wave function solution to the Schrodinger equation. This appendix describes both the cubic and the quintic Hermite polynomials.

C.2 Hermite Polynomial Splines

Each low order polynomial function, or Hermite polynomial, is called a basis function. This appendix describes basis functions that consist of cubic splines (third order polynomials) or quintic splines (fifth order polynomials).

Hermite splines are chosen for this thesis because they are smooth, which is to say they yield a good approximation to the function in the least squares sense. Also they span a small, fixed number of only three knots. That is, they cover two sets of collocation points. Quintic splines have the advantage that their derivatives are also smooth. That is, the second derivative is found

at the knots, which is useful since the Schrodinger equation involves second derivatives.

Approximating a function f(x) on a finite domain, [a,b], using splines requires that the interval be made into a grid by defining a set of natural knots $\{x_{k,0}, \ldots, x_{k,Nk}\}$ that divide the interval into $n = N_k-1$ subintervals.

$$a = x_{k,0} < x_{k,1} < \ldots < x_{k,Nk} = b \qquad \text{Eq. 226}$$

The Cardinal Basis Method of Piecewise Hermite Polynomials is implemented in this thesis. The cardinal basis, $\phi_{r,s}(x)$, are n^{th} order polynomials that are nonzero on two adjoining intervals $(x_{k,r-1}, x_{k,r})$ and $(x_{k,r}, x_{k,r+1})$, and zero elsewhere. The index r indicates the center knot for this basis function. The index s is described in the following paragraph.

The total number of n^{th} order basis functions required to cover all the intervals between knots is N_k*N_f, where N_k is the total number of knots and $N_f = (n-1)/2+1$, n = 3 for cubic and 5 for quintic. For example $N_f = 2$ if cubic splines are implemented or $N_f = 3$ if quintic splines are implemented. In the notation for the spline function, $\phi_{r,s}(x)$, the index r represents the r^{th} center knot and s represents the s^{th} spline on that interval, $0 <= s <= N_f$.

The basis functions are continuous and differentiable across the knots. If $N_f = 3$ the second derivative also exists across the knots. To ensure the basis functions with have continuous n^{th} derivatives across the knots, the splines must satisfy the following condition for each of the $x_{k,s}$ natural knots

$$\frac{d^n \phi_{r,s}(x_{k,i})}{dx^n} = \delta_{n,s}\delta_{r,i} \qquad \text{Eq. 227}$$

where $0 < x < N_k$, and $0 < s < N_f - 1$.

The analytical formulas for the cubic Hermite splines are

$$\phi_{i,0}(x) = \begin{cases} \frac{1}{h_i^3}((h_i - (x_{k,i} - x))^2 (h_i + 2(x_{k,i} - x))) & x_{k,i-1} \le x \le x_{k,i} \\ \frac{1}{h_{i+1}^3}((h_{i+1} - (x - x_{k,i}))^2 (h_{i+1} + 2(x - x_{k,i}))) & x_{k,i} \le x \le x_{k,i+1} \\ 0 & \textit{otherwise} \end{cases} \qquad \text{Eq. 228}$$

$$\phi_{i,1}(x) = \begin{cases} -\frac{1}{h_i^2}((h_i - (x_{k,i} - x))^2 (x_{k,i} - x)) & x_{k,i-1} \le x \le x_{k,i} \\ \frac{1}{h_{i+1}^2}((h_{i+1} - (x - x_{k,i}))^2 (x - x_{k,i})) & x_{k,i} \le x \le x_{k,i+1} \\ 0 & \textit{otherwise} \end{cases} \qquad \text{Eq. 229}$$

where $h_i = x_{k,i} - x_{k,i-1}$ and $h_{i+1} = x_{k,i+1} - x_{k,i}$. A plot of each spline basis is given in Figure 37.

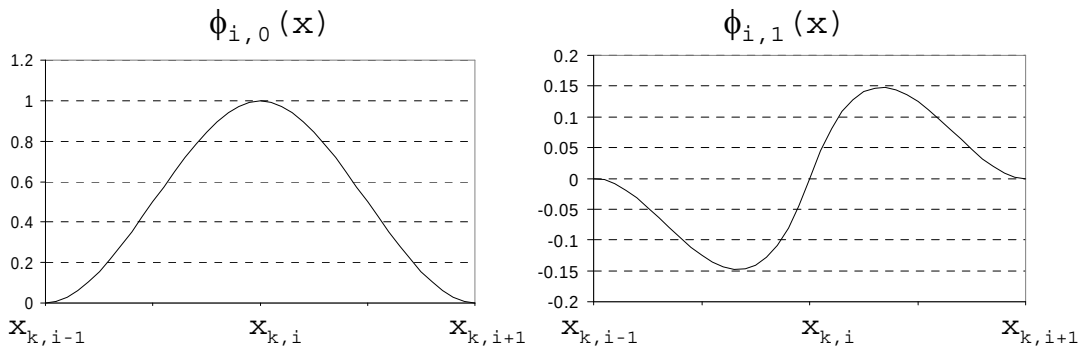

Figure 37. Cubic B-spline Basis.

The analytical formulas for the quintic Hermite splines are

$$\phi_{i,0}(x)=\begin{cases}\dfrac{(x-x_{i-1})^3}{h_i^5}(6(x-x_i)^2-3(x-x_i)h_i+h_i^2) & x_{i-1}\le x\le x_i\\ \dfrac{(x-x_{i+1})^3}{h_{i+1}^5}(-6(x-x_i)^2-3(x-x_i)h_{i+1}-h_{i+1}^2) & x_i\le x\le x_{i+1}\\ 0 & \textit{otherwise}\end{cases} \qquad \text{Eq. 230}$$

$$\phi_{i,1}(x)=\begin{cases}\dfrac{(x-x_{i-1})^3}{h_i^4}((x-x_{i-1})(x-x_i)-4(x-x_i)^2) & x_{i-1}\le x\le x_i\\ \dfrac{(x-x_{i+1})^3}{h_{i+1}^4}((x-x_{i+1})(x-x_i)-4(x-x_i)^2) & x_i\le x\le x_{i+1}\\ 0 & \textit{otherwise}\end{cases} \qquad \text{Eq. 231}$$

$$\phi_{i,2}(x)=\begin{cases}\dfrac{(x-x_{i-1})^3(x-x_i)^2}{2h_i^3} & x_{i-1}\le x\le x_i\\ -\dfrac{(x-x_{i+1})^3(x-x_i)^2}{2h_{i+1}^3} & x_i\le x\le x_{i+1}\,x\\ 0 & \text{otherwise}\end{cases} \qquad \text{Eq. 232}$$

where $h_i = x_{k,i} - x_{k,i-1}$ and $h_{i+1} = x_{k,i+1} - x_{k,i}$. A plot of each spline basis is given in Figure 38.

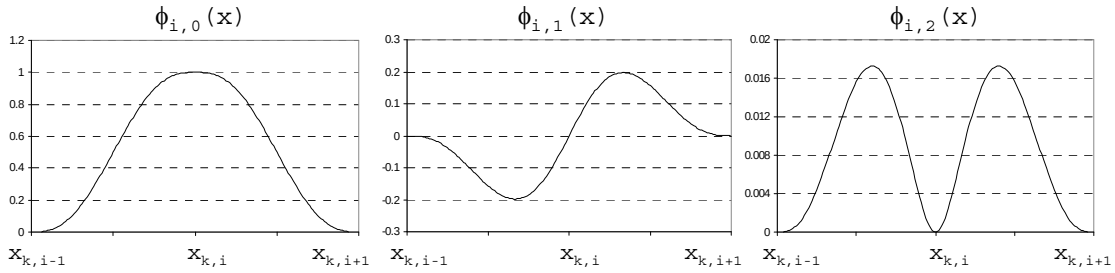

Figure 38. Quintic B-spline Basis.

The approximation to f(x) using the basis functions is written as

$$\tilde{f}(x) = \sum_{r=0}^{N_k-1} \sum_{s=0}^{N_f-1} A_{r,s} \phi_{r,s}(x) \qquad \text{Eq. 233}$$

From the properties of the splines, Eq. 227, the coefficients are immediately known

$$\tilde{f}(x) = \sum_{r=0}^{N_k-1} \sum_{s=0}^{N_f-1} \frac{d^s f(x_{k,r})}{dx^s} \phi_{r,s}(x) \qquad \text{Eq. 234}$$

Of course the purpose of using the spline approximation is that the function f(x) and its derivatives are generally not known at all the knots and thus the coefficients must be obtained via some indirect method. In this thesis they are obtained by solving a differential equation for f(x).

An ordinary differential equation can be approximated by replacing the function, f(x), by the spline approximation (Eq. 233) and requiring the equation to be satisfied at a finite number of collocation points. This

is called the collocation method. Proper choice of the collocation points allows the solution to converge rapidly.

Optimal collocation points are the Gauss-Legendre integration points of the subintervals. This is called orthogonal collocation, and is based on the same idea as the Gauss quadrature integration technique. For cubic splines there are two collocation points between each knot. This gives four points (two on each side of the central knot) for the third order curve fit. For quintic splines there are three collocation points. This gives six points (three on each side of the central knot) for the fifth order curve fit.

For the interval [0,1] the two point Gauss-Legendre points are given by $(1\pm1/\sqrt{3})/2$. For the interval [-1,1] they are given by $\pm1/\sqrt{3}$. In general, for the interval [a,b] the two point Gauss-Legendre points are given by $(b-a)(1\pm1/\sqrt{3})/2+a=(b+a)/2\pm(b-a)/2\sqrt{3}$.

The general formula for the three point Gauss-Legendre points for the interval [a,b] is given by the set $\{\,(b+a)/2,\ (b+a)/2\pm(b-a)\sqrt{3/20}\,\}$.

C.3 Interpolation Of A Function Using Hermite Polynomial Splines

A simple example of using Hermite polynomial splines to approximate a function is simply that of fitting a function f(x) which is known at the collocation points.

The approximant is written as

$$\tilde{f}(x) = \sum_{r=0}^{N_k-1} \sum_{s=0}^{N_f-1} A_{r,s}\phi_{r,s}(x) \qquad \text{Eq. 235}$$

For notation let the single index rs represent the pair of indices (r,s), for example rs = r*N_f+s, the approximant is written as

$$\tilde{f}(x) = \sum_{rs=0}^{N_k N_f-1} A_{rs}\phi_{rs}(x) \qquad \text{Eq. 236}$$

Requiring that

$$\tilde{f}(x_i) = f(x_i) \qquad \text{Eq. 237}$$

at every collocation point x_i allows the above equations to be combined to yield the matrix equation

$$\underline{\underline{\phi}}\,\overline{A} = \bar{f} \qquad \text{Eq. 238}$$

where

$\underline{\underline{\phi}}$ = the matrix with elements $\underline{\underline{\phi}}_{i,rs} = \phi_{rs}(x_i)$

$\overline{A}$ = expansion coefficient vector with coefficients A_{rs}

$\bar{f}$ = the vector of function values, $f(x_i)$

There are a total of $N_k N_f$ basis functions and basis function expansion coefficients. Using the Gauss-Legendre collocation points between each adjacent pair of knots yields $(N_k-1)N_f$ collocation points. In addition to Eq. 238 there must be N_f additional equations or boundary conditions to make the matrix square. For this example additional equations are obtained by adding N_f extra points to the collocation set. For example adding knots, $f(x_{k,i})$ for $i = 0...N_f$.

The matrix, $\underline{\underline{\phi}}$, has a banded structure due to the limited support of the basis functions in each knot interval. This matrix equation is solved using standard linear algebraic techniques.

C.4 Generic Equation Using Hermite Polynomial Splines

The following differential equation is solved by inserting the interpolation function into the differential equation.

$$a(x)f''(x) + b(x)f'(x) + c(x)f(x) = d(x) \qquad \text{Eq. 239}$$

Again for notation let the single index rs represent the pair of indices (r,s). Then

$$f(x) = \sum_{rs=0}^{N_k N_f - 1} A_{rs}\phi_{rs}(x) \qquad \text{Eq. 240}$$

$$f'(x) = \sum_{rs=0}^{N_k N_f - 1} A_{rs} \phi'_{rs}(x) \qquad \text{Eq. 241}$$

$$f''(x) = \sum_{rs=0}^{N_k N_f - 1} A_{rs} \phi''_{rs}(x) \qquad \text{Eq. 242}$$

Substituting and evaluating at the i^{th} collocation point yields

$$a(x_i) \sum_{rs=0}^{N_k N_f - 1} A_{rs} \phi''_{rs}(x_i) + b(x_i) \sum_{rs=0}^{N_k N_f - 1} A_{rs} \phi'_{rs}(x_i) + c(x_i) \sum_{rs=0}^{N_k N_f - 1} A_{rs} \phi_{rs}(x_i) = d(x_i) \qquad \text{Eq. 243}$$

or

$$\sum_{rs=0}^{N_g N_f - 1} A_{rs} (a(x_i)\phi''_{rs}(x_i) + b(x_i)\phi'_{rs}(x_i) + c(x_i)\phi_{rs}(x_i)) = d(x_i) \qquad \text{Eq. 244}$$

This is put into the matrix equation

$$\underline{\underline{\phi}}\,\overline{A} = \overline{d} \qquad \text{Eq. 245}$$

where

$\overline{A}$ = expansion coefficient vector with coefficients A_{rs}

$\overline{d}$ = the vector of function values, $d(x_i)$

$\underline{\underline{\phi}}$ = the matrix with elements $\underline{\underline{\phi}}_{i,rs}$ =

$$a(x_i)\phi''_{rs}(x_i) + b(x_i)\phi'_{rs}(x_i) + c(x_i)\phi_{rs}(x_i)$$

As in the previous example there are $(N_k\text{-}1)N_f$ Gauss-Legendre collocation points and $N_k N_f$ basis function coefficients. To make $\underline{\underline{\phi}}$ a square matrix the differential equation boundary conditions must be added to the equation set. For example if, at the boundaries, the first and

last knots, the $\frac{d^s f(x_{k,0})}{dx^s}$ and $\frac{d^s f(x_{k,N_k-1})}{dx^s}$ are known, then the following equations may be added to the matrix equation

$$A_{rs} = \frac{d^s f(x_{k,0})}{dx^s}, \quad rs = 0*Nf+s \qquad \text{Eq. 246}$$

$$A_{rs} = \frac{d^s f(x_{k,N_k-1})}{dx^s}, \quad rs = (N_k-1)*Nf+s \qquad \text{Eq. 247}$$

Figure 39 illustrates this example using cubic splines, s = 0 and 1.

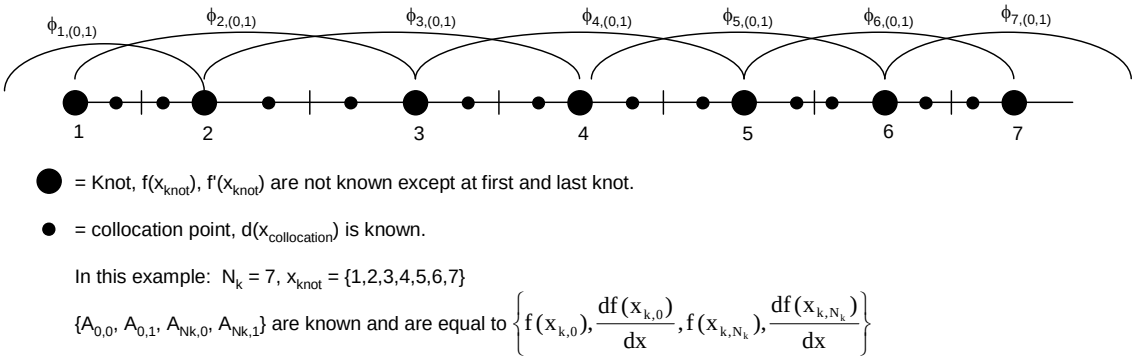

Figure 39. Cubic Spline Collocation Points Between Knots And Boundary Conditions.

The derivatives of the cubic spline functions are given by

$$\frac{d\phi_{i,0}(x)}{dx} = \begin{cases} \frac{6(x_i - x)}{h_i^3}(h_i - (x_i - x)) & x_{i-1} \le x \le x_i \\ -\frac{6(r - r_i)}{h_{i+1}^3}(h_{i+1} - (x - x_i)) & x_i \le x \le x_{i+1} \\ 0 & otherwise \end{cases} \qquad \text{Eq. 248}$$

$$\frac{d\phi_{i,1}(x)}{dx} = \begin{cases} \frac{1}{h_i^2}((h_i - (x_i - x))(h_i - 3(x_i - x))) & x_{i-1} \le x \le x_i \\ \frac{1}{h_{i+1}^2}((h_{i+1} - (x - x_i)(h_{i+1} - 3(x - x_i))) & x_i \le x \le x_{i+1} \\ 0 & otherwise \end{cases} \qquad \text{Eq. 249}$$

$$\frac{d^2\phi_{i,0}(x)}{dx^2} = \begin{cases} -\frac{6}{h_i^3}(h_i - 2(x_i - x)) & x_{i-1} \le x \le x_i \\ -\frac{6}{h_{i+1}^3}(h_{i+1} - 2(x - x_i)) & x_i \le x \le x_{i+1} \\ 0 & \textit{otherwise} \end{cases}$$

Eq. 250

$$\frac{d^2\phi_{i,1}(x)}{dx^2} = \begin{cases} \frac{-2}{h_i^2}(-2h_i + 3(x_i - x)) & x_{i-1} \le x \le x_i \\ \frac{2}{h_{i+1}^2}(-2h_{i+1} + 3(x - x_i)) & x_i \le x \le x_{i+1} \\ 0 & \textit{otherwise} \end{cases}$$

Eq. 251

Figure 40 illustrates this example using quintic splines.

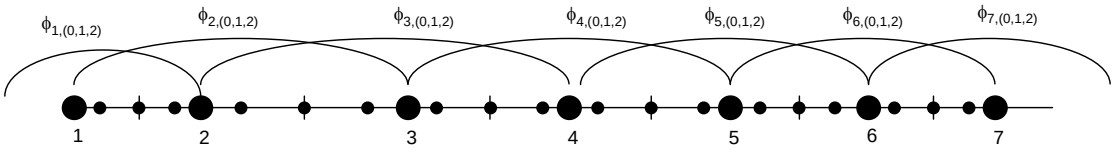

● = Knot, $f(x_{knot})$, $f'(x_{knot})$, $f''(x_{knot})$ are not known except at first and last knot.

● = collocation point, $d(x_{collocation})$ is known.

In this example: $N_k = 7$, $x_{knot} = \{1,2,3,4,5,6,7\}$

$\{A_{0,0}, A_{0,1}, A_{0,2}, A_{Nk,0}, A_{Nk,1}, A_{Nk,2}\}$ are known and equal to $\left\{f(x_{k,0}), \frac{df(x_{k,0})}{dx}, \frac{d^2f(x_{k,0})}{dx^2}, f(x_{k,N_k}), \frac{df(x_{k,N_k})}{dx}, \frac{d^2f(x_{k,N_k})}{dx^2}\right\}$

Figure 40. Quintic Spline Collocation Points Between Knots And Boundary Conditions.

The derivatives of the quintic spline functions are given by

$$\frac{d\phi_{i,0}(x)}{dx} = \begin{cases} \frac{3(x - x_{i-1})^2}{h_i^5}(h_i^2 - 3h_i(x - x_i) + 6(x - x_i)^2 + (x - x_{i-1})(4(x - x_i) - h_i)) & x_{i-1} \le x \le x_i \\ \frac{-3(x - x_{i+1})^2}{h_{i+1}^5}(h_{i+1}^2 + 3(x - x_i)h_{i+1} + 6(x - x_i)^2 + (x - x_{i+1})(4(x - x_i) + h_{i+1})) & x_i \le x \le x_{i+1} \\ 0 & \textit{otherwise} \end{cases}$$

Eq. 252

$$\frac{d\phi_{i,1}(x)}{dx}=\begin{cases}-\frac{(x-x_{i-1})^2}{h_i^4}((6(x-x_i)-(x-x_{i-1}))(2(x-x_i)+(x-x_{i-1}))) & x_{i-1}\le x\le x_{ii}\\ -\frac{(x-x_{i+1})^2}{h_{i+1}^4}((6(x-x_i)-(x-x_{i+1}))(2(x-x_i)+(x-x_{i+1}))) & x_i\le x\le x_{i+1}\\ 0 & otherwise\end{cases} \quad \text{Eq. 253}$$

$$\frac{d\phi_{i,2}(x)}{dx}=\begin{cases}\frac{(x-x_{i-1})^2(x-x_i)(3(x-x_i)+2(x-x_{i-1}))}{2h_i^3} & x_{i-1}\le x\le x_i\\ -\frac{(x-x_{i+1})^2(x-x_i)(3(x-x_i)+2(x-x_{i+1}))}{2h_{i+1}^3} & x_i\le x\le x_{i+1}\\ 0 & otherwise\end{cases} \quad \text{Eq. 254}$$

$$\frac{d^2\phi_{i,0}(x)}{dx^2}=\begin{cases}\frac{6(x-x_{i-1})}{h_i^5}(h_i^2-3h_i(x-x_i)+6(x-x_i)^2+3(x-x_{i-1})(4(x-x_i)-h_i)+2(x-x_{i-1})^2) & x_{i-1}\le x\le x_i\\ \frac{-6(x-x_{i+1})}{h_{i+1}^5}(h_{i+1}^2+3(x-x_i)h_{i+1}+6(x-x_i)^2+3(x-x_{i+1})(4(x-x_i)+h_{i+1})+2(x-x_{i+1})^2) & x_i\le x\le x_{i+1}\\ 0 & otherwise\end{cases} \quad \text{Eq. 255}$$

$$\frac{d^2\phi_{i,1}(x)}{dx^2}=\begin{cases}-\frac{12(x-x_{i-1})(x-x_i)}{h_i^4}(2(x-x_i)+3(x-x_{i-1})) & x_{i-1}\le x\le x_i\\ -\frac{12(x-x_{i+1})(x-x_i)}{h_{i+1}^4}(2(x-x_i)+3(x-x_{i+1})) & x_i\le x\le x_{i+1}\\ 0 & otherwise\end{cases} \quad \text{Eq. 256}$$

$$\frac{d^2\phi_{i,2}(x)}{dx^2}=\begin{cases}\frac{(x-x_{i-1})}{h_i^3}(3(x-x_i)^2+6(x-x_i)(x-x_{i-1})+(x-x_{i-1})^2) & x_{i-1}\le x\le x_i\\ -\frac{(x-x_{i+1})}{h_{i+1}^3}(3(x-x_i)^2+6(x-x_i)(x-x_{i+1})+(x-x_{i+1})^2) & x_i\le x\le x_{i+1}\\ 0 & otherwise\end{cases} \quad \text{Eq. 257}$$

C.5 Hermite Splines In Two Dimensions

For this thesis all matrix element indices are denoted with the row subscript first and the column subscript second.

The two-dimensional splines are a direct product of one-dimensional splines. The approximant is written as (assuming the same order fit for both the x and y directions, e.g. $N_{fx} = N_{fy} = N_f$)

$$\tilde{f}(x,y) = \sum_{r_y=0}^{N_{k_y}-1} \sum_{s_y=0}^{N_f-1} \sum_{r_x=0}^{N_{k_x}-1} \sum_{s_x=0}^{N_f-1} A_{r_y,s_y,r_x,s_x} \phi_{r_y,s_y}(y) \phi_{r_x,s_x}(x) \qquad \text{Eq. 258}$$

with the coefficients given by

$$A_{r_y,s_y,r_x,s_x} = \frac{\partial^{(s_y+s_x)} f(y_{k,r_y}, x_{k,r_x})}{\partial y^{s_y} \partial x^{s_x}} \qquad \text{Eq. 259}$$

Let the single index rs_y represent the pair of indices (r_y, s_y). For example $rs_y = r_y * N_f + s_y$. And a similar single index representation for rs_x the approximant is written as

$$\tilde{f}(x,y) = \sum_{rs_y=0}^{N_{k_y}N_f-1} \sum_{rs_x=0}^{N_{k_x}N_f-1} A_{rs_y,rs_x} \phi_{rs_y}(y) \phi_{rs_x}(x) \qquad \text{Eq. 260}$$

The two-dimensional knots are the direct product of the one-dimensional knots. The two-dimensional collocation points are also the direct product of the one-dimensional collocation points. This is illustrated for quintic splines in Figure 41.

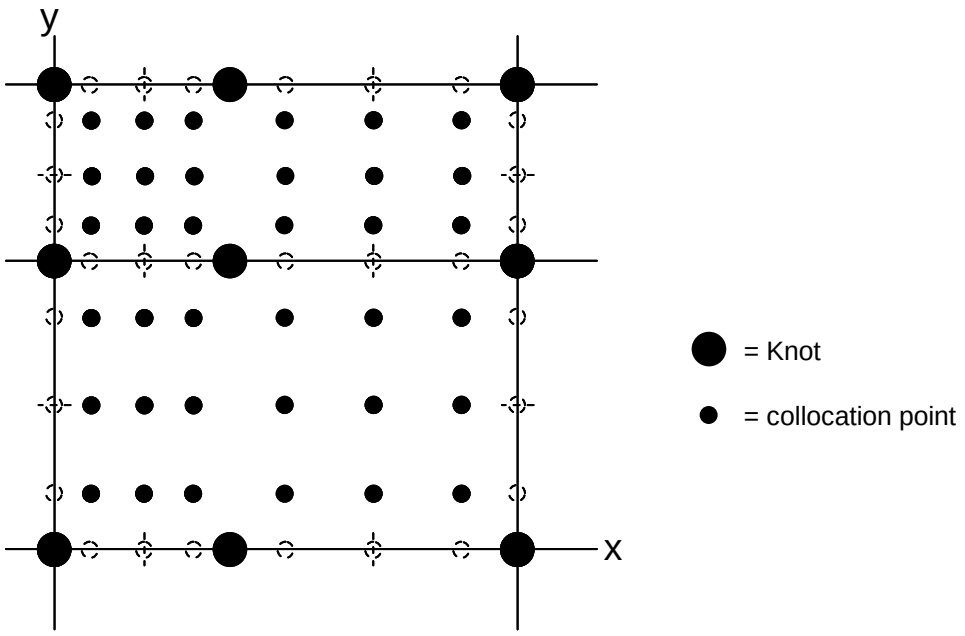

Figure 41. Example Of Two-Dimensional Knots And Collocation Points.

For a given two-dimensional differential equation this approximant is substituted into the equation and evaluated at the collocation points. This yields a matrix equation of the same form as the one-dimensional case. Adding boundary conditions squares up the matrix and the linear equation is solved using standard techniques.

C.6 Interpolation Of A Function Using Basis Functions

If a function does not yield a good approximation by the splines previously described in a specific region then either the region must be further divided into more segments or another method must be implemented to

approximate the function. This may require splines of higher order for that region, or a different type of approximating scheme may be required. In any case at the boundary between the two approximating schemes the function should have the same value. Depending on the quality of the desired results such as continuity and matching derivatives, additional boundary matching may be required.

It is conjectured that the quintic splines are not of high enough order to fit the wave function in the region near y = 0. The positron-proton scattering basis functions were introduced into the radial y-axis wave function approximation in an attempt to mitigate this deficiency.

Specific to this thesis, the positron-proton Coulomb scattering basis functions are introduced near the interaction region on the y-axis in place of the Hermite splines. In this region the positron-proton interaction should be dominate over the positron-electron or proton-electron interaction since the probability of the electron being in this region is small (see Figure 5).

The positron-proton Coulomb scattering basis functions and their derivatives are expanded about zero

and the expansions are used as basis functions in the wave function approximation. The expansions are given by

$$F_{l_y}(y) = \sqrt{2\pi} e^{-iky} C_{l_y} (ky)^{l_y+1} [1+...] \qquad \text{Eq. 261}$$

$$F'_{l_y}(y) = F_{l_y}(ky)[(l+1)/y - ik] \qquad \text{Eq. 262}$$

$$F''_{l_y}(y) = F_{l_y}(ky)[l(l+1) - k^2 y^2 - i2k(l+1)y]/y^2 \qquad \text{Eq. 263}$$

where

$$C_l^2 = \left[\frac{2^l}{(2l+1)!}\right]^2 (l^2+1/k^2)((l-1)^2+1/k^2)...(1+1/k^2)\frac{2\pi/k}{e^{2\pi/k}-1}$$

$$C_1^2 = \left[\frac{2}{(3)!}\right]^2 (1+1/k^2)\frac{2\pi/k}{e^{2\pi/k}-1} \qquad \text{Eq. 264}$$

$$C_0^2 = \frac{2\pi/k}{e^{2\pi/k}-1}$$

Since only the form of the basis function is required and the constants are not, the basis functions implemented are given by

$$F_{l_y}(y) = e^{-iky}(ky)^{l_y+1} \qquad \text{Eq. 265}$$

and its derivatives.

These functions are chosen since, near y = 0 (interaction region), the probability of the hydrogen electron interfering with the incoming positron is small. However, the basis functions are complex enough at higher angular momentum quantum numbers that Hermite splines provide a poor approximation to the wave function, unless

the density of the splines is increased to such a high value that solving the equations for the coefficients becomes unwieldy on today's computer resources.

When the scattering basis functions are implemented along with the splines then a two-dimensional function approximation is given by

$$\tilde{f}(x,y) = \begin{cases} \sum_{rs_y=0}^{N_{k_y}N_f-1} \sum_{rs_x=0}^{l_{y,\max}} A_{rs_y,rs_x} F_{rs_y}(y)\phi_{rs_x}(x) & y \le y_t \\ \sum_{rs_y=0}^{N_{k_y}N_f-1} \sum_{rs_x=0}^{N_{k_x}N_f-1} A_{rs_y,rs_x} \phi_{rs_y}(y)\phi_{rs_x}(x) & otherwise \end{cases} \qquad \text{Eq. 266}$$

Using the positron-proton basis functions also allows for an additional set of boundary conditions near y = 0 by matching not only the wave function but also its derivatives.

Appendix D describes the boundary conditions for matching $\tilde{f}(x,y_t)$ when Hermite splines are implemented and when the basis functions are implemented for the function approximation.

APPENDIX D

SOLVING THE SCHRODINGER EQUATION USING DVR BASIS FUNCTIONS AND SPLINES

This appendix summarizes the solution to the Schrodinger Equation in atomic units using the DVR basis function expansion technique. For the two-particle case mass-scaled center of mass coordinates are used. For the three-particle case mass-scaled Jacobi coordinates are used. The more familiar two-particle case is discussed so that it can be referenced analogous to the less familiar three-particle case.

More in depth details are found in references 1 to 13, 15, 19, 29, 30, 31 and 43.

D.1 Two-Particle Schrodinger Equation

As shown in Appendix A, the two-particle mass-scaled Schrodinger equation (center of mass removed) is

$$(\bar{p}^2 + V(r))\Psi = E\Psi \qquad \text{Eq. 267}$$

Separating the momentum operator into radial and angular terms yields

$$(p_r^2 + \frac{L^2}{2r} + V(r))\Psi = E\Psi \qquad \text{Eq. 268}$$

where

p_r = radial momentum operator, $-\frac{\partial^2 r}{r\partial r^2}$

L = orbital angular momentum operator

If Ψ is separable into the product of a radial term R and an angular term Y_{lm} that is proportional to the spherical harmonics, then $\Psi = RY_{lm}$ is substituted into the equation to yield a differential equation for the radial term

$$(-\frac{\partial^2 r}{r\partial r^2}+\frac{l(l+1)}{r^2}+V(r))R = ER \qquad \text{Eq. 269}$$

The term $\frac{l(l+1)}{r^2}+V(r)$ is the "effective potential". The first term being the angular momentum barrier, which goes to infinity as r approaches 0. This term acts as a repulsive core so the system cannot collapse.

An effective method to solve the radial equation is to let R = U/r. The radial equation for U becomes

$$(-\frac{\partial^2}{\partial r^2}+\frac{l(l+1)}{r^2}+V(r))U = EU \qquad \text{Eq. 270}$$

From Appendix B, the wave function is expanded using the DVR basis functions

$$\Psi(r,\Omega) \approx \sum_{j=1}^{N}\sum_{\nu=1}^{n}\sqrt{w_j}(S_{j\nu})^* S_\nu(\Omega)\psi_j(r) \qquad \text{Eq. 271}$$

where the functions $S_\nu(\Omega)$ are linear combinations of the spherical harmonics, $J_\nu(\Omega)$

$$S_\nu(\Omega) = \sum_{\nu'=1}^{N} C_{\nu\nu'} J_{\nu'}(\Omega) \qquad \text{Eq. 272}$$

For convenience let this expansion instead be

$$\Psi(r,\Omega) \approx \frac{\tilde{\Psi}(r,\Omega)}{r} = \frac{1}{r}\sum_{j=1}^{N}\sum_{\nu=1}^{n}\sqrt{w_j}\,(S_{j\nu})^* S_\nu(\Omega)\psi_j(r) \qquad \text{Eq. 273}$$

where

$$\tilde{\Psi}(r,\Omega) = \sum_{j=1}^{N}\sum_{\nu=1}^{n}\sqrt{w_j}\,(S_{j\nu})^* S_\nu(\Omega)\psi_j(r) \qquad \text{Eq. 274}$$

Substitution into the Schrodinger equation yields the following equation for the radial expansion coefficients, $\psi_j(r)$

$$\begin{aligned} 0 = &-\sum_{j=1}^{N}\sum_{\nu=1}^{N} S_\nu(\Omega)(S_{j\nu})^*\sqrt{w_j}\,\psi''_j(r) \\ &+\frac{1}{r^2}\sum_{j=1}^{N}\sum_{\nu=1}^{N} L^2 S_\nu(\Omega)(S_{j\nu})^*\sqrt{w_j}\,\psi_j(r) \\ &+(V(r)-E)\sum_{j=1}^{N}\sum_{\nu=1}^{N} S_\nu(\Omega)(S_{j\nu})^*\sqrt{w_j}\,\psi''_j(r) \end{aligned} \qquad \text{Eq. 275}$$

Note that the angular operator acting on $S_\nu(\Omega)$ yields the following

$$L^2 S_\nu(\Omega) = \sum_{\nu'=1}^{N} C_{\nu\nu'} l'(l'+1) J_{\nu'}(\Omega) \qquad \text{Eq. 276}$$

where l' is the angular momentum quantum number corresponding to ν' = (l', m'). Thus the equation becomes

$$0 = -\sum_{j=1}^{N}\sum_{\nu=1}^{N} S_{\nu}(\Omega)(S_{j\nu})^{*}\sqrt{w_j}\psi''_j(r)$$
$$+\frac{1}{r^2}\sum_{j=1}^{N}\sum_{\nu=1}^{N}\sum_{\nu'=1}^{N}[C_{\nu\nu'}l'(l'+1)J_{\nu'}(\Omega)](S_{j\nu})^{*}\sqrt{w_j}\psi_j(r) \qquad \text{Eq. 277}$$
$$+(V(r)-E)\sum_{j=1}^{N}\sum_{\nu=1}^{N} S_{\nu}(\Omega)(S_{j\nu})^{*}\sqrt{w_j}\psi''_j(r)$$

Evaluating this equation at a DVR angular grid point, denoted with index k, angle Ω_k, with $S_\nu(\Omega_k) = S_{k\nu}$, multiplying by $\sqrt{w_k}$, and using the DVR properties yields the following differential equation

$$0 = \sum_{j=1}^{N}\left[\left(V(r)-E-\frac{\partial^2}{\partial r^2}\right)\delta_{k,j}+\frac{SLS_{k,j}}{r^2}\right]\psi_j(r) \qquad \text{Eq. 278}$$

where

$$SLS_{k,j} = \sqrt{w_k w_j}\sum_{\nu=1}^{N}\sum_{\nu'=1} C_{\nu\nu'}(l'(l'+1))J_{k\nu'}(S_{j\nu})^{*} \qquad \text{Eq. 279}$$

Since there are N DVR indices, k = 1 to N, a set of coupled differential equations is obtained for the set of radial coefficients, $\psi_j(r)$.

Using the spline expansion described in Appendix C, each $\psi_j(r)$ is expanded as follows

$$\psi_j(r) = \sum_{rs=0}^{N_k N_f - 1} A_{j,rs}\phi_{rs}(r) \qquad \text{Eq. 280}$$

Substituting this into the DVR set of differential equations yields the following set of coupled linear differential equations for $A_{j,rs}$

$$0 = \sum_{j=1}^{N} \sum_{rs} A_{j,rs} \left\{ \left[(V(r) - E)\delta_{k,j} + \frac{SLS_{k,j}}{r^2} \right] \phi_{rs}(r) - \phi''_{rs}(r)\delta_{k,j} \right\} \qquad \text{Eq. 281}$$

This set of equations is then solved for each radial spline coefficient, $A_{j,rs}$, using the spline technique described in Appendix C.

D.2 Full Two-Particle Boundary Condition

There are many boundary conditions that may be implemented to solve these equations. A boundary condition that is reasonable to use near zero is the following

$$\psi_j(0) = 0 \qquad \text{Eq. 282}$$

for all j.

For the other boundary conditions no one method may be numerically convenient for all situations. A reasonable set of conditions to implement are a set that takes advantage of the asymptotic boundary conditions.

As r goes to infinity, the scattered particle is far enough away from the influence of the potential that the

wave function has the form of the sum of a spherical scattered wave and the incoming plane wave.

$$\Psi(\bar{r}) = A(e^{i\bar{k}\bullet\bar{r}} + \frac{e^{ikr}}{r} f(\theta)) \qquad \text{Eq. 283}$$

where $\bar{k}$ is the incoming particle momentum vector, $\bar{r}$ is the outgoing vector direction and $f(\theta)$ or the scattering amplitude is the shift in the outgoing wave function amplitude. The directions of $\bar{k}$ and $\bar{r}$ are given by the angular grid directions, Ω_i.

Equivalently this is written as

$$\tilde{\Psi}(\bar{r}) = A(re^{i\bar{k}\bullet\bar{r}} + e^{ikr} f(\theta)) \qquad \text{Eq. 284}$$

Asymptotic boundary conditions are obtained by manipulating this equation. Two techniques based on matching the outgoing wave function with the interior expanded wave function are given. The first description is given without using the outgoing expansion approximation.

Evaluating these equations for two different asymptotic range values r and r' and eliminating $f(\theta)$ yields the following boundary condition

$$(\tilde{\Psi}(\bar{r}) - \frac{r'}{r} e^{ik(r-r')} \tilde{\Psi}(\bar{r}')) = A(e^{i\bar{k}\bullet\bar{r}} - \frac{r'}{r} e^{i\bar{k}\bullet\bar{r}' - ik(r'-r)}) \qquad \text{Eq. 285}$$

Evaluating this equation for an incoming angle on the DVR grid, $\bar{k}=(k,\Omega_k)$, and an outgoing angle on the DVR grid, $\bar{r}=(r,\Omega_j)$, $\bar{r}'=(r',\Omega_j)$, yields the following asymptotic boundary condition

$$\psi(r,\Omega_j)-e^{ik(r-r')}\psi(r',\Omega_j)=A(re^{ikrcos(\theta_{kr})}-r'e^{ikr'cos(\theta_{kr})-ik(r'-r)})\sqrt{w_j} \qquad \text{Eq. 286}$$

where $\cos(\theta_{kr})$ is the cosine of the angle between the incoming and outgoing vectors and is given by

$$\cos(\theta_{kr})=\cos(\theta_k)\cos(\theta_r)+\sin(\theta_k)\sin(\theta_r)\cos(\phi_k-\phi_r) \qquad \text{Eq. 287}$$

The derivative with respect to r of the asymptotic wave equation yields

$$\tilde{\Psi}'(\bar{r})=A(ikcos(\theta_{kr})e^{ikrcos(\theta_{kr})}+\frac{e^{ikr}}{r}f(\theta_{kr})) \qquad \text{Eq. 288}$$

Following the previous example yields another boundary condition using the wave function derivative

$$\psi'(r,\Omega_j)-e^{ik_{in}(r-r')}\psi'(r',\Omega_j)=A\sqrt{w_j}((1+ikr\cos(\theta_{kr}))e^{ikrcos(\theta_{kr})}- (1+ikr'\cos(\theta_{kr}))e^{ikr'cos(\theta_{kr})-ik(r'-r)}) \qquad \text{Eq. 289}$$

As an example another set of boundary conditions is obtained by evaluating the derivative at a radial point r and then using the wave function at r to solve for $f(\theta_{kr})$ and substituting this solution into the derivative. This yields the following boundary condition

$$\psi'_k(r)-ik\psi_k(r)=\sqrt{w_k}Ae^{ikrcos(\theta_{kr})}(1+ikr(\cos(\theta_{kr})-1)) \qquad \text{Eq. 290}$$

Repeating using the second derivative yields

$$\psi''_{k}(\mathrm{r}) + k^2\psi_k(\mathrm{r}) = \sqrt{w_k}Ak^2 r\mathrm{e}^{\mathrm{i}ky\cos(\theta_{kr})} - \sqrt{w_k}Ak\mathrm{e}^{\mathrm{i}ky\cos(\theta_{kr})}(kr\cos^2(\theta_{kr}) - 2i\cos(\theta_{kr})) \quad \text{Eq. 291}$$

D.3 Approximating Two-Particle Boundary Condition

The goal of this thesis is to find an approximating wave function that allows the derivation of the amplitude function to determine the scattering cross section. Since an approximated wave function is being implemented using a finite number of partial angular momentum an approximated boundary condition for that wave function should also be implemented to obtain a reasonable match at the asymptotic boundary.

Using the DVR as the basis functions and approximating the wave function by summing up to a maximum partial angular momentum, l_{max}, given in v = (l,m), the outgoing asymptotic wave function $\mathrm{e}^{\mathrm{i}\bar{k}\bullet\bar{r}}$ is also be expanded and only terms from l = 0 to l = l_{max} are retained.

Starting with

$$\tilde{\Psi}(\bar{r}) = \mathrm{A}(\mathrm{re}^{\mathrm{i}\bar{k}\bullet\bar{r}} + \mathrm{e}^{\mathrm{i}kr}\mathrm{f}(\theta_{kr})) \quad \text{Eq. 292}$$

and expanding the first term using angular basis functions and simplifying yields

$$e^{ikr\cos(\theta_{kr})} = \sum_l e^{il\pi/2}(2l+1)\,j_l(kr)P_l(\cos(\theta_{kr}))$$ Eq. 293

Then putting the second term in a conveniently similar form

$$f(\theta_{kr}) = \frac{1}{2ik}\sum_l (2l+1)(s_l - 1)P_l(\cos(\theta_{kr}))$$ Eq. 294

the wave function is written as

$$\tilde{\Psi}(\bar{r}) \approx Ar\sum_l e^{il\pi/2}(2l+1)\,j_l(kr)P_l(\cos(\theta_{kr})) + Ae^{ikr}\frac{1}{2ik}\sum_l (2l+1)(s_l - 1)P_l(\cos(\theta_{kr}))$$ Eq. 295

where the sum is from l = 0 to l = l_{max}. s_l represents the l^{th} diagonal element of the scattering or S operator. The actual value of s_l is not computed nor required for asymptotic matching.

Note that

$$e^{il\pi/2} = (i)^l$$ Eq. 296

Substituting the finite expansions into the previously derived first set of boundary conditions yields the following set of boundary conditions for the asymptotic region

$$\psi_k(r) - e^{ik(r-r')}\psi_k(r') = A\sqrt{w_k}(S_{k,r}(r) - e^{ik(r-r')}S_{k,r}(r'))$$ Eq. 297

$$\psi'_k(r) - e^{ik(r-r')}\psi'_k(r') = A\sqrt{w_k}(S'_{k,r}(r) - e^{ik(r-r')}S'_{k,r}(r'))$$ Eq. 298

where

$$S_{k,r}(r) \approx \sum_l i^l r j_l(kr)(2l+1)P_l(\cos(\theta_{kr})) \qquad \text{Eq. 299}$$

$$S'_{k,r}(r) \approx \sum_l i^l (2l+1)P_l(\cos(\theta_{kr}))(j_l(kr) + krj'_l(kr)) \qquad \text{Eq. 300}$$

and the amplitude function is found by

$$f(\theta_{kr})\big|_{k,j} = \frac{e^{-iky}\psi_j}{A\sqrt{w_j}} - e^{-iky}S_{k,r}(r) \qquad \text{Eq. 301}$$

D.4 Three-Particle Schrodinger Equation

As shown in Appendix A, the three-particle mass-scaled Schrodinger equation (center of mass removed) for the α three-body Jacobi coordinates is given by

$$(p_{x_\alpha}^2 + p_{y_\alpha}^2 + V(x_\alpha) + V(x_\beta) + V(x_\gamma))\Psi = E\Psi \qquad \text{Eq. 302}$$

In terms of the rotational angular momentum of the bound pair, $\hat{l}_{x_\alpha}$, and of the orbital angular momentum of the free particle about the bound pair, $\hat{l}_{y_\alpha}$, the quantum-mechanical form of the mass-scaled Schrodinger equation, with pairwise Coulomb potentials, is thus

$$\left(-\frac{1}{x_\alpha}\frac{\partial}{\partial x_\alpha^2}x_\alpha - \frac{1}{y_\alpha}\frac{\partial}{\partial y_\alpha^2}y_\alpha + \frac{\hat{l}_{x_\alpha}^2}{x_\alpha^2} + \frac{\hat{l}_{y_\alpha}^2}{y_\alpha^2} + \frac{q_\alpha}{x_\alpha} + \frac{q_\beta}{x_\beta} + \frac{q_\gamma}{x_\gamma}\right)\Psi = E\Psi \qquad \text{Eq. 303}$$

where the coordinates x_β and x_γ are found via the previously derived mass-scaled Jacobi coordinate transformation equations with inputs (x_α, y_α).

For notation convenience, the α notation is dropped with the understanding that this equation is for the α = 1 Jacobi coordinates

$$\left(-\frac{1}{x}\frac{\partial}{\partial x^2}x-\frac{1}{y}\frac{\partial}{\partial y^2}y+\frac{\hat{l}_x^2}{x^2}+\frac{\hat{l}_y^2}{y^2}+\frac{q}{x}+\frac{q_2}{x_2}+\frac{q_3}{x_3}\right)\Psi=E\Psi \qquad \text{Eq. 304}$$

For convenience let the wave function be represented by

$$\Psi(x,y,\Omega_x,\Omega_y)\approx\frac{\tilde{\Psi}(x,y,\Omega_x,\Omega_y)}{xy} \qquad \text{Eq. 305}$$

where

Ω_x = angle representation of the pair of polar and azimuthal angles (θ_x,ϕ_x) that indicate the direction of the x coordinate axis

Ω_y = angle representation of the pair of polar and azimuthal angles (θ_y,ϕ_y) that indicate the direction of the y coordinate axis

The wave function differential equation is

$$-\frac{\partial^2\tilde{\Psi}}{\partial x^2}-\frac{\partial^2\tilde{\Psi}}{\partial y^2}+\frac{\hat{l}_x^2\tilde{\Psi}}{x^2}+\frac{\hat{l}_y^2\tilde{\Psi}}{y^2}-E\tilde{\Psi}+\left(\frac{q}{x}+\frac{q_2}{x_2}+\frac{q_3}{x_3}\right)\tilde{\Psi}=0 \qquad \text{Eq. 306}$$

Following the same procedure as shown in the two-particle case the wave function is expanded using the two-dimensional DVR

$$\tilde{\Psi}(x,y,\Omega)=\sum_{j=1}^{N}\sum_{\nu=1}^{N}\sqrt{W_j}(S_{j\nu})^{*}S_{\nu}(\Omega)\psi_j(x,y) \qquad \text{Eq. 307}$$

where, as defined in Appendix B, Ω represents the pair (Ω_x, Ω_y), and the functions $S_\nu(\Omega)$ are linear combinations of the bipolar basis functions, $Y_\nu(\Omega)$.

Substitution of the DVR expansion into the differential equation yields

$$\begin{aligned}0=&-\sum_{j=1}^{N}\sum_{\nu=1}^{N}S_{\nu}(\Omega)(S_{j\nu})^{*}\sqrt{W_j}\frac{\partial^2\psi_j(x,y)}{\partial x^2}\\&-\sum_{j=1}^{N}\sum_{\nu=1}^{N}S_{\nu}(\Omega)(S_{j\nu})^{*}\sqrt{W_j}\frac{\partial^2\psi_j(x,y)}{\partial y^2}\\&+\frac{1}{x^2}\sum_{j=1}^{N}\sum_{\nu=1}^{N}\hat{l}_x^2S_{\nu}(\Omega)(S_{j\nu})^{*}\sqrt{W_j}\psi_j(x,y)\\&+\frac{1}{y^2}\sum_{j=1}^{N}\sum_{\nu=1}^{N}\hat{l}_y^2S_{\nu}(\Omega)(S_{j\nu})^{*}\sqrt{W_j}\psi_j(x,y)\\&+\left(\frac{q}{x}+\frac{q_2}{x_2}+\frac{q_3}{x_3}-E\right)\sum_{j=1}^{N}\sum_{\nu=1}^{N}S_{\nu}(\Omega)(S_{j\nu})^{*}\sqrt{W_j}\psi_j(x,y)\end{aligned} \qquad \text{Eq. 308}$$

Note that the angular operators acting on $S_\nu(\Omega)$ yields the following

$$\hat{l}_x^2S(\Omega)=\sum_{\nu'=1}^{N}C_{\nu\nu'}(l'_x(l'_x+1))Y_{\nu'}(\Omega) \qquad \text{Eq. 309}$$

where l'_x is the angular momentum quantum number corresponding to $\nu' = (L', M', l'_x, l'_y)$.

and

$$\hat{l}_y^2 S(\Omega) = \sum_{\nu'=1}^{N} C_{\nu\nu'}(l'_y(l'_y+1))Y_{\nu'}(\Omega) \qquad \text{Eq. 310}$$

where l'_y is the angular momentum quantum number corresponding to $\nu' = (L', M', l'_x, l'_y)$.

The differential equation is

$$\begin{aligned}
0 = &-\sum_{j=1}^{N}\sum_{\nu=1}^{N} S_\nu(\Omega)(S_{j\nu})^* \sqrt{W_j}\frac{\partial^2\psi_j(x,y)}{\partial x^2} \\
&-\sum_{j=1}^{N}\sum_{\nu=1}^{N} S_\nu(\Omega)(S_{j\nu})^* \sqrt{W_j}\frac{\partial^2\psi_j(x,y)}{\partial y^2} \\
&+\frac{1}{x^2}\sum_{j=1}^{N}\sum_{\nu=1}^{N}\left(\sum_{\nu'=1}^{N} C_{\nu\nu'}(l'_x(l'_x+1))Y_{\nu'}(\Omega)\right)(S_{j\nu})^*\sqrt{W_j}\psi_j(x,y) \qquad \text{Eq. 311} \\
&+\frac{1}{y^2}\sum_{j=1}^{N}\sum_{\nu=1}^{N}\left(\sum_{\nu'=1}^{N} C_{\nu\nu'}(l'_y(l'_y+1))Y_{\nu'}(\Omega)\right)(S_{j\nu})^*\sqrt{W_j}\psi_j(x,y) \\
&+\left(\frac{q}{x}+\frac{q_2}{x_2}+\frac{q_3}{x_3}-E\right)\sum_{j=1}^{N}\sum_{\nu=1}^{N} S_\nu(\Omega)(S_{j\nu})^*\sqrt{W_j}\psi_j(x,y)
\end{aligned}$$

Evaluating this equation at a DVR angular grid point, denoted with index k, angle Ω_k, with $S_\nu(\Omega_k) = S_{k\nu}$, multiplying by $\sqrt{W_k}$, and using the DVR properties yields the following differential equation

$$\begin{aligned}
0 = \sum_{j=1}^{N}\Bigg[&\left(-\frac{\partial^2}{\partial x^2}-\frac{\partial^2}{\partial y^2}+\left(\frac{q}{x}+\frac{q_2}{x_2\big|_{\Omega_k}}+\frac{q_3}{x_3\big|_{\Omega_k}}-E\right)\right)\delta_{k,j} \\
&+\frac{Sl_x S_{k,j}}{x^2}+\frac{Sl_y S_{k,j}}{y^2}\Bigg]\psi_j(x,y)
\end{aligned} \qquad \text{Eq. 312}$$

where

$$Sl_x S_{k,j} = \sqrt{W_k W_j}\sum_{\nu=1}^{N}\sum_{\nu'=1} C_{\nu\nu'}(l'_x(l'_x+1))Y_{k\nu'}(S_{j\nu})^* \qquad \text{Eq. 313}$$

$$Sl_y S_{k,j} = \sqrt{W_k W_j} \sum_{\nu=1}^{N} \sum_{\nu'=1} C_{\nu\nu'}(l'_y (l'_y+1)) Y_{k\nu'}(S_{j\nu})^* \qquad \text{Eq. 314}$$

$x_\beta\big|_{\Omega_k}$ is the transformation of the x β-Jacobi coordinate to the x α-Jacobi coordinates using the coordinate transformation for the lengths as described in Appendix A with z_α being the cosine of the angle between the β-Jacobi coordinates defined by angles Ω_k. In this description α = 1 and β = 2 or 3.

Since there are N DVR indices, k = 1 to N, a set of coupled differential equations is obtained for the set of radial coefficients, $\psi_j(x,y)$.

Using the spline expansion described in Appendix B, each $\psi_j(x,y)$ is expanded as follows

$$\psi_j(x,y) = \sum_{rs_y=0}^{N_{k_y} N_f - 1} \sum_{rs_x=0}^{N_{k_x} N_f - 1} A_{j,rs_y,rs_x} \phi_{rs_y}(y) \phi_{rs_x}(x) \qquad \text{Eq. 315}$$

Substituting this into the DVR set of differential equations yields the following set of coupled linear equations for A_{j,rs_y,rs_x}

$$0=\sum_{j=1}^{N}\sum_{rs_y=0}^{N_f N_{ky}-1}\sum_{rs_x=0}^{N_f N_{kx}-1} A_{j,rs_y,rs_x}\left\{\left[\left(\frac{q}{x}+\frac{q_2}{x_2\big|_{\Omega_k}}+\frac{q_3}{x_3\big|_{\Omega_k}}-E\right)\delta_{k,j}\right.\right.$$
$$\left.+\left(\frac{Sl_x S_{k,j}}{x^2}+\frac{Sl_y S_{k,j}}{y^2}\right)\right]\phi_{rs_x}(x)\phi_{rs_y}(y) \qquad \text{Eq. 316}$$
$$\left.-\left(\phi_{rs_y}(y)\frac{\partial^2\phi_{rs_x}(x)}{\partial x^2}+\phi_{rs_x}(x)\frac{\partial^2\phi_{rs_y}(y)}{\partial y^2}\right)\delta_{k,j}\right\}$$

This set of equations is then solved for each radial spline coefficient, A_{j,rs_y,rs_x}, using the spline technique described in Appendix C.

D.5 Three-Particle Near Zero Boundary Condition Using Basis Functions And Splines

There are many boundary conditions that may be implemented to solve these equations. A boundary condition that is reasonable to use near zero is the following

$$\psi_j(x,0)=0 \qquad \text{Eq. 317}$$

$$\psi_j(0,y)=0 \qquad \text{Eq. 318}$$

for all j.

As discussed in the Appendix C, when a linear combination of positron-proton basis functions are used to approximate the wave function near zero and splines are used elsewhere, each approximating scheme must match at

the transition, y_t, where one approximation scheme ends and the next begins.

The wave function evaluated at the DVR angle k is given by

$$\psi_{\mathrm{k}}(\mathrm{x},\mathrm{y}) = \begin{cases} \sum_{\mathrm{rs_x}=0}^{N_f N_{kx}-1} \sum_{rs_y=0}^{l_{y,\max}} A_{k,rs_y,rs_x} F_{rs_y}(y)\phi_{rs_x}(x) & \mathrm{y} \le \mathrm{y_t} \\ \sum_{\mathrm{rs_x}=0}^{N_f N_{kx}-1} \sum_{rs_y=l_{y,\max}+1}^{N_f N_{ky}-1+(l_{y,\max}+1)-N_f} A_{k,rs_y,rs_x} \phi_{rs_y}(y)\phi_{rs_x}(x) & \text{otherwise} \end{cases} \qquad \text{Eq. 319}$$

where ϕ_{rsx}, are spline functions for the x component and ϕ_{rsy} and F_{rsy} are spline functions and positron-proton basis functions respectively for the y component and are discussed in the spline appendix.

The boundary conditions at the transition point, y_t is

$$\sum_{\mathrm{rs_x}=0}^{\mathrm{N_f N_{kx}}-1} \sum_{\mathrm{rs_y}=l_{y,\max}+1}^{N_f N_{ky}-1+(l_{y,\max}+1)-N_f} \mathrm{A_{k,rs_y,rs_x}}\, \phi_{\mathrm{rs_y}}(\mathrm{y})\phi_{\mathrm{rs_x}}(\mathrm{x}) - \sum_{\mathrm{rs_x}=0}^{N_f N_{kx}-1} \sum_{rs_y=0}^{l_{y,\max}} A_{k,rs_y,rs_x} F_{rs_y}(y)\phi_{rs_x}(x) = 0 \qquad \text{Eq. 320}$$

$$\sum_{\mathrm{rs_x}=0}^{\mathrm{N_f N_{kx}}-1} \sum_{\mathrm{rs_y}=l_{y,\max}+1}^{N_f N_{ky}-1+(l_{y,\max}+1)-N_f} \mathrm{A_{k,rs_y,rs_x}}\, \phi'_{\mathrm{rs_y}}(\mathrm{y})\phi_{\mathrm{rs_x}}(\mathrm{x}) - \sum_{\mathrm{rs_x}=0}^{N_f N_{kx}-1} \sum_{rs_y=0}^{l_{y,\max}} A_{k,rs_y,rs_x} F'_{rs_y}(y)\phi_{rs_x}(x) = 0 \qquad \text{Eq. 321}$$

$$\sum_{\mathrm{rs_x}=0}^{\mathrm{N_f N_{kx}}-1} \sum_{\mathrm{rs_y}=l_{y,\max}+1}^{N_f N_{ky}-1+(l_{y,\max}+1)-N_f} \mathrm{A_{k,rs_y,rs_x}}\, \phi''_{\mathrm{rs_y}}(\mathrm{y})\phi_{\mathrm{rs_x}}(\mathrm{x}) - \sum_{\mathrm{rs_x}=0}^{N_f N_{kx}-1} \sum_{rs_y=0}^{l_{y,\max}} A_{k,rs_y,rs_x} F''_{rs_y}(y)\phi_{rs_x}(x) = 0 \qquad \text{Eq. 322}$$

D.6 Three-Particle Non-Approximated Asymptotic Boundary Condition

For the other boundary conditions no one method may be numerically convenient for all situations. A

convenient set of conditions to implement are the asymptotic boundary conditions.

As r goes to infinity, the scattered particle is far enough away from the influence of the potential that the wave function has the form of the direct product of bound asymptotic wave function and the scattered asymptotic wave function. The scattered wave function is the same form as in the two-particle case, the sum of a spherical scattered wave and the incoming plane wave. Thus the three-particle asymptotic wave function is

$$\Psi(\bar{x},\bar{y}) = A\phi(\bar{x})(e^{i\bar{k}\bullet\bar{y}} + \frac{e^{iky}}{y} f(\theta_{ky})) \qquad \text{Eq. 323}$$

where A is the normalizing constant, $\bar{k}$ is the incoming particle momentum vector, $\bar{y}$ is the outgoing vector direction, the scattering amplitude $f(\theta_{ky})$ is the shift in the outgoing wave function amplitude and θ_{ky} is the angle between the incoming direction vector and the Jacobi y-axis vector. The directions of $\bar{k}$ and $\bar{y}$ are given by the angles on the y-axis angular grid (θ_y,ϕ_y). $\phi(\bar{x})$ is the bound particle hydrogen wave function.

$$\phi(\bar{x}) = R_{nl}(x)Y_{lm}(\theta_x,\phi_x); \quad R_{nl}(x) = \phi^h(x)/x \qquad \text{Eq. 324}$$

$R_{nl}(x)$ is the radial wave function.

Note that

$$\int |\phi(\bar{x})|^2 d\bar{x} = 1 \quad \text{and} \quad \int_0^\infty \left| \frac{\phi^h(x)}{x} \right|^2 x^2 dx = \int_0^\infty |\phi^h(x)|^2 dx = 1$$

Equivalently ($\Psi(\bar{x},\bar{y}) = \tilde{\Psi}(\bar{x},\bar{y})/xy$) the asymptotic wave function is written as

$$\begin{aligned} \tilde{\Psi}(\bar{x},\bar{y}) &= A(yx\phi(\bar{x})e^{i\bar{k}\bullet\bar{y}} + x\phi(\bar{x})e^{iky} f(\theta_{ky})) \\ &= A(y\phi^h(\bar{x})e^{i\bar{k}\bullet\bar{y}} + \phi^h(\bar{x})e^{iky} f(\theta_{ky})) \end{aligned} \qquad \text{Eq. 325}$$

where $x\phi(\bar{x}) = \phi^h(\bar{x}) = \phi^h(x)\,Y_{1m}(\theta_x, \phi_x)$.

Asymptotic boundary conditions is obtained by manipulating this equation.

Using the asymptotic wave function without the outgoing wave approximation, and using the approximated DVR wave function evaluated at the j^{th} DVR angle and evaluating at two different scattering distances y and y' to eliminate $f(\theta_{ky})$ yields the following asymptotic boundary condition

$$\psi(x,y,\Omega_j) - e^{ik(y-y')}\psi(x,y',\Omega_j) = A\phi^h(\bar{x})\sqrt{W_j}\,(ye^{ikycos(\theta_{kj})} - y'e^{iky'cos(\theta_{kj})-ik(y'-y)}) \qquad \text{Eq. 326}$$

where θ_{kj} is the angle between the incoming direction vector and the Jacobi y-axis vector given by the j^{th} DVR angles, $\Omega_j = (\theta_{j_{\theta_x}}, \phi_{j_{\phi_x}}, \theta_{j_{\theta_y}}, \phi_{j_{\phi_y}})$, and is given by

$$\cos(\theta_{kj}) = \cos(\theta_k)\cos(\theta_{j_{\theta_y}}) + \sin(\theta_k)\sin(\theta_{j_{\theta_y}})\cos(\phi_k - \phi_{j_{\phi_y}}) \qquad \text{Eq. 327}$$

Denoting $\psi_j(x,y) = \psi(x,y,\Omega_j)$ this boundary condition is written as

$$\psi_j(x,y) - e^{ik(y-y')}\psi_j(x,y') = A\phi^h(\bar{x})\sqrt{W_j}(ye^{ikycos(\theta_{kj})} - y'e^{iky'cos(\theta_{kj})-ik(y'-y)}) \qquad \text{Eq. 328}$$

Using the derivative at two different scattering distances yields an additional boundary condition

$$\psi'_j(x,y) - e^{ik(y-y')}\psi'_j(x,y') = A\phi^h(\bar{x})\sqrt{W_j}((1+iky\cos(\theta_{kj}))e^{ikycos(\theta_{kj})} - (1+iky'\cos(\theta_{kj}))e^{iky'cos(\theta_{kj})-ik(y'-y)}) \qquad \text{Eq. 329}$$

Taking the derivative and evaluating at a single point yields the following boundary condition

$$\psi'_j(x,y) - ik\psi_j(x,y) = A\sqrt{W_j}\phi^h(\bar{x})e^{ikycos(\theta_{kj})}(1+iky(\cos(\theta_{kj})-1)) \qquad \text{Eq. 330}$$

or using the second derivative

$$\psi''_j(x,y) + k^2\psi_j = A\sqrt{W_j}k^2y\phi^h(\bar{x})e^{ikycos(\theta_{kj})} - A\sqrt{W_j}k\phi^h(\bar{x})e^{ikycos(\theta_{kj})}(ky\cos^2(\theta_{kj}) - 2i\cos(\theta_{kj})) \qquad \text{Eq. 331}$$

D.7 Three-Particle Approximated Asymptotic Boundary Condition

Since the wave function is approximated by a finite number of terms, N, for numerical stability the asymptotic boundary conditions should be represented by the approximated asymptotic wave function using only terms up to the maximum partial angular momentum used in the DVR expansion.

As in the two-particle example, the expanded form of $e^{i\bar{k}\bullet\bar{y}} = e^{ikycos(\theta_{ky})}$ is given by

$$e^{ikycos(\theta_{ky})} = \sum_{l_y} e^{il_y/2}(2l_y+1)\,j_{l_y}(kr)P_{l_y}(\cos(\theta_{ky})) \qquad \text{Eq. 332}$$

The expanded asymptotic wave function is given by

$$\tilde{\Psi}(\bar{x},\bar{y}) = A\phi^h(\bar{x})y\sum_{l_y} e^{il_y/2}(2l_y+1)\,j_{l_y}(kr)P_{l_y}(\cos(\theta_{ky})) + A\phi^h(\bar{x})e^{iky}f(\theta_{ky}) \qquad \text{Eq. 333}$$

The amplitude function, $f(\theta_{ky})$, is also represented by

$$f(\theta_{ky}) = \frac{1}{2ik}\sum_{l_y}(2l_y+1)(s_{l_y}-1)P_{l_y}(\cos(\theta_{ky})) \qquad \text{Eq. 334}$$

where s_{ly} represents the l^{th} diagonal element of the scattering or S operator. The actual value of s_{ly} is not computed nor required for asymptotic matching.

In each of these expansions the sum over l_y goes from 0 to infinity. If this sum is truncated then these expansion equations become approximations. In the approximated asymptotic wave function the sum over l_y goes from 0 to the maximum l_y given in the DVR quartet of quantum numbers (L, M, l_x, l_y) used for the wave function approximation.

Using this notation the asymptotic wave function is represented by

$$\tilde{\Psi}_{\text{asym}}(\bar{x},\bar{y}) \approx A\phi^{h}(\bar{x}) y \sum_{l_y} e^{il_y\pi/2}(2l_y+1)\, j_{l_y}(ky) P_{l_y}(\cos(\theta_{ky})) + A\phi^{h}(\bar{x}) e^{iky} \frac{1}{2ik} \sum_{l_y} (2l_y+1)(s_{l_y}-1) P_{l_y}(\cos(\theta_{ky})) \quad \text{Eq. 335}$$

Which is rewritten as

$$\tilde{\Psi}_{\text{asym}}(\bar{x},\bar{y}) \approx A\phi^{h}(\bar{x}) S_{yk}(y) + A\phi^{h}(\bar{x}) e^{iky} G_{yk} \quad \text{Eq. 336}$$

where

$$S_{yk}(y) = \sum_{l_y} i^{l_y} y j_{l_y}(ky)(2l_y+1) P_{l_y}(\cos(\theta_{ky})) \quad \text{Eq. 337}$$

$$f(\theta_{ky}) \approx G_{yk} = \frac{1}{2ik} \sum_{l_y} (2l_y+1) P_{l_y}(\cos(\theta_{ky}))(s_{l_y}-1) \quad \text{Eq. 338}$$

Evaluating the wave function at the DVR angle j for the outgoing y-axis finds

$$\psi_{j}(x,y) \approx A\phi^{h}(\bar{x}) S_{jk}(y) + A\phi^{h}(\bar{x}) e^{iky} G_{jk} \quad \text{Eq. 339}$$

where

$$S_{jk}(y) = \sum_{l_y} i^{l_y} y j_{l_y}(ky)(2l_y+1) P_{l_y}(\cos(\theta_{kj})) \quad \text{Eq. 340}$$

$$f(\theta_{kj}) \approx G_{jk} = \frac{1}{2ik} \sum_{l_y} (2l_y+1) P_{l_y}(\cos(\theta_{kj}))(s_{l_y}-1) \quad \text{Eq. 341}$$

where θ_{kj} is the angle between the incoming vector and the outgoing vector corresponding to the j^{th} y-axis vector.

Using the approximated asymptotic wave function, evaluating at two different asymptotic scattering

distances y and y', and eliminating G_{jk} yields the following asymptotic boundary condition

$$\psi_j(x,y) - e^{ik(y-y')}\psi_j(x,y') = A\sqrt{W_j}\phi^h(\bar{x})(S_{jk}(y) - e^{ik(y-y')}S_{jk}(y')) \quad \text{Eq. 342}$$

Or using the derivative at two different scattering distances yields

$$\psi'_j(x,y) - e^{ik(y-y')}\psi'_j(x,y') = A\sqrt{W_j}\phi^h(\bar{x})(S'_{jk}(y) - e^{ik(y-y')}S'_{jk}(y')) \quad \text{Eq. 343}$$

Continuing, the second derivative yields

$$\psi''_j(x,y) - e^{ik(y-y')}\psi''_j(x,y') = A\sqrt{W_j}\phi^h(\bar{x})(S''_{jk}(y) - e^{ik(y-y')}S''_{jk}(y')) \quad \text{Eq. 344}$$

with

$$S'_{j,k}(y) = \sum_{l_y} i^{l_y}(2l_y+1)P_{l_y}(\cos(\theta_{kj}))(j_{l_y}(ky) + kyj'_{l_y}(ky)) \quad \text{Eq. 345}$$

and

$$S''_{j,k}(y) = \sum_{l_y} i^{l_y}(2l_y+1)P_{l_y}(\cos(\theta_{kj}))(2kj'_{l_y}(ky) + k^2yj''_{l_y}(ky)) \quad \text{Eq. 346}$$

Note that the amplitude function is written as

$$f(\theta_{ky})\Big|_{kj} = \frac{e^{-iky}\psi_j(x,y)}{AY_0^0(\hat{x}_j)\phi^h(x)\sqrt{W_j}} - e^{-iky}S_{jk}(y) \quad \text{Eq. 347}$$

It should be noted that the amplitude function derivation was performed for only 1 input angular y direction, k, and for all output angular y directions, j = 1 to N. However, this equation is valid for all input

angular grid directions and the equation gives the full scattering amplitude NxN matrix for k = 1 to N and j = 1 to N.

REFERENCES

[1]Igarashi, A., S. Nakazaki, A. Ohsake. "Phase Shifts of e+Ps Scatterings and Photodetachment Cross Sections of Ps", *Physical Review A*, 61:032710-1-5, September 2000.

[2]Sultanov, R.A., W. Sandhas, V.B. Belyaev. "Semiclassical Approach to the Three-body Muon-transfer Collisions", *European Physics Journal D.* 5:33-37, 1999.

[3]Ward, S.J., J.H. Macek. "Effective Range Analysis of Positron-Hydrogen Collisions", *Physical Review A*, Vol. 62, No. 5, October 2000.

[4]Faddeev, L.D., S.P. Merkuriev. *Quantum Scattering Theory for Several Particle Systems*. Springer Academic Publishers, 1993.

[5]Hu, Chi-Yu. "The Modified Faddeev Equation and Multichannel Positron-Hydrogen Scattering Calculation", *Journal Of Physics B*, Vol 32, No. 12:3077-3090, 1999.

[6]Elster, Ch., W. Schadow, A. Nogga, W. Glockle. "Three-Body Bound-State Calculations Without Angular-Momentum Decomposition", *Few-Body Systems* 27:83-105, 1999.

[7]Schadow, W. Ch. Elster, W. Glockle. "Three-Body Scattering Below Breakup Threshold: An Approach Without Using Partial Waves", *Few-Body Systems*, 28:15-34, 2000.

[8]Fachruddin, I., Ch. Elster, W. Glockle. "Nucleon-Nucleon Scattering in a Three Dimensional Approach", *Physical Review C*, 62:044002-1-19, 2000.

[9]Baertschy, Li. "Solution of a Three-Body Problem in Quantum Mechanics Using Sparse Linear Algebra on Parallel Computers", *Supercomputing, ACM, IEEE 2001 Conference*, 2001

[10]Kvitsinsky, A.A., Chi-Yu Hu, "Faddeev Calculations of Muonic-atom Collisions: Scattering and Fusion in Flight", *Physical Review A.*, Vol. 53, No. 1:255-271, January 1996.

[11]Kvitsinsky, A.A., Chi-Yu Hu, "Resonances and Excitation of n=2 Levels in e- + H Scattering Via the Faddeev Approach", *Journal Physics B. Atomic Molecular and Optical Physics*, 29:2059-2077, 1996.

[12]Parker, G.A., R.B. Walker, B.K. Kendrick. "Accurate Quantum Calculations on Three-body Collisions in Recombination and Collisions-induced Dissociation. I. Converged Probabilities For The H+Ne2 System", *Journal Of Chemical Physics*, Vol. 117, No. 13:6083-6102, October 2002.

[13]Korobov, V.I. "Multichannel Scattering with Velocity-dependent Asymptotic Potentials", *Journal Of Physics B*, Vol. 27, No. 4:733-745, November 1994.

[14]Hu, Chi-Yu, Kvitsinsky, A.A., "Faddeev Calculations of pu+p Collisions: Effect of Hyperfine Splitting on the Cross Sections", *Journal of Physics B. Atomic Molecular and Optical Physics*. 28:2629-3641, 1995.

[15]Kvitsinsky, A.A., "Low-energy Scattering in the p+pu System Via the Faddeev Approach: Virtual-state Effects", *Physical Review A*, Vol. 47, No. 5:3476-3478, 1993.

[16]Pokorny, Cornel. *Computer Graphics, an Object-Oriented Approach to the Art and Science*, Franklin, Beedle & Associates, Incorporated, 1994.

[17]Hu, Chi-Yu, "The Modified Faddeev Equation and Multichannel Positron-hydrogen Scattering Calculation", *Journal Physics B. Atomic Molecular and Optical Physics*. 32:3077-3090, 1999.

[18]Hou, H.S., H.C. Andrews. "Cubic Splines for Image Interpolation and Digital Filtering", *IEEE Transactions On Acoustics, Speech, and Signal Processing*, Vol. ASP-26, No 6:508-517, December 1978.

[19]Keys, R.G. "Cubic Convolution Interpolations for Digital Image Processing", *IEEE Transactions On Acoustics, Speech, and Signal Processing*, Vol ASP-29, No 6:1153-1160, December 1981.

[20]Prenter, P.M. *Splines and Variational Methods*, John Wiley & Sons, 1989.

[21]Hu, Chi-Yu, Kvitsinsky, A.A. "Solution of the Faddeev Equations for Coulombic Systems", *Hyperfine Interactions*, 82:59-72, 1993.

[22]Schafer, R.W., Rabiner, L.R. "A Digitial Signal Processing Approach to Interpolation" *Proceedings Of The IEEE*, Vol. 61, pp 692, 1973.

[23]Schellingerhout, W.W. "Factorizability in the Numerical Few-Body Problem", Ph. D. Thesis, *Rijksuniversiteit Groningen*, August 1995.

[24]Lill, J.V., G.A. Parker, J.C. Light. "Discrete Variable Representations and Sudden Models in Quantum Scattering Theory", *Chemical Physics Letters*. Vol 89, No 6:483-489, July 1982.

[25]Karabulut, H., E. Sibert. "Trigonometric Discrete Variable Representations", *Journal Physics B. Atomic Molecular and Optical Physics*. 30:513-516, 1997.

[26]Harris, D.O., G.G. Engerholm, W.D. Gwinn. "Calculation of Matrix Elements for One-Dimensional Quantum-Mechanical Problems and The Application to Anharmonic Oscillators", *Journal of Chemical Physics*, Vol. 43, No. 5:515, 1965.

[27]Dickinson, A.S., P.R. Certain, "Calculation of Matrix Elements for One-Dimensional Quantum-Mechanical Problems", *Journal of Chemical Physics*, Vol. 49, No. 9:4209, 1968.

[28]Szalay, V., C. Czako, A. Nagy. "On One-Dimensional Discrete Variable Representations with General Basis Functions", *Journal Of Chemical Physics*, Vol. 119, No 20:10512-10518, November 2003.

[29]Groenenboom, G.C. “The Discrete Variable Representation”, *Lecture notes from Post Graduate Course On Theoretical Chemistry And Spectroscopy*, 2001.

[30]Neto, J.J.S., L.S. Costa. "Numerical Generation of Optimized Discrete Variable Representations", *Brazilian Journal Of Physics*, Vol 28, No 1:1-11, March 1998.

[31]Melezhik, V.S. "New Method for Solving Multidimensional Scattering Problem", *Journal Of Computational Physics*. 92:64-81, 1991.

[32]Melezhik, V.S., Chi-Yu Hu. "Ultra-cold Atom-atom Collisions at Nonresonant Laser Field", *Physics Review Letters*. 90:083202, 2003.

[33]Melezhik, V.S., D. Baye. "Nonperturbative Time-dependent Approach to Breakup of Halo Nuclei", *Physical Review C*, Vol. 59, No. 6:3232-3239, June 1999.

[34]Zhang, F., M. Goldgeier, P.S. Krishnaprasad. "Control of Small Formations Using Shape Coordinates", *Robotics and Automation*, *Proceedings Of The IEEE*. 2:2510-2515, September 2003.

[35]Groenenboom, G. C., D.T. Colbert. "Combining the Discrete Variable Representation with the S-Matrix Kohn Method for Quantum Reactive Scattering", *Journal Of Chemical Physics*, Vol. 99, No. 12:9681-9696, December 1993.

[36]Jacobi, C.G.J., C.W. Borchardt, A. Clebsh, E. Lottner. *Vorlesungen Uber Dynamik*. G. Reimer, Berlin 1884.

[37]Aquilanti, V., Cavalli, S. "Coordinates for Molecular Dynamics: Orthogonal Local System", *Journal Of Chemical Physics*, Vol. 85, No. 3:1355-1362, 1986.

[38]Littlejohn, R, Reinsch, M. "Gauge Fields in the Separation of Rotation and Interanl Motions in the n-body Problem", *Reviews Of Modern Physics*, Vol. 69, No. 1:213-276, 1997.

[39]Abramowitz, M., I.A. Stegun. *Handbook of Mathematical Functions.*, Dover, New York, 1970.

[40]Press, W.H. *Numerical Recipes in C, the Art of Scientific Computing.* Cambridge University Press, New York, 1991.

[41]Lebedev, V.I. "Important Units and Weights of Quadrature Formula Such as The Gauss-Markov for the Series From 9^{th} to 17^{th} Order Accuracy, Invariant Relative to Groups Octagons With Inversion", *Journal Of Mathematics and Mathematical Physics*, 15:48-54, 1975.

[42]Claude, L., L.B. Fraly, K. Liu, M.J. Elrod. "Fully Coupled Six-Dimensional Calculations of the Water Dimer Vibration-Rotation-Tunneling States with a Split Wigner Pseudo Spectral Approach", *Journal Of Chemical Physics*, Vol. 106, No 20:8527-8544, May 1997.

[43]Sakurai, J.J. *Modern Quantum Mechanics Revised Edition*. Addison-Wesley Publishing Company, 1994.

[44]Kuang, Y.R., T.T. Gien. "Positron-Hydrogen Collisions at Low Energies", *Physical Review A*, Vol. 55, No. 1:256-264, Janurary 1996.

[45]Gould, N.I.M., Y. Hu, J.A. Scott. "A Numerical Evaluation of Sparse Direct Solvers for the Solution of Large Sparse, Symmetric Linear Systems Of Equations", *Technical Report RAL-TR-2005-05*, May 2005.

[46]Schneider, H. *Matrices and Linear Algebra*. Dover Publications, Inc., New York, 1989.